

Florida Institute of Technology

Scholarship Repository @ Florida Tech

Theses and Dissertations

5-2021

Design and Synthesis of Polymeric Metastable State Photoacid and Photo CO-Releasing Materials

Adnan Abdallah Muftah Elgattar

Follow this and additional works at: <https://repository.fit.edu/etd>



Part of the [Chemistry Commons](#)

Design and Synthesis of Polymeric Metastable State Photoacid and Photo CO-Releasing Materials

by

Adnan Abdallah Muftah Elgattar

A dissertation submitted to the College of Engineering and Science at
Florida Institute of Technology
in partial fulfillment of the requirements
for the degree of

Doctor of Philosophy
in
Chemistry

Melbourne, Florida
May 2021

We the undersigned committee hereby approve the attached dissertation,
“Design and Synthesis of Polymeric Metastable State Photoacid and Photo CO-
Releasing Materials” by
Adnan Abdallah Muftah Elgattar

Yi Liao, Ph.D.
Professor
Biomedical and Chemical Engineering and Sciences
Committee Chairperson

Rudolf Wehmschulte, Ph.D.
Professor
Biomedical and Chemical Engineering and Sciences
Committee Member

Robert Usselman, Ph.D.
Assistant Professor
Biomedical and Chemical Engineering and Sciences
Committee Member

Ersoy Subasi, Ph.D.
Assistant Professor
Computer Engineering and Sciences
Committee Member

Andrew Knight, Ph.D.
Professor and Department Head
Biomedical and Chemical Engineering and Sciences

Abstract

Design and Synthesis of Polymeric Metastable State Photoacid and Photo CO-Releasing Materials

Author: Adnan Elgattar

Advisor: Yi Liao, PhD

Metastable state photoacids (mPAHs) are molecules that possess a photoinduced metastable state with high acidity and good reversibility. The metastable state lasts long enough to produce a high proton concentration, which can drive various proton transfer processes. MPAHs have been intensively studied in recent years and applied to different chemical, material, biomedical areas. Covalently linking many mPAHs in a polymer allows the generation of a local proton concentration higher than that of the overall system. This dissertation described my PhD work on the synthesis of mPAH polymers using different radical and ring-opening polymerization methods. These polymers can repeatedly produce a high local concentration of proton even in a pH buffer. In addition, my work on nanoparticles containing a photo carbon monoxide releasing molecule is also described.

Preface

This dissertation focuses on the polymerization of mPAHs to provide a large localized concentration of protons in aqueous conditions. My dissertation consists of six chapters.

Chapter 1 provides a basic introduction of mPAHs including structures, desired properties, classifications, and applications.

Chapter 2 reveals a successful synthesis of a mPAH polymer with 2 mol % mPAH loading via free radical copolymerization. PH pulses of 1.4-1.9 units can be repeatedly generated on a micrometer film of this polymer in a PBS buffer. The article “Localized pH Pulses in PBS Buffer Repeatedly Induced by Visible Light,” published by the American Chemical Society in the *Journal of Physical Chemistry*, is reprinted in the dissertation.

Chapter 3 describes a series of attempts to prepare high loading mPAH polymers using free-radical polymerization methods with different techniques, including homopolymerization, copolymerization, and post-polymerization. The highest loading of mPAHs achieved was about 2 mol %.

Chapter 4 describes a series of new mPAH monomers that were successfully synthesized by assembling NH-mPAHs and norbornene molecules. Mmonomer-6 is capable of polymerizing via ring opening metathesis polymerization (ROMP) but transforms to a close-ring form (CRF). Using Monomer-7 leads to a novel mPAH homopolymer, providing the first successful

example of using ROMP to homopolymerize mPAHs. This work shows that we can indeed synthesize well-defined mPAH polymer using ROMP.

Chapter 5 describes a side project of mine regarding a nanoparticle drug delivery system. The article “Polybutylcyanoacrylate Nanoparticle Containing an Organic PhotoCORM,” published by The Royal Society of Chemistry in the *Journal Photochemical and Photobiological Sciences*, is reprinted in the dissertation. The novel organic CO-releasing molecule DK4 was synthesized and incorporated in a polybutylcyanoacrylate (PBCA) nanoparticles. The DK4/PBCA nanoparticle, which showed good biocompatibility and low toxicity, is useful for the study of the biological functions of CO.

Table of Contents

Abastract	iii
Preface.....	iv
Table of Contents	vi
List of Figures	x
List of Schemes	xiii
List of Abbreviations and Acronyms.....	xv
Acknowledgement.....	xvi
Dedication	xviii
Chapter 1 Introduction.....	1
1.1. Significance of Dissertation Research.....	1
1.2. Photoacid Types.....	2
1.3. Structure and Dessired Properties of mPAHs.....	3
1.4. Classification and Application of mPAHs.....	4
1.4.1. Phenol Derivatives Metastable State Photoacid.....	5
1.4.2. Indazole Derivatives Metastable State Photoacid.....	8

1.5. Carbon Monoxide Releasing Molecules (CORMs).....	10
1.6. References.....	12
Chapter 2 Localized pH Pulses in PBS Buffer Repeatedly Induced by Visible Light	21
2.1. Introduction.....	20
2.2. Design and Synthesis of P1NH-mPAH.....	23
2.3. Indicator Selection and Synthesis	26
2.4. Results and Discussion.....	28
2.5. Conclusion.....	35
2.6. References.....	36
Chapter 3 Synthesis of NH-mPAHs Using Free Radical Polymerization.....	40
3.1. Introduction.....	40
3.2. Design and Synthesis of Indazole MeI NH-mPAH Monomers- 2 and- 3	41
3.3. Homopolymerisation pf Photo Photoacid Monomers-2 and 3.....	43
3.4. Copolymerization of NH-mPAH1.....	44
3.5. Post-functionalization of Photoacid.....	45
3.6. Oligomer Metastable State Photoacid.....	50
3.6.1. Trimer Carboxamide Bezothiazolium Iodide.....	50
3.6.2. Trimer-benzyloxy Thiazolium Iodide.....	51
3.7. References.....	56

Chapter 4 ROMP of Norbornenes Containing mPAHs.....	57
4.1. Introduction.....	59
4.2. NB Carboxamide-mPAH Polymerization.....	59
4.3. Exo-NB Imide mPAH Polymerization.....	63
4.4. Norbornenyloxy Benzothiazolium Polymer.....	69
4.5. Future Expansion of NH-mPAH Polymer.....	72
4.6. References.....	74
Chapter 5 Poly(butylcyanoacrylate) Nanoparticle Containing an Organic PhotoCORM.....	78
5.1. Introduction.....	78
5.2. DK4 Incorporated with PBCAs Nanoparticles.....	84
5.3. Cytotoxicity Screening.....	88
5.4. Conclusion.....	90
5.5. References.....	90
Chapter 6 Experimental.....	98
6.1. Materials and Instrumentation.....	98
6.2. Chapter 2 Synthesis and Characterization.....	99
6.3. Chapter 3 Synthesis and Characterization.....	104
6.4. Chapter 4 Synthesis and Characterization.....	111
6.5. Chapter 5 Synthesis and Characterization.....	121
6.6. References.....	127

6.7. Appendices.....	128
6.7.1. Selected NMR Spectra for Chapter 2.....	128
6.7.2. Selected NMR Spectra for Chapter 3.....	131
6.7.3. Selected NMR Spectra for Chapter 4.....	135
6.7.4. Selected NMR Spectra for Chapter 5.....	142

List of Figures

Figure 1.1. Examples of a PGA and ePAHs.	3
Figure 1.2. General structure and mechanism of an mPAH	4
Figure 1.3. Liao's group's proposed mechanism for the first OH-mPAH1.....	5
Figure 1.4. Liao's group's proposed mechanism for OH-mPAH2, TCFtype.....	6
Figure 1.5. OH-mPAH3 structure, based on DAD	7
Figure 1.6. Liao's group's proposed mechanism for the first NH-mPAH1.....	9
Figure 1.7. NH-mPAH2 structure.....	10
Figure 1.8. Liao's group organic photo CORMs structures.....	11
Figure 2.1. UV-vis spectra of a P1NH-mPAH film in PBS before and after irradiation.....	25
Figure 2.2. UV-vis spectra of a P-MR film in water before after protonation with HCl.....	28
Figure 2.3. UV-vis spectra of a film of P-mPAH and P-MR in PBS buffer before irradiation 6, 18, and 72s under irradiation. Experimental setup for monitoring the absorption change during the irradiation (insert).....	31

Figure 2.4. Absorption of the P1NH-mPAH/P-MR film at 550 nm (left) and 438 nm (right) during and after irradiation.....	31
Figure 2.5. Changes in the absorption of the P1NH-mPAH/P-MR film at 550 nm (up) and 438 nm (down) during the irradiation and recovery cycles.....	34
Figure 3.1. ¹ H-NMR spectra of post-polymerization reaction in d6-DMSO.....	47
Figure 3.2. ¹ H-NMR spectra of post-polymerization reaction in d6-DMSO.....	49
Figure 3.3. ¹ H NMR overlay of trimer-benzyloxy thiazolium-NH-mPAH and indazole-7-carbaldehyde in d6-DMSO	53
Figure 4.1. Common polymerization routes of NB-derivatives.....	58
Figure 4.2. H-NMR (DMSO-6d) Spectrum of Monomer-6 before irradiation (top) and after irradiation, CRF (bottom).....	66
Figure 4.3. ¹ H NMR spectrum (DMSO-d6) diagnostic of the polymer synthesized from the monomer-6 and shows the disappearance of the monomer olefinic peaks at 6.4 ppm was observed (red circle, bottom) and new olefinic resonances of product appeared 5.9-5.3 ppm (blue circle, bottom).	68
Figure 5.1. UV-Vis spectra of DK4 in DMSO (9×10 ⁻⁵ M) before and after irradiation [left, inserted figure: spectrum of di-t-butyl anthracene (the expected photoproduct)], and in 1% DMSO aqueous solution (4×10 ⁻⁵ M) before and after irradiation [right, inserted figure: spectra of the irradiated solution after addition of DMSO].....	84

Figure 5.2. Size distribution of the PBCA/DK4 nanoparticle measured by DSL (up) and UV-Vis spectra of the nanoparticle in water and in DMSO before and after irradiation (down).....86

Figure 5.3. DNA Analysis of Endothelial Cells seeded on TCPS treated with varying concentrations of DK4 Nanoparticle solutions ($n=6$). No significance was determined. Bottom: Live/Dead (green / red) confocal images of endothelial cells with varying dose at A) no drug delivery of 0 $\mu\text{g/mL}$; B) low dose of 0.5 $\mu\text{g/mL}$, and C) at high concentration of 50 $\mu\text{g/mL}$ for DK4 Nanoparticle solution at Day 11.....89

List of Schemes

Scheme 2.1. Synthesis of the photoacid monomer-1 and polymer P1NH-mPAH..	24
Scheme 2.2. Synthesis of the indicator polymer P-MR	27
Scheme 3.1. Synthetic route for NH-PAH monomers-2 and -3.....	42
Scheme 3.2. Attempted homopolymerization of Monomer-2 and -3.....	43
Scheme 3.3. Synthesis of photoacid polymer-2 (P1NH-mPAH)	45
Scheme 3.4. (A) Free-radical copolymerization of benzothiazolium monomer and Isopropyl acrylamide. (B) Post-polymerization functionalization of the bhenothiazinium-units to form photoacid polymer.....	48
Scheme 3.5. Synthetic Route for the Compound 7 and 8.....	51
Scheme 3.6. Synthetic route for the trimer-benzyloxy NH-mPAH.....	53
Scheme 4.1. Synthesis of monomer-4	60
Scheme 4.2. Attempted Thiol-ene Polymerization and ROMP of Monomer-4.....	62
Scheme 4.3. Synthesis monomer-5.....	64
Scheme 4.4. Synthesis monomer-6	65
Scheme 4.5. Synthesis of the monomer-7	70

Scheme 4.6. Polymerization of the monomer-7 to form the respective P3-mPAH.....	71
Scheme 5.1. (a) Structures of DK4 and PBCA, (b) photoreaction of DK4, (c) the potential hydration reaction, and (d) synthesis of DK4.....	81

List of Abbreviations and Acronyms

Metastable-state photoacids	mPAHs
Polymer metastable state photoacids	P-mPAHs
Proton transfer	PT
Photoacid generators	PAGs
Excited-state proton transfer	ESPT
Excited-state photoacids	ePAHs
Close ring form	CRF
Open ring form	ORF
Methyl trifluoromethanesulfonate; Methyl triflate	MeOTf
Thin layer chromatography	TLC
2,2-Azobisisobutyronitrile	AIBN
Free-radical polymerization	FRP
Butylated hydroxytoluene	BHT
2-Hydroxyethylene methacrylate	HEMA
Hexafluoroisopropanol	HFIP
Second generation Grubbs	G2
Ethyl vinyl ether	EVE
Endothelial cells	ECs
Trifluoroacetic acid	TFA
Polybutyl cyanoacrylate	PBCA
Nanoparticles	NPs

Acknowledgments

First, I thank God for providing me with wisdom, strength, and passion. Second, I extend and express my most profound appreciation and sincere gratitude to Dr. Yi Liao for his support, guidance, and encouragement provided throughout my graduate study. His patience and belief in me greatly enhanced my research. I give special thanks to my PhD committee members Dr. Rudolf Wehmschulte, Dr. Robert Usselman, and Dr. Ersoy Subasi for their direction, constructive criticism and inspiration.

I express my sincere thanks to the Department of Biomedical and Chemical Engineering and Sciences at the Florida Institute of Technology. Special acknowledgment goes to Dr. Alan Brown, Dr. Nasri Nesnas and Dr. Norito Takenaka for their instruction, support, and appreciation of my work. I am truly grateful to Dr. Bashar and his group for sharing their biological studies.

I would like to thank my research group members Thaaer, Osamah, Nawodi, Zhuozhi, Somayeh, and Abdelhamid for their invaluable help, advice, and optimism about lab-related issues during my study at the Florida Institute of

Technology. The rewarding journey we all experienced could not have been made without their contributions. I am extremely proud to have been involved in such amazing discussions with them.

I give special thanks for my wife Nona who reinforced me with endless love and care all these years. I am so grateful to my three children for cheering me up every day and reminding me how beautiful life is.

Support from the National Science Foundation and the Ed Ethel Moore Alzheimer Research Grant is gratefully acknowledged.

Dedication

I dedicate my work to my family, especially my mother for her love and prayers, and with special respect to my father who cannot see this dissertation completed

Chapter 1

Introduction

1.1. Significance of Dissertation Research

Proton transfer is one of the most studied phenomena in chemistry. Light-controlled pH change has an important application in biomedical and biotechnology. Photoacids, molecules that transform to a strong acid after absorbing light, are useful in controlling proton transfer processes with light and are applied in many crucial chemical technologies.¹ Metastable state photoacids (mPAHs) are molecules that have a photoinduced metastable state with high acidity and good reversibility. The structural design of mPAHs allows the metastable state to last long enough to produce a high proton concentration which can be reversibly produced with moderate light intensity.²

Therefore, linking mPAH units to synthesize a new polymeric material of mPAHs that can produce a localized proton concentration with high efficiency and good reversibility under visible light is important. Furthermore, covalently linking mPAH monomers to become a polymer prevents leakage problems without irradiation and improves the compatibility of materials in different media. The polyphotoacids significantly impact future development and application in different areas such as advanced polymer chemistry, material science, and nanotechnology.

1.2. Photoacid Types

Generally, photoacids can be classified based on their high acidic state or reversibility.² Photoacid generators (PAGs) are irreversible photoacids undergoing a photo-destructive irradiation process, which generates strong acids. N-Hydroxy-naphthalimide-triflate and triphenyl sulfonium-triflate are common examples of nonionic and ionic PAGs (Figure 1. 1).^{3,4} Their ability to form strong acid and create a high concentration of protons has often been used as photo initiators of cationic polymerization⁵⁻⁹ and in photography.¹⁰

There are two types of reversible photoacids including excited-state photoacids (ePAHs) and metastable-state photoacids (mPAH). Each has different mechanisms and properties that make them essential in various applications. The reversible ePAHs, like pyrene derivatives (Figure 1.1), have a high-acidity excited state upon irradiation and quick proton reassociation once light is turned off. Thus, the ePAHs can be utilized to study the mechanisms that require fast proton transfer processes due to the short life of the excited state.¹¹⁻¹³

The mPAH, which can generate a high proton concentration, undergoes photoreaction and transforms into a metastable structure (strong acid). The metastable state lasts from seconds to hours after the light is turned off, allowing protons to accumulate at a high concentration.¹⁴ The chemical properties and mechanism of mPAH are discussed in detail in the next section.

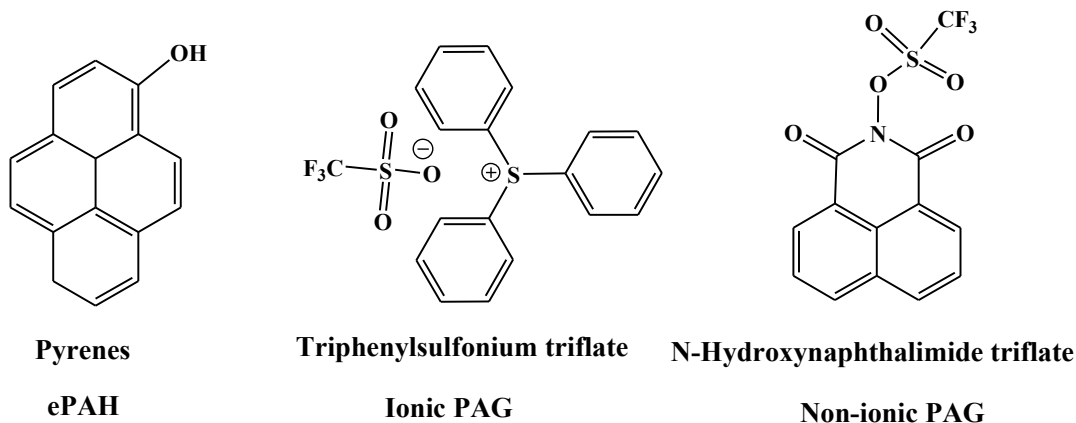


Figure 1. 1. Examples of a PGA and ePAH.

1.3. Structure and Desired Properties of mPAHs

The structure of mPAHs is generally designed to have an electron-accepting (EA) moiety and a weakly acidic nucleophilic moiety (NuH) linked by a double bond. Under illumination, mPAHs absorb the light and undergo a trans-cis photoisomerization reaction and then transform to a highly acidic metastable form (Figure 2). The metastable state is maintained for a certain time after turning the light off, allowing the protons to dissociate and then thermally relax to the ground state.^{14,15}

Based on these desirable properties, mPAHs become molecules that produce a large proton concentration with high efficiency and good reversibility under visible light. Thus, mPAHs are utilized in various proton transfer processes that require a process controlled by switching a light on and off.

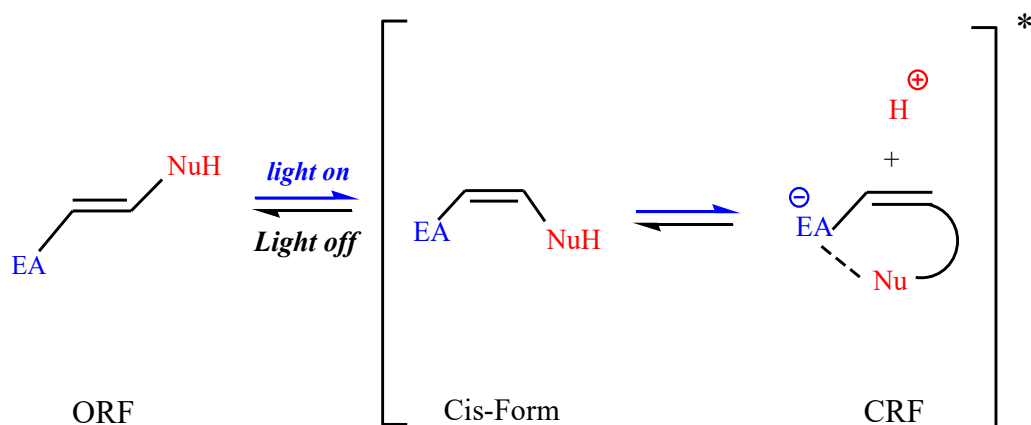


Figure 1.2. General structure and mechanism of an mPAH.

1.4. Classification and Application of mPAHs

Liao's group discovered the first mPAH1 in 2011 and developed the structure by linking different moieties and studying structure-property relationships, photoactivity, and stability to expand their applications.¹⁴ In 2015, a different type of mPAHs based on donor-acceptor structure was reported by his group.¹⁵ Both structures have been the most commonly used since being discovered. Herein, we consider that mPAHs can be subdivided into two major classes: phenol derivatives-photoacid (OH-mPAH), which have phenol as the nucleophilic moiety, and indazole derivatives-photoacid (NH-mPAH), which have indazole as the nucleophilic moiety.

1.4.1. Phenol Derivatives Metastable State Photoacids

Phenol derivatives as the nucleophilic moiety OH-mPAH1 are commonly used in mPAHs and are well known as merocyanine or spiropyran photoacids since they undergo photoirradiation to form a spiropyran photochromic structure. The zwitterionic structure of this type of OH-mPAH has phenol as the nucleophilic moiety linked to indolinium with a propyl sulfonate moiety as the electron acceptor, which gives the ability to transform under moderate light into an acidic spiro-form with high efficiency and good reversibility. The SO_3^- anion increases the stability of the indolinium cation and the ORF. The structure and mechanism for a reversible photoreaction of OH-mPAH1 are proposed (Figure 1.3).

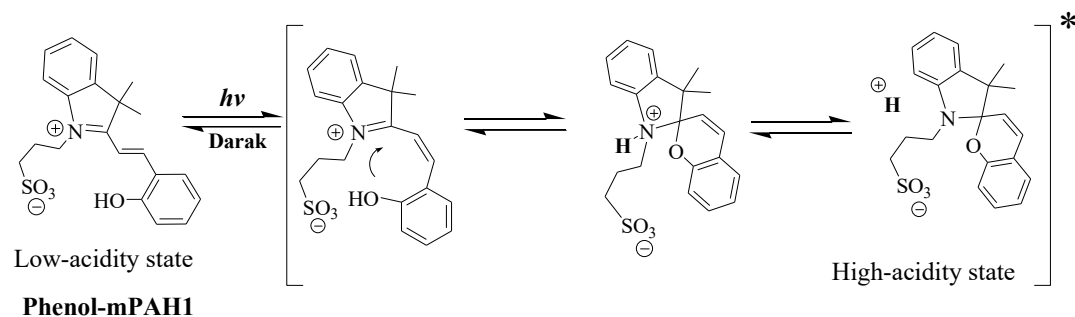


Figure 1.3. Liao's group's proposed mechanism for the first OH-mPAH1.

Another OH-mPAH type was designed without the zwitterionic indolinium moiety, called tricyanofuran (TCF) photoacid. Liao's group developed a TCF-type mPAH in 2016, and the structure was designed with tricyanofuran (TCF) as an

electron-accepting moiety and phenol as the nucleophilic moiety. This photoacid displayed much better solubility in different organic solvents and a comparatively faster reverse reaction than the previous type of OH-mPAHs.¹⁶ Compared to the merocyanine mPAH, the TCF mPAH showed lower dark acidity, which is desirable; on the other hand, lower photoacidity is disadvantageous. Liao's group proposed a photoreaction mechanism for the TCF photoacid (Figure 1.4). The photoacid is soluble in common organic solvents such as alcohols, DCM, DMSO, THF, and EtOAc but was insoluble in water.

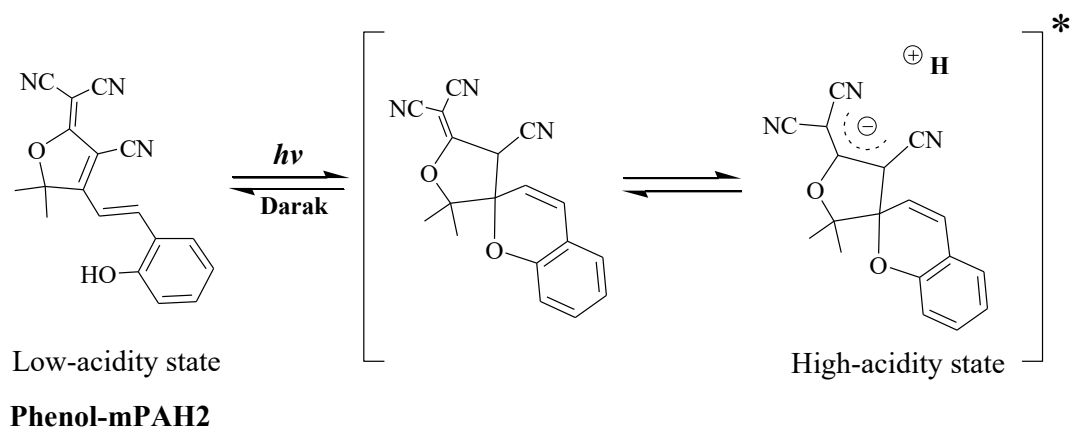
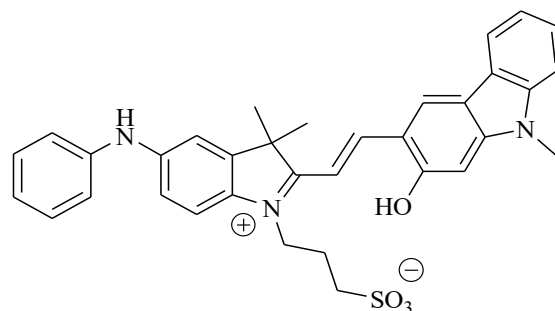


Figure 1.4. Liao's group's proposed mechanism for OH-mPAH2, TCF type.

Different OH-mPAHs have been developed and successfully utilized in various applications that need photo-controlled proton transfer. For example, controlled polymerization reactions^{17,18}, energy transformation¹⁹⁻²¹, molecular switches²², molecular machines^{23,24}, patterning^{25,26}, supramolecular assembly²⁷⁻³⁰,

cationic sensors^{31,32}, photochromic systems^{33,34}, nanoparticles³⁵⁻³⁸, odorant releases³⁹, facilitating drug releases⁴⁰, and antibacterial agents.⁴¹

Our group studied an OH-mPAH to achieve an activating wavelength in the tissue penetration window (650–1350 nm) for in vivo bioapplication. Many drug-release studies have successfully been completed for photo-molecules that can be activated by a wavelength in this window⁴²⁻⁴⁵. In 2019, our group successfully developed and reported a novel OH-mPAH3 (Figure 1.5), which responds to 660 and 700 nm red light. The molecule has a donor-acceptor-donor (DAD) structure, which helps it to respond to long wavelengths (Figure 1.6). This work was published in our article “Red-Light Responsive Metastable-State Photoacid,” published in the journal *Dyes and Pigments* in 2019.



OH-mPAH3

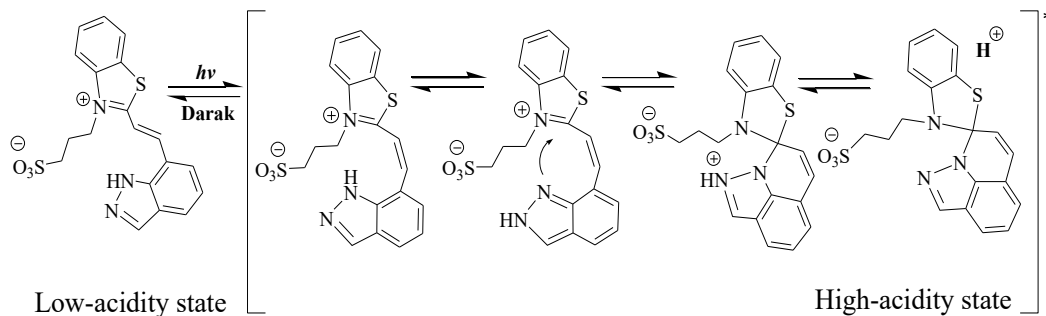
In 2019

Figure 1.5. OH-mPAH3 structure, based on the DAD structure.

1.4.2. Indazole Metastable State Photoacid

In 2015, Liao's group reported the first indazole mPAH1 (figure 1.6). The structure was designed to have indazole as the nucleophilic moiety and benzothiazolium moiety as the electron accepting moiety. Indazole photoacid was discovered to function with a phosphate buffered saline (PBS) with a pH of 7.4 under light. PBS is the most used buffer in biological studies because of its pH of 7.4, which is close to the pH of the human body.¹⁵

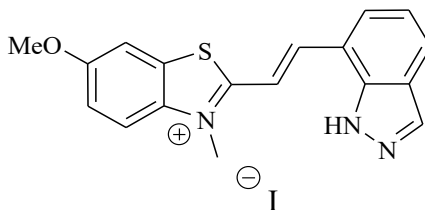
The phenol-mPAH photoreaction in the PBS showed that 83% of the phenol released protons in the PBS buffer without irradiation. The pKa of the mPAH is less than 7.4 after the phenol is coupled with the strongly electron-withdrawing indolinium moiety. The proton dissociation occurs in the dark without irradiation due to the equilibrium shifting thermally to the CRF. However, the pKa of indazole is 13.9, almost 4 units greater than phenol, which lowers the dark acidity of the corresponding mPAH and allows this type of mPAH to function at a pH of 7.4 (Figure 1.6).



Indazol-MPAH1

Figure 1.6. Liao's group's proposed mechanism for the first NH-mPAH1.

Some practical applications may require photo-response materials to function in aqueous solution. Therefore, the NH-mPAH has a great advantage over OH-mPAH. However, the reverse reaction requires hours to days, which may be too long for some practical applications. Therefore, creating new photoacids that can be switched back by light is desirable. Recently, our group developed a new indazole-mPAH for such applications. NH-mPAH2 (in figure 1.7) can be switched alternatively between high-acidity and low-acidity states with different wavelengths of light, which are 470 nm and 365 nm. This work was published in our article "A Reversible Photoacid Switched by Different Wavelengths of Light" in the journal *ChemPhotoChem* in 2020.



NH-mPAH2

In 2020

Figure 1.7. NH-mPAH2 structure.

1.5. Carbon Monoxide Releasing Molecules (CORMs)

Carbon monoxide (CO) is now well known as a gasotransmitter in the body. However, the inhalation of CO causes disorders of the nervous system and asphyxiation. Exposure to a CO-rich atmosphere reduces the oxygen in blood and tissues, causing death. On the other hand, delivering a controlled dose of CO has beneficial effects such as reducing inflammation and cardiovascular disorders.^{46, 47} Therefore, controlling the quantities of CO gas delivered to the human body to avoid toxic and side effects is crucial. CORMs, which are compounds designed to control the release of CO^{48, 49}, showed promising therapeutic effects such as anti-apoptotic, anti-inflammatory, anti-hypertensive, renal protective, and anti-ischemic properties.⁵⁰

In 2013, a new type of organic CORM was reported by the Liao group. The structure was based on unsaturated cyclic α -diketones (DKs), which could be activated by visible light.⁵¹ The structure of the DKs plays an important role in

carrying and releasing CO in cellular systems. The first DK is 9,10-dihydro-9,10-ethanoanthracene-11,12-dione (DK1), which generated CO and fluorescent anthracene under visible light.^{52, 53} In my work, a new CORM was developed: 2, 6-di-tertbutyl-4, 9, 9, 10-tetrahydro-9, 10-ethanoanthracene-11, 12-dione (DK4). DK4 functions in a 1% DMSO aqueous solution, in which other DKs are deactivated due to hydration (figure 1.8). We encapsulated DK4 in polybutylcyanoacrylate (PBCA) nanoparticles. More details about the structure, synthesis, and biological properties are found in chapter 5.

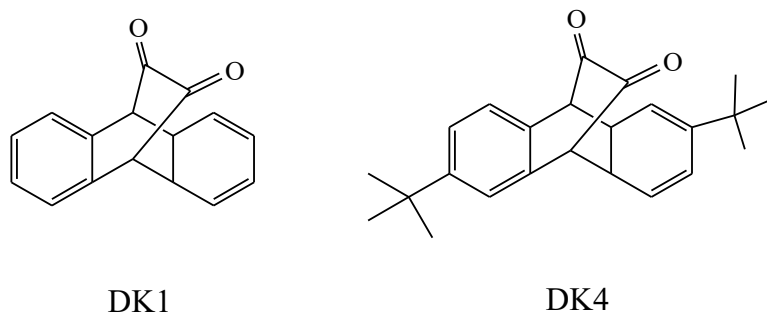


Figure 1.8. Liao's group organic photo CORMs structures.

1.6. References

1. Ivan, M. G.; Scaiano, J. C. Photoimaging and Lithographic Processes in Polymers. In *Photochemistry and Photophysics of Polymer Materials*; Allen, N. S., Ed., John Wiley & Sons: Hoboken, **2010**.
2. Liao, Y. Design and Applications of Metastable-State Photoacids, *Acc. Chem. Res.*, **2017**, *50*, 1956-1964.
3. Ireland, J. F.; Wyatt, P. A. H. Acid-Base Properties of Electronically Excited States of Organic Molecules. *Adv. Phys. Org. Chem.* **1976**, *12*, 131-160.
4. Tolbert, L.; Solntsev, K. M. Excited-State Proton Transfer: From Constrained Systems to “Super” Photoacids to Superfast Proton Transfer, *Acc. Chem. Res.*, **2002**, *35*, 19-27.
5. Shirai, M.; Tsunooka, M. Photoacid and photobase generators: Chemistry and applications to polymeric materials. *Prog. Polym. Sci.*, **1996**, *21*, 1-45.
6. Iwachima, C.; Imai, G.; Okamura, H., Tsunooka, M.; Shirai, M. Synthesis of i- and g-Line Sensitive Photoacid Generators and their Application to Photopolymer Systems, *Photopolym Sci Tec.*, **2003**, *16*, 91-96.
7. Crivello, J. V. Design of photoacid generating systems, *J. Photopolym. Sci. Technol.*, **2009**, *22*, 575-582.

8. Martin, C. J.; Rapenne, G.; Nakashima, T. and Kawai, T. Recent progress in development of photoacid generators, *J. Photochem. Photobiol. C.* , **2018**, 34, 41-51.
9. Kuznetsova, N.A.; Malkov, V.; Gribov, B.G. Photoacid generators. Application and current state of development, *Russ. Chem. Rev.*, **2020**, 89.2 ,173.
10. Klikovits, N.; Knaack, P.; Bomze, D.; Krossing, I.; Liska, R. Novel photoacid generators for cationic photopolymerization. *Polym Chem.*, **2017**, 8, ,14-21.
11. Ayothi, R.; Yi, Y.; Cao, H. B.; Yueh, W.; Putna, S.; Ober, C.K. Arylonium Photoacid Generators Containing Environmentally Compatible Aryloxyperfluoroalkanesulfonate Groups, *Chem. Mater.* , **2007**, 19, 34-44.
12. Ireland, J. F.; Wyatt, P. A. H. Acid-Base Properties of Electronically Excited States of Organic Molecules, *Adv. Phys. Org. Chem.*,**1976**, 12, 131-221.
13. Tolbert, L.; Solntsev, K. M. Excited-State Proton Transfer: From Constrained Systems to “Super” Photoacids to Superfast Proton Transfer, *Acc. Chem. Res.*, **2002**, 35, 19-27.
14. Shi, Z.; Peng, P.; Strohecker, D.; Liao, Y. Long-Lived Photoacid Based upon a Photochromic Reaction. *J. Am. Chem. Soc.*, **2011**, 133, 14699–14703.
15. Abeyrathna, N. and Liao, Y. A Reversible Photoacid Functioning in PBS Buffer under Visible Light. *J. Am. Chem. Soc.*, **2015**, 137, 11282-11284.

16. Yang, C.; Khalila, T.; Liao, Y. Photocontrolled proton transfer in solution and polymers using a novel photoacid with strong C–H acidity. *RSC Adv.*, **2016**, *6*, 85420-85426.
17. Fu, C.; Xu, J.; Boyer, C. Photoacid-Mediated Ring Opening Polymerization Driven by Visible Light, *Chem. Commun.*, **2016**, *52*, 7126-7129.
18. Zayas, M. S.; Dolinski, N. D.; Self, J. L.; Abdilla, A.; Hawker, C. J.; Bates, C. M. and Alaniz, J. R. D. Tuning Merocyanine Photoacid Structure to Enhance Solubility and Temporal Control: Application in Ring Opening Polymerization, *Chem. Photo. Chem.*, **2019**, *3*, 467-472.
19. Xu, Y.; Fei, J.; Li, G.; Yuan, T.; Li, Y.; Wang, C.; Li, X. and Li, J. Enhanced Photophosphorylation of a Chloroplast-Entrapping Long-Lived Photoacid, *Angew. Chem. Int. Ed. Engl.*, **2017**, *56*, 12903-12907.
20. Go, D.; Rommel, D.; Liao, Y.; Haraszti, T.; Sprakel, J.; Kuehne, A. J. C. Dissipative disassembly of colloidal microgel crystals driven by a coupled cyclic reaction network, *Soft Matt*, **2018**, *14*, 910-915.
21. Bao, H.; Li, F.; Lei, L.; Yang, B.; Li, Z. ON/OFF states of a microbial fuel cell controlled by an optical switching system. *RSC Adv.*, **2014**, *4*, 27277-27280.

22. Patel, P.K., Arias, J.E., Gongora, R.S., Hernandez, F.E., Moncomble, A., Aloïse, S.; Chumbimuni-Torres, K.Y. Visible light-triggered fluorescence and pH modulation using metastable-state photoacids and BODIPY. *Phys. Chem. Chem. Phys.*, **2018**, 20, 26804-26808.
23. Tatum, L. A.; Foy, J. T.; Aprahamian, I. Waste Management of Chemically Activated Switches: Using a Photoacid To Eliminate Accumulation of Side Products, *J. Am. Chem. Soc.*, **2014**, 136, 17438-17441.
24. Yang, L.; Jia, F.; Cui, J.; Lu, S.; Jiang, W. Light-Controlled Switching of a Non-photoresponsive Molecular Shuttle, *Org. Lett.*, **2017**, 19, 2945-2948.
25. Zhang, T.; Sheng, L.; Liu, J.; Ju, L.; Li, J.; Du, Z.; Zhang, W.; Li, M.; Zhang, S. X. Photoinduced Proton Transfer between Photoacid and pH - Sensitive Dyes: Influence Factors and Application for Visible - Light - Responsive Rewritable Paper, *Adv. Funct. Mater.*, **2018**, 28, 1705532.
26. Khalil, T.; Alharbi, A.; Baum, C.; Liao, Y. Facile Synthesis and Photoactivity of Merocyanine-Photoacid Polymers, *Macromol. Rapid Commun.*, **2018**, 39, 1800319-1800323.
27. Maity, C.; Hendriksen, W. E.; Van Esch, J. H.; Eelkema, R. Spatial structuring of a supramolecular hydrogel by using a visible-light triggered catalyst, *Angew. Chem. Int. Ed. Engl.*, **2015**, 54, 998-1001.

28. Li, X.; Fei, J.; Xu, Y.; Li, D.; Yuan, T.; Li, G.; Wang, C.; Li, J. A. Photoinduced Reversible Phase Transition in a Dipeptide Supramolecular Assembly, *Angew. Chem. Int. Ed. Engl.*, **2018**, *57*, 1903-1907.
29. Samanta, D.; Galaktionova, D.; Gemen, J.; Shimon, L. J. W.; Diskin-Posner, Y.; Avram, L.; Kral, P.; Klajn, R. Reversible chromism of spiropyran in the cavity of a flexible coordination cage. *Nat. Commun.*, **2018**, *9*, 1-9.
30. Jansze, S. M.; Cecot, G.; Severin, K. Reversible disassembly of metallasupramolecular structures mediated by a metastable-state photoacid, *Chem. Sci.*, **2018**, *9*, 4253-4257.
31. (a) Johns, V. K.; Patel, P. K.; Hassett, S.; Calvo-Marzal, P.; Qin, Y.; Chumbimuni-Torres, K. Y. Visible Light Activated Ion Sensing Using a Photoacid Polymer for Calcium Detection, *Anal. Chem.*, **2014**, *86*, 6184-6187.
(b) Patel, P. K.; Chumbimuni-Torres, K. Y. Visible light-induced ion-selective optodes based on a metastable photoacid for cation detection, *Analyst*, **2016**, *141*, 85-89.
32. Liu, L.; Su, X.; Yu, Q.; Guo, H.; Wang, K.; Yu, B.; Li, M.; Zou, B.; Liu, Y.; Zhang, S. X. Photoacid-Spiropyran Exhibits Different Mechanofluorochromism before and after Modification of Tetraphenylethene under Grinding and Hydrostatic Pressure, *J. Phys. Chem. C*, **2019**, *123*, 25366-25372.

33. Chen, H.; Liao, Y. Photochromism based on reversible proton transfer *J. Photochem. Photobiol. A.*, **2015**, 300, 22-26.
34. (a) Mahvidi, S.; Takeuchi, S.; Kusumoto, S.; Sato, H.; Nakagawa, T.; Yokoyama, Y. Gated Photochromic System of Diarylethene with a Photon-Working Key. *Org. Lett.*, 2016,18, 5042-5045. (b) Kusumoto, S.; Nakagawa, T.; Yokoyama, Y. All-Optical Fine-Tuning of Absorption Band of Diarylethene with Photochromic Acid-Generating Spiropyran. *Adv. Opt. Mater.*, **2016**, 4, 1350-1353
35. Wang, Z.; Liao, Y. Reversible dissolution/formation of polymer nanoparticles controlled by visible light. *Nanoscale* , **2016**, 8, 14070-14073.
36. (a) Zhang, H.; Zeng, H.; Priimagi, H.; Ikkala, O. Programmable responsive hydrogels inspired by classical conditioning algorithm, *Nat. Commun.*, **2019**, 10, 1-8. (b) Zhang, H.; Muhammad, J.; Liu, K.; Ras, R. H. A.; Ikkala, O. Light-induced reversible hydrophobization of cationic gold nanoparticles via electrostatic adsorption of a photoacid, *Nanoscale*, **2019**, 11, 14118-14122.
37. Kundu, P. K.; Manna, D.; Leizrowice, R.; Margulis, B.; Zhao, H.; Borner, M.; Udayabhaskararao, T.; Manna, D.; Klajn, R. Light-controlled self-assembly of non-photoresponsive nanoparticles, *Nat. Chem.*, **2015**, 7, 646-652.
38. Guo, J.; Zhang, H.; Zhou, Y.; Liu, Y. Light-controlled reversible self-assembly of nanorod suprastructures, *Chem. Comm.*, **2017**, 53, 6089-6092.

39. Wang, Z.; Johns, V. K.; Liao, Y. Controlled Release of Fragrant Molecules with Visible Light. *Chem. Eur. J.*, **2014**, *20*, 14637-14640.
40. Han, R.; Wu, S.; Tang, K.; Hou, Y. Facilitating drug release in mesoporous silica coated upconversion nanoparticles by photoacid assistance upon near-infrared irradiation. *Adv. Powder Technol.*, **2020**, *31*, 3860-3866.
41. Luo, Y.; Wang, C.; Peng, P.; Hossain, M.; Jiang, T.; Fu, W.; Liao, Y.; Su, M. Visible Light Mediated Killing of Multidrug-Resistant Bacteria Using Photoacids, *J. Mater. Chem. B*, **2013**, *1*, 997-1001.
42. Peterson, J. A.; Wijesooriya, C.; Gehrman, E. J.; Mahoney, K. M.; Goswami, P. P.; Albright, T. R.; Syed, A.; Dutton, A. S.; Smith, E. A.; Winter, A. H. Family of BODIPY Photocages Cleaved by single Photons of Visible / Near-Infrared Light. *J. Am. Chem. Soc.*, **2018**, *140*, 7343-7346.
43. Gorke, A. P.; Nani, R.; Schnermann, M. J. Harnessing Cyanine Reactivity for Optical Imaging and Drug Delivery. *Acc. Chem. Res.*, **2018**, *51*, 3226–3235.
44. Al-Afyouni, M. H.; Rohrabough, T. N. J.; Al-Afyouni, K. F.; Turro, C. New Ru(II) Photocages Operative with Near-IR Light: New Platform for Drug Delivery in the PDT Window. *Chem Sci.*, **2018**, *9*, 6711-6720.

45. Sun, W.; Li, S.; Haeupler, B.; Liu, J.; Jin, S.; Steffen, W.; Schubert, U.S.; Butt, H-J.; Liang, X-J.; Wu, S. Drug Therapy: An Amphiphilic Ruthenium Polymetallo drug for Combined Photodynamic Therapy and Photochemotherapy in vivo. *Adv. Mater.*, **2017**, *29*, 1603702.
46. Tenhunen, R.; Marver, H.; Schmid, R. Microsomal heme oxygenase. Characterization of the enzyme, *J. Biol. Chem.* **1969**, *244*, 6388-94.
47. R. Motterlini, Carbon monoxide-releasing molecules (CO-RMs): vasodilatory, anti-ischaemic; anti-inflammatory activities, *Biochem. Soc. Trans.* **2007**, *35*, 1142-1146.
48. Palao, E.; Slanina, T.; Muchová, L.; Šolomek, T.; Vitek, L.; Klán, P. Transition Metal-Free CO-Releasing BODIPY Derivatives Activatable by Visible to NIR Light as Promising Bioactive Molecules, *J. Am. Chem. Soc.*, **2016**, *138*, 126-133.
49. Heinemann, S. H.; Hoshi, T.; Westerhausen, M.; Schiller, A. Carbon monoxide-physiology, detection and controlled release, *Chem. Commun.* **2014**, *50*, 3644.
50. (a) Motterlini, R.; Otterbein, L. E. The therapeutic potential of carbon monoxide, *Nat. Rev. Drug Discovery*, **2010**, *9*, 728-743. (b) Alberto, R. Motterlini, R. Chemistry and biological activities of CO-releasing molecules (CORMs) and transition metal complexes, *Dalton Trans.*, **2007**, *17*, 1651-1660

51. Peng, P.; Wang, C.; Shi, Z.; Johns, V. K.; Ma, L.; Oyer, J.; Copik, A.; Igarashi, R.; Liao, Y. Visible-light activatable organic CO-releasing molecules (PhotoCORMs) that simultaneously generate fluorophores. *Org. Biomol. Chem.*, **2013**, *11*, 6671-6674.
52. Michael, E.; Abeyrathna, N.; Patel, A. V.; Liao, Y.; Bashur, C. A. Incorporation of photo-carbon monoxide releasing materials into electrospun scaffolds for vascular tissue engineering. *Biomedical Materials*, **2016**, *11*, 025009.
53. Washington, K. Controlling CO Dose from CORM-loaded Electrospun Scaffolds with Diffusion-based Modeling and Experimental Assessment of Endothelial Cell. *Diss.* **2019**.

Chapter 2

Localized pH Pulses in PBS Buffer Repeatedly Induced by Visible Light

“Reprinted with permission from **Elgattar**, A.; Abeyrathna N. Liao Y.” A Localized pH pulses in PBS buffer repeatedly induced by visible light. *The Journal of Physical Chemistry B*. **2019**, 123 (3) 648–654. Copyright © 2019, American Chemical Society.

2.1. Introduction

A suitable pH of a biological system is critical for the activity of enzymes, and abnormal cellular pH is related to many diseases including cancer, cardiovascular diseases, Alzheimer’s disease, etc. A method that allows spatial and temporal modulation of pH with light will be useful for studying the pH effects on enzymatic functions and disease mechanisms and may lead to new drug delivery and therapeutic methods. It is worth mentioning that photoinduced proton transfer at molecular level has been extensively studied using ultrafast spectroscopy.^{1,2} Our goal is to controllably produce a large proton concentration with measurable pH change and significant macroscopic effects.

Metastable-state photoacids (mPAH) can produce a large proton concentration with high efficiency and good reversibility under visible light.³ Reversible pH change over two units has been demonstrated previously.⁴ Over the past years, mPAH has become a useful tool for controlling various proton transfer processes with light. Applications of mPAH in energy conversion⁵⁻⁷, sensor^{8,9}, polymerization¹⁰, patterning¹¹⁻¹³, nanomaterials^{9,14-15}, molecular machines¹⁶⁻¹⁸, photochromic materials^{13,19-21}, fragrance release²², and biomedical^{23,24} areas have been reported by our group and other groups. For example, Gray, Dougherty and coworkers showed that ion channels associated with vision and pain can be reversibly activated with light using an mPAH.²³ Li group demonstrated that chloroplast entrapped with an mPAH produced 2.9 times more ATP than natural chloroplast.⁵ Chumbimuni-Torres group developed a Calcium biosensor by incorporating *mPAHs* in polymer thin films.⁸ Su group in collaboration with our group showed that the photoacidity of an mPAH was enough to kill drug-resistant bacteria and assist the antibacterial activity of Colistin.²⁴

Although the potential of mPAHs have been clearly demonstrated in these works, no photo-induce pH change in a pH buffer has been reported. Non-buffered solutions of mPAHs were often used for modulating pH with light. The challenge is apparent for the buffer is against the pH change. However, since all biological systems are in pH buffers, it is expected that a localized pH change in a pH buffer

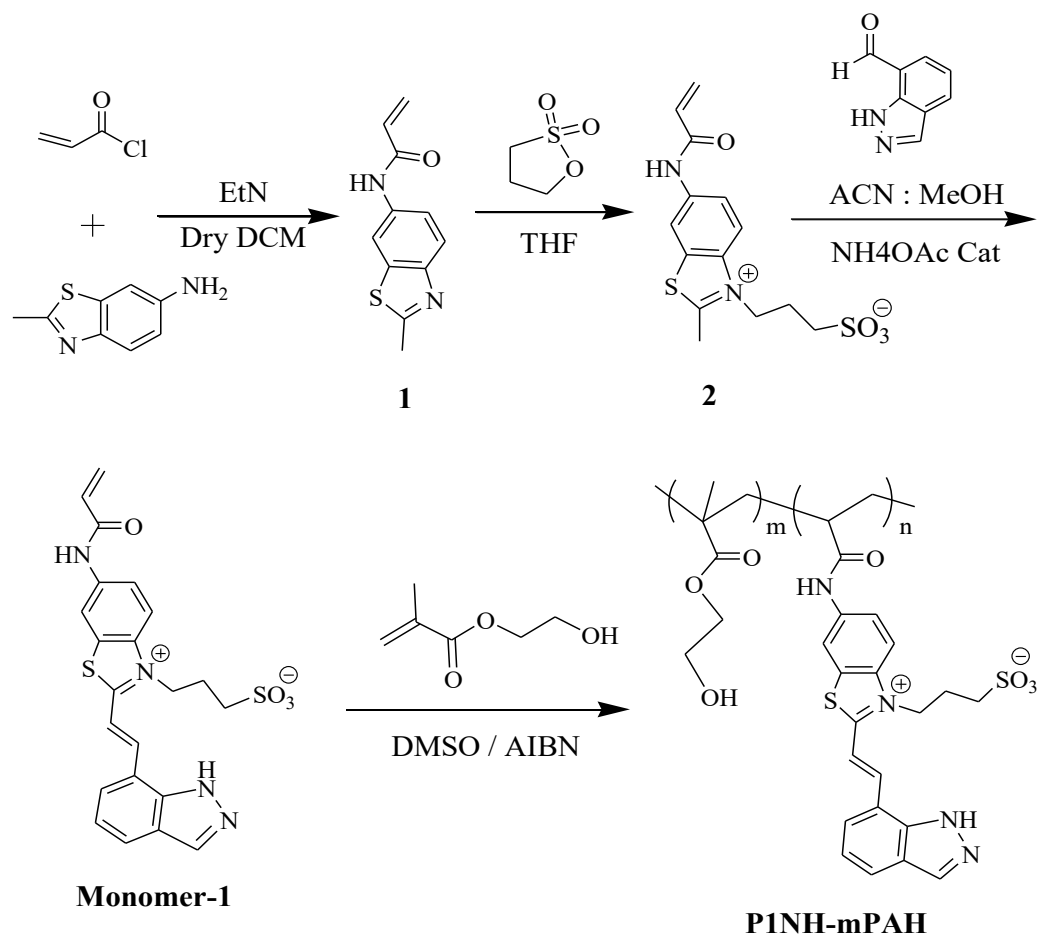
is required for most biomedical applications. In an open system that allows proton exchange, the photo-induced pH drop will be neutralized by the buffer, which will result in a pH pulse. Since mPAH is reversible, another pulse can be generated after the photoacid recovers in the dark. The key is that the pH pulse must be large and long enough to generate a useful effect. In this work, we show that pH pulses of 1.4-1.9 units can be repeatedly generated in a micrometer film of a hydrophilic mPAH polymer in PBS buffer. The pH pulse is strong enough to induce a quick release of a weakly basic molecule from the thin film to the buffer.

2.2. Design and Synthesis of P1NH-mPAH

Our group reported previously that an NH-mPAH released its proton in PBS buffer under visible light but not in the dark.²⁶ (Scheme 1.3). Therefore, the indazole mPAH monomer-1 was synthesized as in scheme 2.1. and then copolymerized with hydroxyethyl methacrylate to yield the first NH-mPAH polymer (P1NH-mPAH) that has hydrophilic properties.

As shown in Scheme 2.1., 6-amino-2-methylbenzothiazole was reacted with acryloyl chloride to yield acrylamide **1**, which was then reacted with propane sultone in THF to yield compound **2**. Compound **2** was coupled with indazole-7-carboxylaldehyde via a Knoevenagel reaction using ammonium acetate as the catalyst, which gave the monomer-**1** as an orange precipitate. P1NH-mPAH was

then synthesized by copolymerizing the monomer-1 (5 wt %) and HEMA via an AIBN initiated radical polymerization. The stable amide linker between the polymer and the NH-mPAH avoids hydrolysis in either basic or acidic conditions. The loading of the NH-mPAH on the polymer was 5 wt %. The detailed synthetic procedures of all compounds are described in chapter 6.



Scheme 2.1. Synthesis of the photoacid monomer-1 and polymer P1NH-mPAH.

A thin film of P1-mPAH was prepared by drop coating a solution of the polymer in methanol on a glass substrate. The film was dried on a heat plate (plate temperature 70 °C) for 15 min and then kept in a ventilation hood overnight. It was soaked in water for 15 min and then in PBS buffer for 30 min. The sample was then put in a quartz cell filled with PBS buffer and studied by UV-Vis spectroscopy. UV-Vis spectrum of the film showed a strong absorption peak at 438 nm. (Figure 2.1.) Upon irradiation with a 470 nm LED from the top of the cell, the 438 nm peak was diminished and absorption near 320 nm substantially increased indicating the formation of the acidic form.²⁶

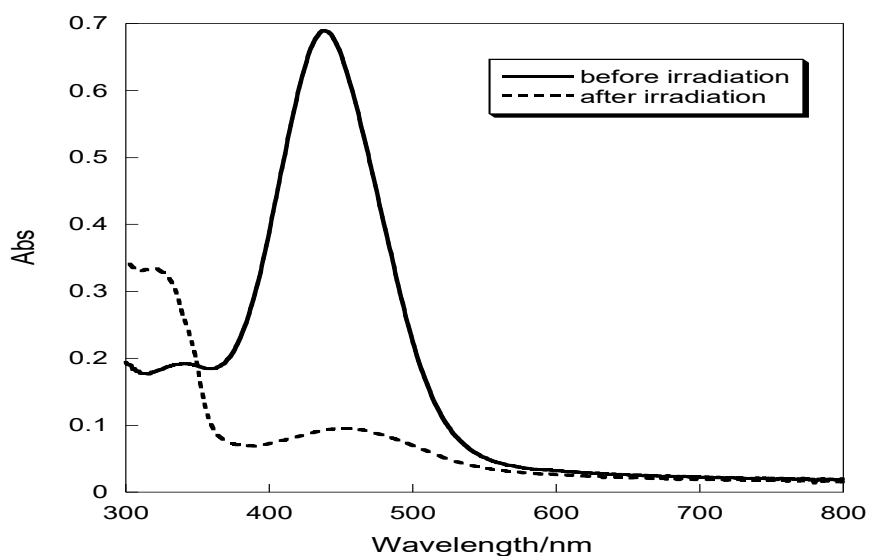
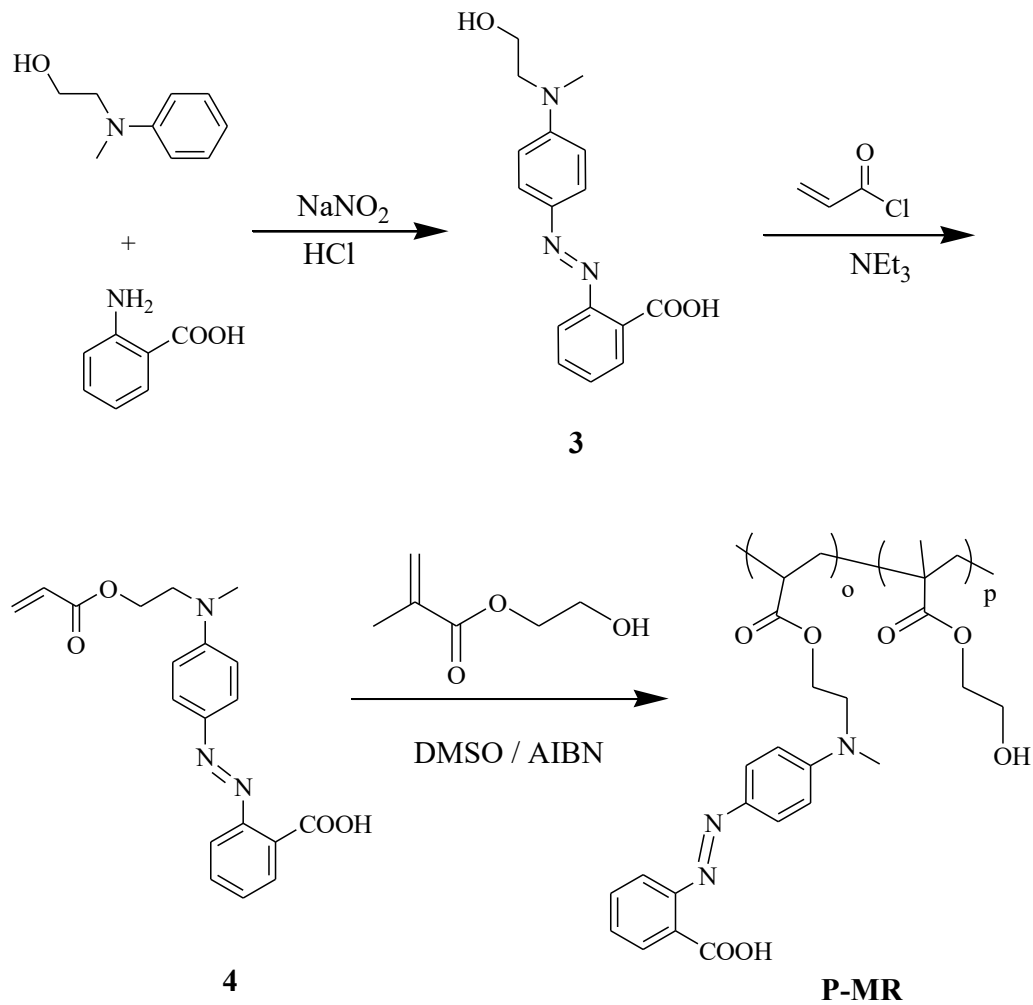


Figure 2.1. UV-vis spectra of a P1NH-mPAH film in PBS before and after irradiation.

2.3. Indicator Selection and Synthesis

Photo-induced pH change will be evaluated by using a common pH indicator as model proton acceptors so that the proton transfer in the NH-mPAH can be monitored by the UV-Vis absorption of the indicator. To demonstrate the photo-induced pH change in P1NH-mPAH, a copolymer of methyl red (MR 5 wt %) and HEMA was synthesized as showing in Scheme 2.2. The synthesis was started by using a diazonium coupling reaction between anthranilic acid and 2-(Nmethylanilino)ethanol to give diazo product **3**. Then acryloyl chloride was added to give acrylic ester diazo derivative, which is MR monomer **4**. The (5 wt %) of the monomer **4** was copolymerizing with HEMA via free radical polymerization to give the methyl red indicator polymer (P-MR). The detailed synthetic procedures of all compounds that were resulted are described in chapter 6.

The MR was chosen as the indicator because it has a pKa of 5.1 and is suitable for measuring pH between 6 and 4. As described below, the photo-induced pH in the P1NH-mPAH film fell in this range. Another reason is that part of the absorption band of the protonated MR (MRH^+) does not overlap with the absorption band of the indazole mPAH.



Scheme 2.2. Synthesis of the indicator polymer P-MR.

To demonstrate that a film of MR polymer (P-MR) was prepared by drop coating in methanol and putting it into quartz cell which is filled with water for UV-vis spectra study. The highest absorption peak was at 420 nm, after protonated by HCl it was shifted to 501 nm as showing in Figure 2.2. A thin film of the MR

polymer (P-MR) in water has a strong absorption band centered at 420 nm. After addition of HCl, the absorption peak of the protonated P-MR shifted to 501 nm. While P1NH-mPAH has no significant absorption above 550 nm, the protonated P-MR substantially absorbs light between 550 and 600 nm, which allows us to observe the protonation of MR by the photoacid. It is worth mentioning that it is necessary to use the polymers instead of molecules of the photoacid and the indicator to avoid leakage during the tests.

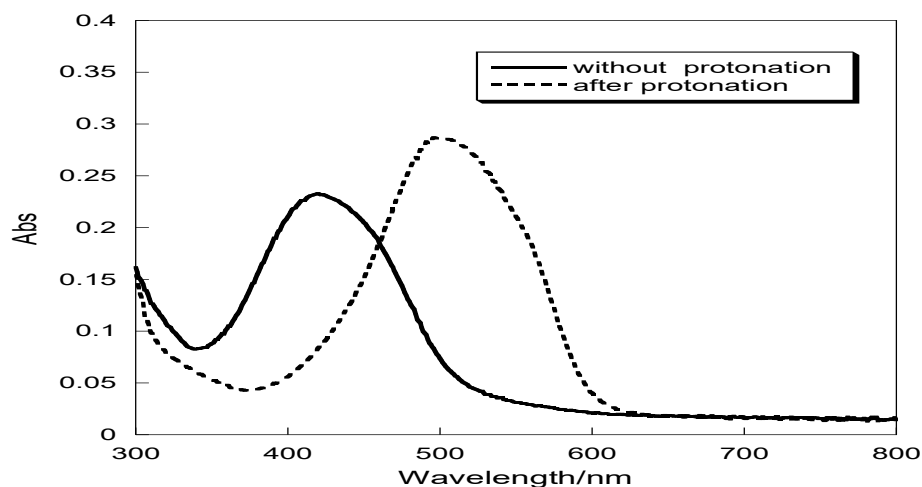


Figure 2.2. UV-vis spectra of a P-MR film in water before after protonation with HCl.

2.4. Results and Discussion

PBS buffer (1X, pH=7.4) was chosen since it is commonly used for biological study. To produce a localized pH change, a high local concentration of mPAH is

required. Therefore, a copolymer of an indazole mPAH and hydroxyethyl methacrylate (HEMA) was synthesized as Scheme 2.1. Poly(hydroxyethyl methacrylate) is a well-known biocompatible hydrophilic polymer. It has been used as a host material for the preparation of mPAH thin films in previous work.²⁵ Although phenolic mPAHs are most commonly used for different applications, they release a significant amount of protons without irradiation in PBS buffer due to relatively high dark acidity.²⁶ Our group reported previously that an NH-mPAH released its proton in PBS buffer under visible light but not in the dark.²⁶ (Scheme 1.3.). Therefore, the indazole monomer-1 was synthesized and then copolymerized with hydroxyethyl methacrylate to yield the first P1NH-mPAH as in scheme 2.1. The loading of the monomer-1 on the polymer was 5 wt %. We found it was difficult to achieve a higher loading using this monomer. When 10 wt % of the monomer-1 was used in the polymerization, the resultant polymer contained less than 5 wt % of the mPAH. It is likely that the bulky photoacid sterically hinders the polymerization since it is close to the reactive acryloyl group. To demonstrate the photoinduced pH change, a copolymer of methyl red (MR 5 wt %) and HEMA was synthesized (Scheme 2.2).

A thin film containing 80 wt % of P1-mPAH and 20 wt % of P-MR was prepared by drop coating a methanol solution of the mixture on a glass slide and dried on a heat plate. The detailed procedure is described in chapter 6. The

thickness of the film was measured to be 8 μm . After soaked in water and then PBS buffer, the sample was put in a quartz cell filled with PBS buffer and studied by UV-Vis spectroscopy. The setup is illustrated in Figure 3. This setup allows us to monitor the change of UV-Vis absorption while the sample is under irradiation. The sample in PBS buffer was irradiated by a 470 nm LED from the top of the cell. The photon flux at the center of the sample was $\sim 425 \mu\text{mol s}^{-1} \text{m}^{-2}$ (11 mW/cm^2) measured by a quantum meter. UV-Vis spectra were recorded every 6s. As shown in Figures 3 and 4, upon irradiation the absorption at 438 nm quickly decreased due to the photoreaction of the NH-mPAH. In the meantime, the absorption between 500 nm and 600 nm increased indicating the formation of MRH^+ .

The absorption of MRH^+ at 550 nm maximized at $\sim 18\text{s}$, and then gradually decreased with time even though the sample was still under irradiation. (Figure 2.4) The absorption at 438 nm kept decreasing after 18 s until the irradiation was stopped at 72s. The results show that the proton concentration in the thin film increased upon irradiation and reached its maximum at $\sim 18\text{s}$, after which the proton concentration decreased although more acids were generated from NH-mPAHs.

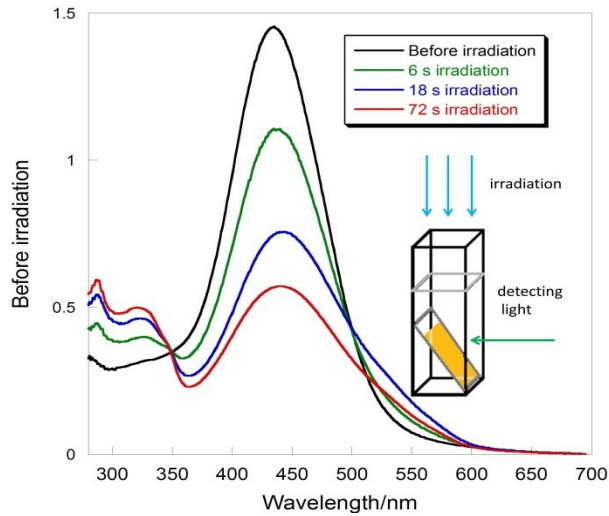


Figure 2.3. UV-vis spectra of a film of P-mPAH and P-MR in PBS buffer before irradiation 6, 18, and 72s under irradiation. Experimental setup for monitoring the absorption change during the irradiation (insert).

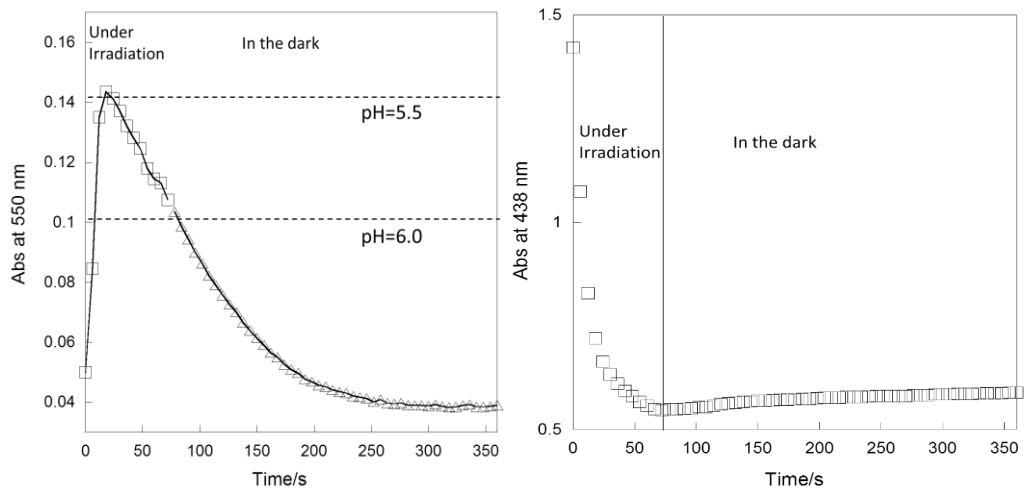


Figure 2.4. Absorption of the P1NH-mPAH/P-MR film at 550 nm (left) and 438 nm (right) during and after irradiation.

Upon irradiation, the NH-mPAHs were quickly converted to their acidic state and released protons. The released protons acidified the film and protonated MR. In the meantime, the H^+/OH^- exchange between the film and PBS buffer basified the film. In the first 18s, the acidification is faster than basification, which resulted in increase of MRH^+ . After 18s, the basification was faster than acidification even though more acids were generated from the NH-mPAHs. This is likely due to two reasons. The rate of acid generation decreased with time due to decreased amount of the mPAHs. In addition, when the protons were transferred from the photoacids to MR or PBS, the photoacids became anions and formed salts with MRH^+ or the cations from PBS, which increased the hydrophilicity of the film and consequently accelerated the H^+/OH^- exchange. The two factors led to the decrease of MRH^+ in the film after 18s. On the basis of the absorbance change at 438 nm (Figure 2.4), we estimated that $\sim 3 \times 10^{-2}$ M of NH-mPAHs had changed to the acidic form and released their protons in the $\sim 8 \mu\text{m}$ film during the first 18 s. As described below, the pH in the film was ~ 5.5 at 18 s. The proton concentration was $\sim 3 \times 10^{-6}$ M, which was 4 orders of magnitude lower than the concentration of the acidic form of the NH-mPAH. This indicates that most of the protons were quickly neutralized by the buffer soaked in the film before irradiation and diffused into the film during irradiation

Since the NH-mPAH is reversible, the pH pulse can be reproduced after the NH-mPAH recovers in the dark. To test this, the sample was kept in the dark for 8 h in PBS buffer. The absorption at 438 nm grew back from 0.546 to 1.223 confirming the recovery of most of the photoacid. (Figure 2.5) The sample was then irradiated for a minute. The maximum absorption at 550 nm (MRH⁺ absorption) during the irradiation was 0.112, which was lower than that of the first irradiation (0.143). The absorption at 438 nm decreased to 0.529 after irradiation. The sample was kept in the dark again for 8 h. The absorption at 438 nm went back to 1.152 and the absorption at 550 nm was 0.035, which is close to the value after the first irradiation (0.036). The sample was then irradiated for the third time. The maximum absorption observed at 550 nm was 0.108 and absorption at 438 nm went down to 0.535 after irradiation. To finish the third cycle, the sample was kept in the dark for 8 h. The absorption at 438 nm went back to 1.100 and the absorption at 550 nm was 0.035. The results of the second and the third irradiation were very close showing the reversibility of the system. It is also worth mentioning that the maximum absorption at 550 nm was observed at the third (18 s) or fourth scan (24 s) during the irradiation in all three tests. (As shown in Figure 4, the absorption values at the third and the fourth are very close.)

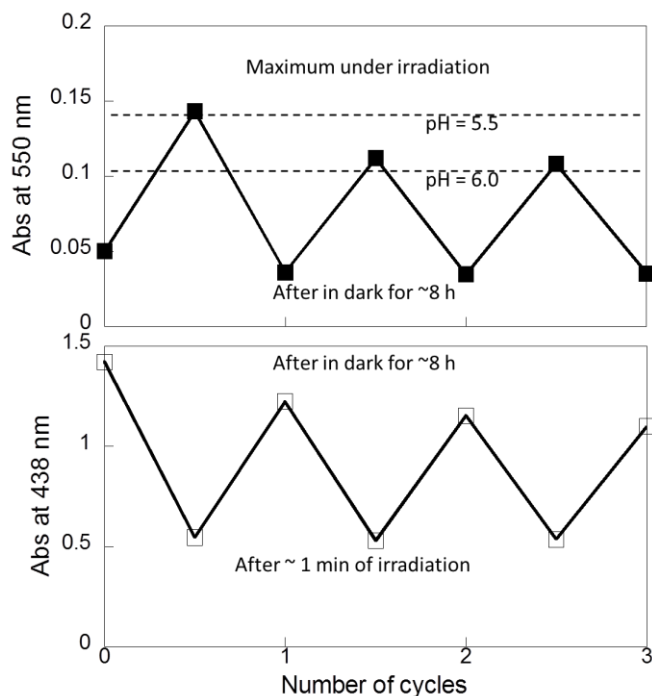


Figure 2.5. Changes in the absorption of the P1NH-mPAH/P-MR film at 550 nm (up) and 438 nm (down) during the irradiation and recovery cycles.

To quantify the pH change induced by irradiation, the very same sample that was tested in the above experiments was immersed in a pH 6 buffer and kept in the dark for 15 min. The absorption at 550 nm increased from 0.035 to 0.104, which is close and slightly lower than the maximum absorption at 550 nm observed during the second and third irradiation and is significantly lower than that of the first irradiation. The pH 6 buffer was then replaced by a pH 5.5 buffer. The 550 nm absorption reached 0.143, which is about the same as the maximum absorption during the first irradiation. These results show that the first irradiation produced a

pH pulse with a magnitude of ~ 1.9 units and a minimum pH at 5.5, and the following irradiations produced smaller but consistent pH pulses of ~ 1.4 unit with a minimum at ~ 6.0 .

2.5. Conclusion

In this work, photo-induced pH change in an NH-mPAH polymer film in PBS has been demonstrated. The hydrophilic polymer film is an open system that allows exchange of protons and small molecules. A quick release of the protons from the NHmPAH and proton exchange between the PBS buffer and the film resulted in a pH pulse. The magnitude of the pulse is 1.4 to 1.9 units with maximum pH change occurred after 18s of the irradiations. Since the NHmPAH is a reversible photoacid, the pH pulse can be repeatedly generated after the photoacid recovered in the dark. This work shows that photo-induced pH change based on NH-mPAH can be applied to biological systems even though their pH is maintained by pH buffers.

2.6. References

1. Tolbert, L.; Solntsev, K. M. Excited-state proton transfer: from constrained systems to “super” photoacids to superfast proton transfer. *Acc. Chem. Res.* , **2002**, *35*, 19-27.
2. Chou, P.-T.; Solntsev, K. M. J Photoinduced Proton Transfer in Chemistry and Biology. *Phys. Chem. B.* **2015**, *119*, 2089.
3. Liao, Y. Design and applications of metastable-state photoacids. *Acc. Chem Res.* ,**2017**, *50*, 1956-1964.
4. Shi, Z.; Peng, P.; Strohecker, D. and Liao, Y. Long-Lived Photoacid Based upon a Photochromic Reaction. *J. Am. Chem. Soc.* **2011**, *133*, 14699–14703.
5. Xu, Y.; Fei, J.; Li, G.; Yuan, T.; Li, Y.; Wang, C.; Li, X.; Li, J. Enhanced Photophosphorylation of a Chloroplast-Entrapping Long-Lived Photoacid. *Angew. Chem. Int. Ed. Engl.* **2017**, *56*, 12903-12907.
6. Go, D.; Rommel, D.; Liao, Y.; Haraszti, T.; Sprakel, J.; Kuehne, A. J. C. Dissipative disassembly of colloidal microgel crystals driven by a coupled cyclic reaction network. *Soft Matt.* **2018**, *14*, 910-915.

7. Bao, H.; Li, F.; Lei, L.; Yang, B.; Li, Z. ON/OFF states of a microbial fuel cell controlled by an optical switching system. *RSC Adv.* **2014**, *4*, 27277-27280.
8. Johns, V. K.; Patel, P. K.; Hassett, S.; Calvo-Marzal, P.; Qin, Y.; Chumbimuni-Torres, K. Y. Visible light activated ion sensing using a photoacid polymer for calcium detection. *Anal. Chem.* **2014**, *86*, 6184-6187.
9. Patel, P. K.; Chumbimuni-Torres, K. Y. Visible light-induced ion-selective optodes based on a metastable photoacid for cation detection. *Analyst*, **2016**, *141*, 85-89.
10. Fu, C.; Xu, J.; Boyer, C. Photoacid-mediated ring opening polymerization driven by visible light. *Chem. Commun.* **2016**, *52*, 7126-7129.
11. Maity, C.; Hendriksen, W. E.; van Esch, J. H.; Eelkema, R. Spatial structuring of a supramolecular hydrogel by using a visible - light triggered catalyst. *Angew. Chem. Int. Ed.* **2015**, *54*, 998-1001.
12. Kundu, P. K.; Samanta, D.; Leizrowice, R.; Margulis, B.; Zhao, H.; Borner, M.; Udayabhaskararao, T.; Manna, D.; Klajn, R. Light-Controlled Self-Assembly of Non-Photoresponsive Nanoparticles. *Nature Chem.*, **2015**, *7*, 646-652.

13. Zhang, T.; Sheng, L.; Liu, J.; Ju, L.; Li, J.; Du, Z.; Zhang, W.; Li, M.; Zhang, X-A. Photoinduced Proton Transfer between Photoacid and pH Sensitive Dyes: Influence Factors and Application for Visible-Light Responsive Rewritable Paper. *Adv. Funct. Mater.* **2018**, 1705532.
14. Wang, Z.; Liao, Y. Reversible dissolution/formation of polymer nanoparticles controlled by visible light. *Nanoscale*, **2016**, 8, 14070-14073.
15. Guo, J.; Zhang, H.-Y.; Zhou, Y.; Liu, Y. Light-controlled reversible self-assembly of nanorod suprastructures. *Chem. Commun.*, **2017**, 53, 6089-6092.
16. Shi, Q.; Meng Z.; Xiang J.-F.; Chen, C.-F. Efficient control of movement in non-photoresponsive molecular machines by a photo-induced proton-transfer strategy. *Chem. Commun.*, **2018**, 54, 3536-3539.
17. Yang, L.-P.; Jia, F.; Cui, J.-S.; Lu, S.-B.; Jiang, W. Light-controlled switching of a non-photoresponsive molecular shuttle. *Org. Lett.*, **2017**, 19, 2945-2948.
18. Tatum, L. A.; Foy, J. T.; Aprahamian, I. Waste management of chemically activated switches: Using a photoacid to eliminate accumulation of side products. *J. Am. Chem. Soc.*, **2014**, 136, 17438-17441.
19. Chen, H.; Liao, Y. J. Photochromism based on reversible proton transfer. *Photochem. Photobio., A*, **2015**, 300, 22-26.

20. Mahvidi, S.; Takeuchi, S.; Kusumoto, S.; Sato, H.; Nakagawa, T.; Yokoyama, Y. Gated photochromic system of diarylethene with a photon-working key. *Org. Lett.*, **2016**, *18*, 5042-5045.
21. Samanta, D.; Galaktionova, D.; Gemen, J.; Shimon, L.; Kral Petr; Diskin-Posner Y.; Avram, L.; Kral, P.; Klajn, R. Reversible chromism of spiropyran in the cavity of a flexible coordination cage. *Nature Commun.*, **2018**, *9*, 641.
22. Wang, Z.; Johns, V. K.; Liao, Y. *Chem. Eur. J.* **2014**, *20*, 14637-14640.
23. Shafaat, O. S; Winkler, J. R; Gray, H. B; Dougherty, D. A. Photoactivation of an Acid-Sensitive Ion Channel Associated with Vision and Pain. *Chembiochem*, **2016**, *17*, 1323-1327.
24. Luo, Y.; Wang, C.; Peng, P.; Hossain, M.; Jiang, T.; Fu, W.; Liao, Y., Su, M. Visible light mediated killing of multidrug-resistant bacteria using photoacids. *J. Mater. Chem. B*, **2013**, *1*, 997-1001.
25. Yang, C.; Khalila, T., Liao, Y. Photocontrolled proton transfer in solution and polymers using a novel photoacid with strong C–H acidity. *RSC Adv.* **2016**, *6*, 85420-85426.
26. Abeyrathna, N.; Liao, Y. A reversible photoacid functioning in PBS buffer under visible light. *J. Am. Chem. Soc.*, **2015**, *137*, 11282-11284.

Chapter 3

Synthesis of NH-mPAH Polymers Using Free Radical Polymerization

3.1. Introduction

The synthesis of polymeric mPAHs with high loading is our goal for controlling the pH change. The low loading of NH-mPAH was demonstrated in chapter 2 and successfully reported. The hydrophilic polymer film of NH-mPAH1 was synthesized with 5 wt % loadings and produced a localized proton concentration under irradiation with a measurable pH change in the PBS buffer. Free-radical polymerization (FRP) of vinyl monomers is one of the successful methods used to obtain mPAH polymers. Worthy to note, other techniques such as anionic and cationic polymerizations would not be useful with such photoacid molecules since the structure possesses positively and negatively charged moieties, which could lead to side reactions.^{1,2}

Designing a polymer of mPAH monomers with good compatibility with media like water is challenging due to the solubility limitations and the bulky structure of mPAH units². The major issue of compatibility can be modified by changing the backbone or side chains of the polymer. Three different approaches for synthesizing high loading mPAH polymers by using free radical polymerization

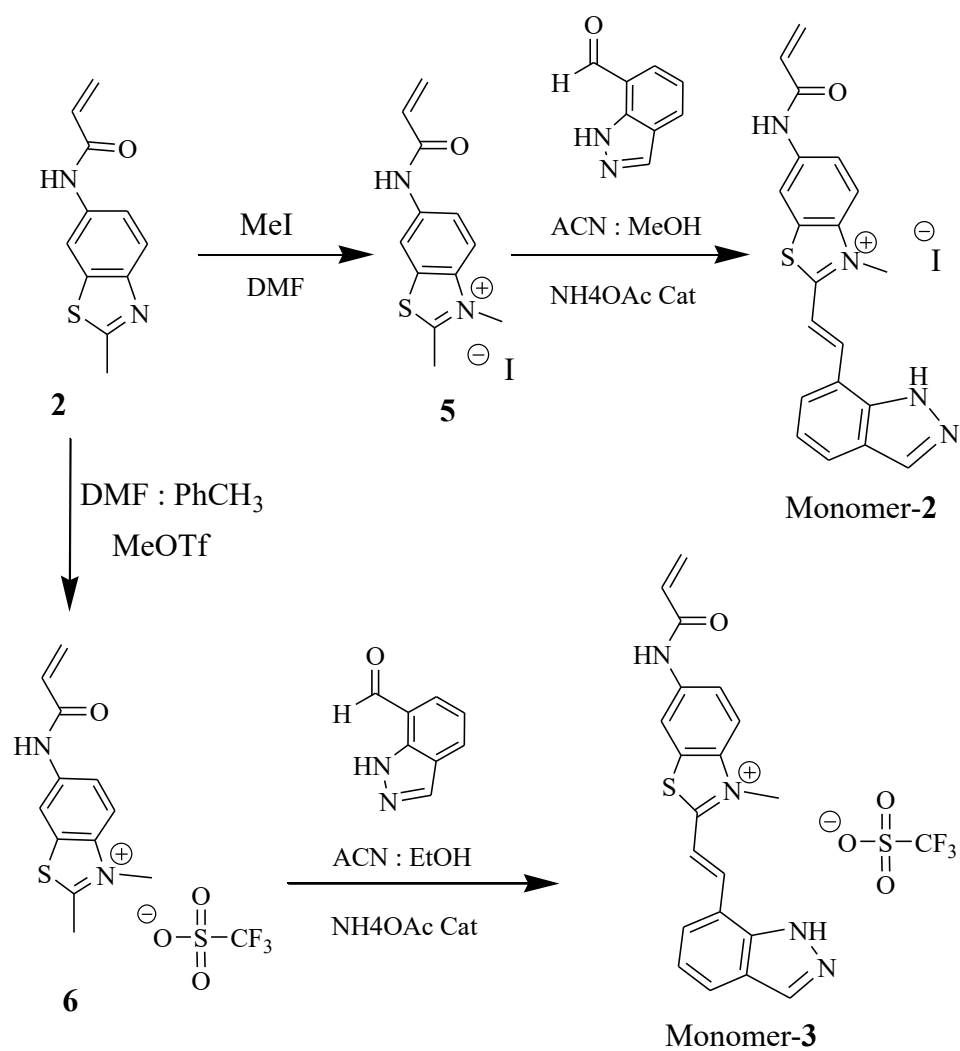
were studied in this chapter: homopolymerization, copolymerization, and post-functionalization. We also investigated how to synthesize oligomer (trimer) of NH-mPAH by using a central benzene core as a start material. Taking a step toward the challenge, we designed a new NH-mPAH-**2** and -**3**, expecting the monomers would be polymerized easily by free radical polymerization to form positively charged polymers. Furthermore, we expected that these polymers would have had great solubility in water and could have been neutralized after irradiation.

3.2. Design and Synthesis of Indazole NH-mPAH

Monomers-2 and -3

Two indazole acrylic amide-photoacid monomers were synthesized (scheme 3.1). The procedure started by esterification between 6-amino-2-methylbenzothiazole and acryloyl chloride to result in acrylamide benzothiazole, **2**. Then iodomethane was added to the solution of **2** in DMF to yield **5**. In the last step, indazole-7-carboxylaldehyde was coupled to **5** in presence of ammonium acetate as the catalyst to result in the monomer-**2** (NH-mPAH₂). In order to increase the solubility of the monomer-**2** in different solvents, a second monomer was synthesized by adding methyl triflate (MeOTf) to **2**. The methyl triflate was added to a solution of **2** to give methyl triflate acrylamide benzothiazolium, **6**. Then, indazole-7-carboxylaldehyde was coupled to yield the monomer-**3** (NH-mPAH₃). The detailed procedure is given in chapter 6. Both monomers were designed with

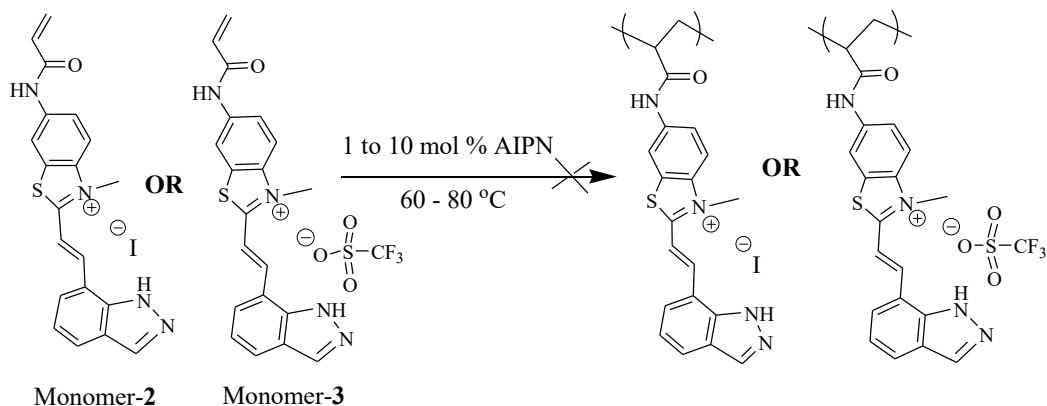
an amide group between the NH-mPAH and the polymerizable vinyl group to give the stability of photoacids and to avoid proton release without irradiation and any hydrolysis problems.



Scheme 3.1. Synthetic route for NH-PAH monomers-2 and -3.

3.3. Homopolymerization of Photoacid Monomers 2 and 3

In order to synthesize a large molecule composed of identical repeating photoacid monomer-2 or -3, a free-radical polymerization was applied in the present azoisobutylnitrile (AIBN) as an initiator. The polymerization was carried out in several attempts under a degassed atmosphere and in a concentrated solution of the monomers using different solvents such as DMSO, DMF, and HFIP. Unfortunately, no one attempt resulted in any polymerization in the polymerizable acrylic group even though the polymerization was promoted up to 10 mol % AIBN to form a low molecular weight molecule. The major problem with this method was that the NH in the indazole moiety could have worked as a radical quencher and led to the termination of the radical polymerization. Another problem was the proximity of the bulky function group in the mPAH and the reactive acrylic amide group in the monomers during steric interactions.



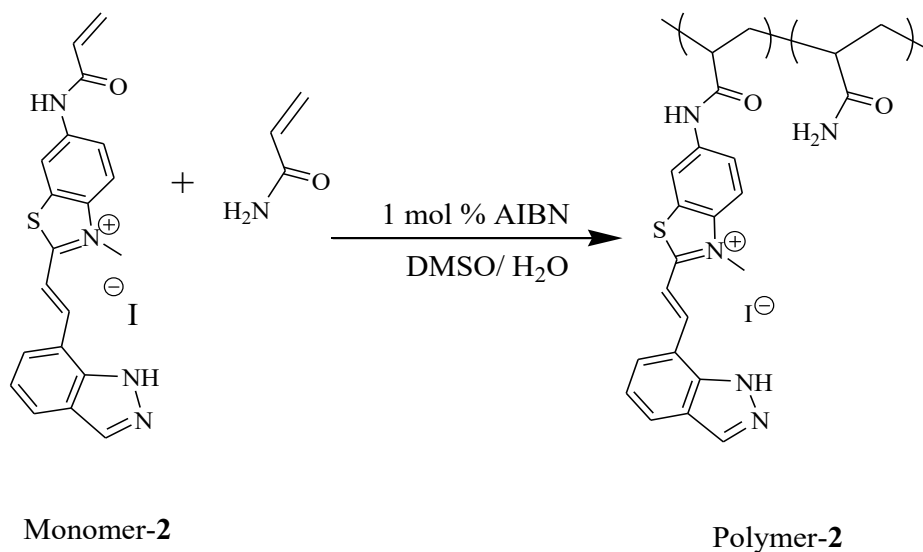
Scheme 3.2. Attempted homopolymerization of Monomers-2 and -3.

3.4. Copolymerization of NH-mPAH1

Covalently linking mPAHs is preferred to copolymerizing with other flexible materials such as methacrylate derivatives. These classes of materials known as polymer hosts are the most preferable host materials. The hosts have diverse solubility characteristics and are easy to be polymerized with many bulky functional groups. Also, they have high thermostability and transparency that help create a material film that can be utilized in different media.⁴⁻⁵ For example, since hydroxyethyl methacrylate (HEMA) is soluble in water, we used a biocompatible hydrophilic polymer copolymerized with the monomer-2 (Chapter 2). In this section, we studied acrylic amide, which is one of the water-soluble polymers for pharmaceutical applications.⁶ This copolymerization technique resulted in a light-responsive film with high loading of the NH-mPAH-2.

The photoacid polymer-2 was synthesized by copolymerizing monomer-2 (1 eq) and HEMA (39 eq) via AIBN initiated radical polymerization (Scheme 3.3). A mixture was prepared in the DMSO and polymerized at 70 °C overnight. The polymer was precipitated in diethyl ether, collected by filtration, and dried in air to yield a dark white solid. A more detailed synthesis procedure is given in Chapter 6. The percentage was difficult to calculate from the corresponding ¹H-NMR due to problems with integrating the weak, broad peaks and the aromatic mPAH monomer

overlapping the NH₂ monomer in the acrylamide. We calculated an average loading of the NH-mPAH₂ of about 2 mol %, which was lower than expected.



Scheme 3.3. Synthesis of photoacid polymer-2 (P1NH-mPAH).

We found to achieve a higher loading using this monomer was difficult even when we applied with more molar equivalents of the monomer-2. The problem was likely due to the same issues described in Chapter 2: the bulky photoacid sterically hindered the polymerization. To study the problem, we planned to use post-polymerization of mPAH photoacid, which is explained in the next section.

3.5. Post-functionalization of Photoacid

Post-functionalization is another approach of copolymerization that was applied. In this method, we studied how NH-photoacids can be grafted covalently

on a prepared copolymer. The technique is simple and efficient in attaching new desirable bulk functionalities covalently to flexible chain that was copolymerized.

In this method, the photoacid polymer was synthesized in two steps. First, acrylamide dimethyl-bezothiazolium, **5** (1eq) was copolymerized with isopropyl acrylamide (4 eq) via AIBN free radical polymerization at 60 °C in dry DMSO. The next day, the polymer was precipitated in diethyl ether and collected by filtration. The mole percentage were calculated from corresponding ¹H-NMR spectra (Figure 3.1) of the purified polymer by comparing the peak of CH (b) at 4.125 ppm to that of CH (d) at 3.786 ppm and the equivalents were ~ (1:4). The result showed us the major problem in previous experiments is not the steric interactions between bulky photoacid and reactive acrylic amide group but was more likely that the NH-indazole moiety of photoacid could be a radical quencher for the polymerization.

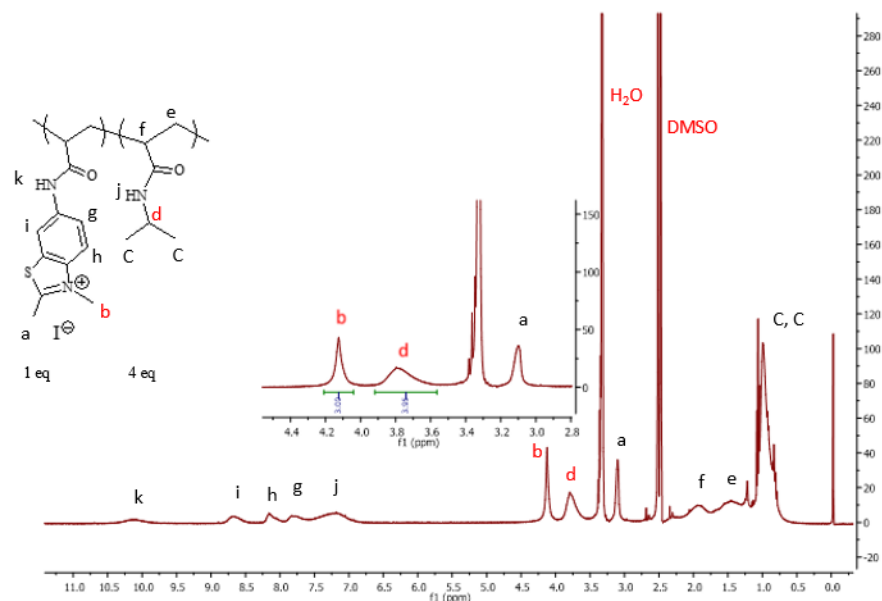
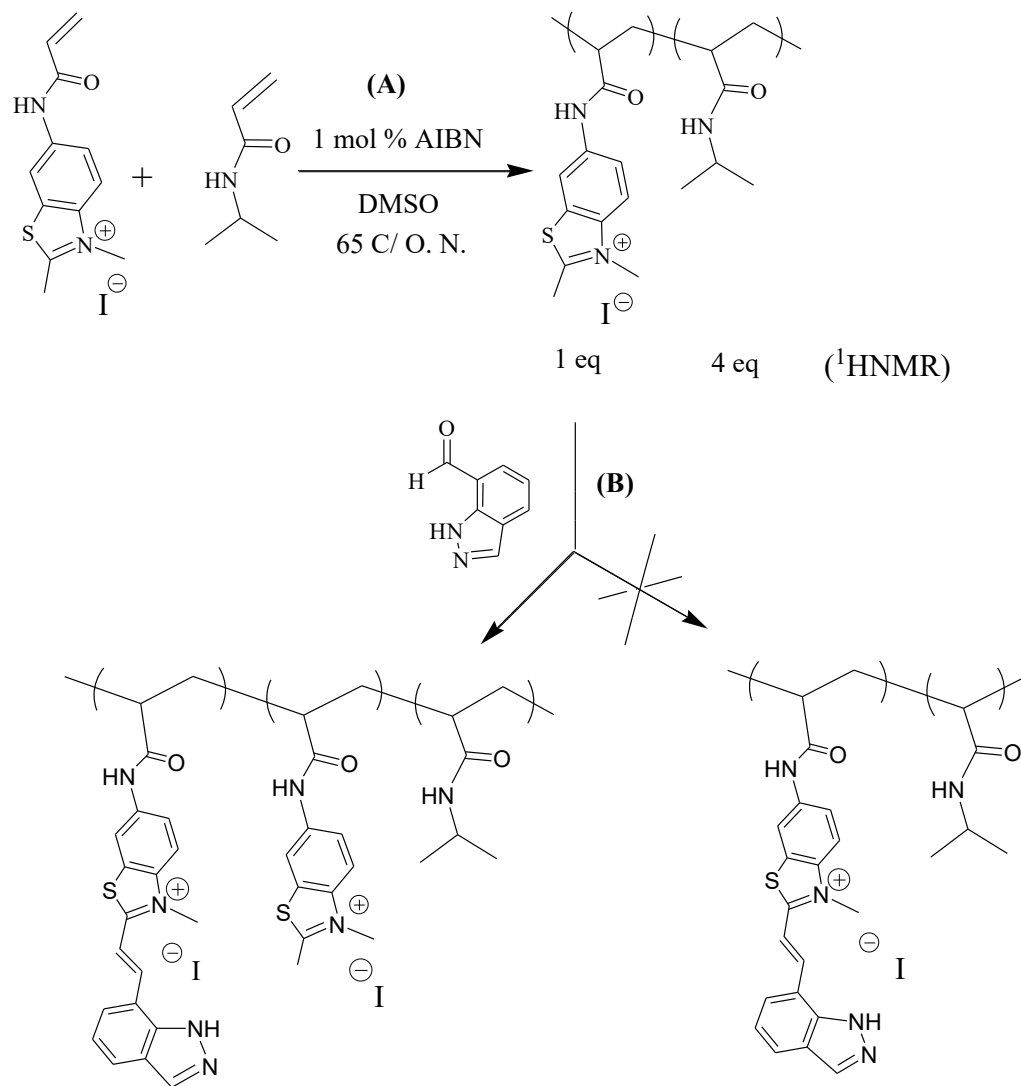


Figure 3.1. ^1H -NMR spectra of bezothiazolium copolymer in DMSO.

Second, Through Knoevenagel condensation, the indazole-7-carboxylaldehyde was coupled with benzothiazolium-units of the copolymer in order to form the corresponding photoacid polymer (Scheme 3.4). The reaction was carried out in different solvents that are suitable for the condensation reaction such as EtOH, DMSO, and H₂O; EtOH, as well as different catalysts, were used, such as NH₄OAc 20 mol%, proline 10 mol %, and piperidine 10 mol %. After the resulting polymer was purified, we confirmed the copolymerization from corresponding ^1H NMR spectra in d₆-DMSO (Figure 3.2).



Scheme 3.4. (A) Free-radical copolymerization of benzothiazolium monomer and Isopropyl acrylamide. (B) Post-functionalization of the phenothiazinium-units to form photoacid polymer.

We cannot see a clear baseline of peaks because of the extensive broadening and overlapping peaks. But we can see that only ~ 1 equivalent of NH-mPAH was

coupled by comparing the peaks c of CH₃ at 4.387 ppm for photoacid unit, d of CH₃ at 3.818 ppm for unreacted benzothiazolium unit, and d of CH at 3.112 ppm for host polymer used (Figure 3.4).

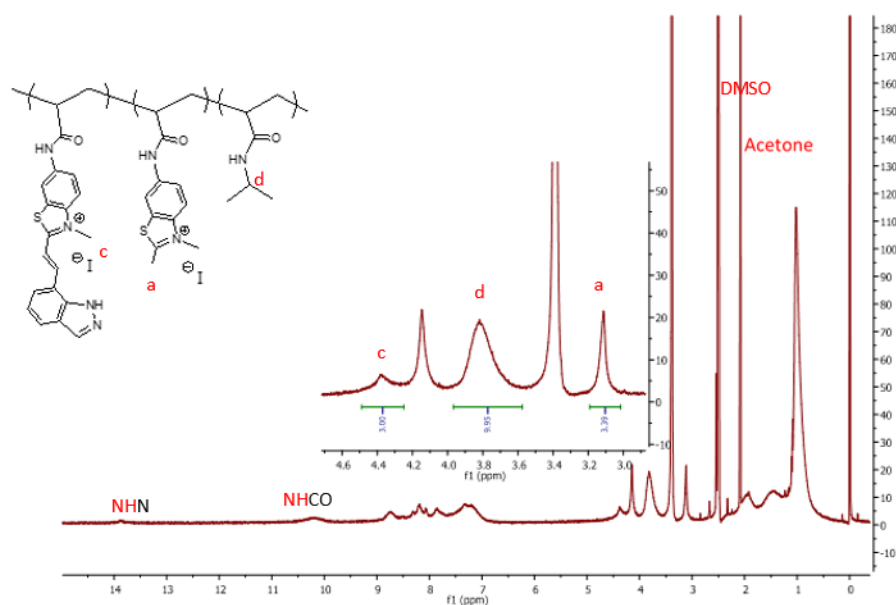


Figure 3.2. ¹H-NMR spectra of post-functionalization reaction in d₆-DMSO.

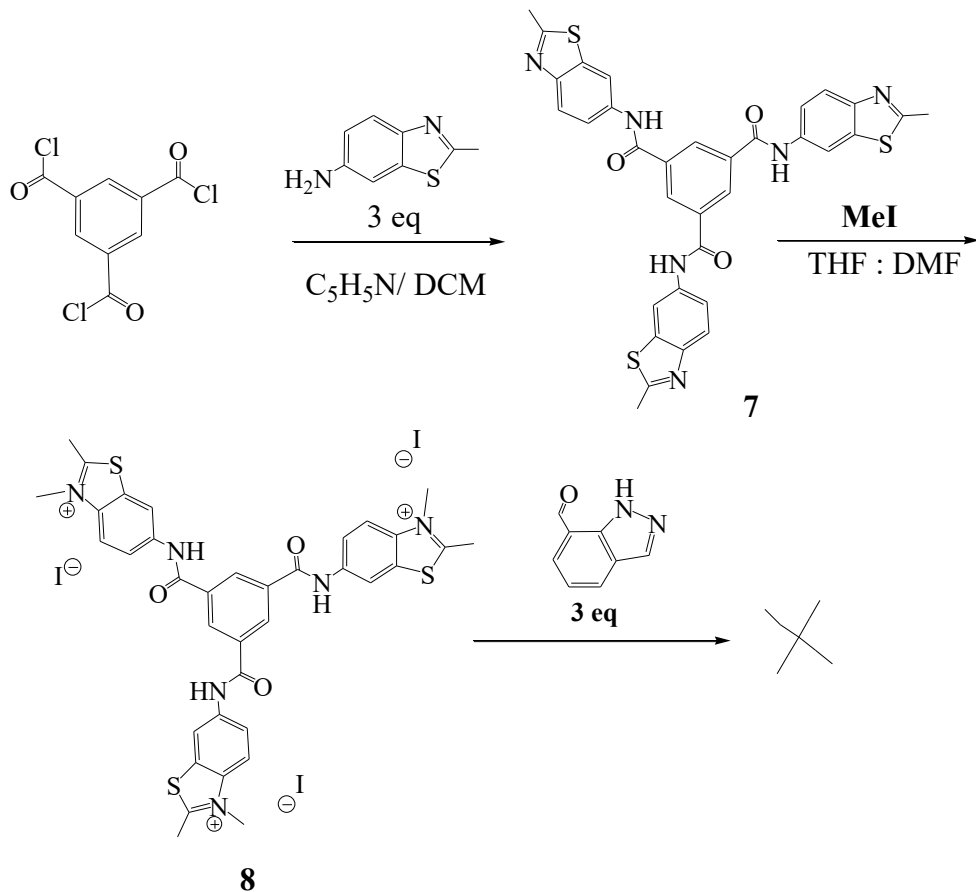
We found that only 1 equivalent of NH photoacid unit could be condensed through Knoevenagel reaction (8 mol %) and this is the best loading factor that we have reached with the post-functionalization reaction after refluxing the mixture overnight in H₂O:EtOH, 3:1. Unfortunately, we kept the mixture refluxing for two days to attain a higher loading and yield, but we found that the loading of the condensation reaction decreased. More likely, hydrolysis took place on the double bond between the two moieties and stopped the reaction.

3.6. Oligomer Metastable State Photoacid

The lack of success in the high loading of the mPAH monomers by free radical polymerization led us to think about the design of oligomeric mPAH, which is a type of polymer that has low molecular weight. The trimer was chosen as a simple model of the mPAHs oligomer. We designed a star polymer shape of photoacid that had a central benzene core. The benzene was chosen due to the stability of chemical modification.

3.6.1. Trimer Carboxamide-Bezothiazolium Iodide

Three equivalents of 6-amino-2-methylbenzothiazole were reacted with three acryloyl chloride groups attached to the central benzene core to yield the corresponding carboxamide product **7**, which was then dissolved in PhCH₃:DMF, 2:1, and refluxed with MeI to give compound **8** (Scheme 3.6). Unsuccessful attempts were made to finish the last step, which was aldehyde condensation via the Knoevenagel reaction to synthesize the trimer mPAH. The solubility of **8** in the concentrated solution was not achieved with suitable solvents such as EtOH or MeOH. Of importance, the linkage of the three stable carboxamides between the photoacid and the benzene core gave rigidity to the structure of the carboxamide-bezothiazolium iodide **8**, which became poorly soluble even in DMSO, which was the best solvent for many insoluble compounds.



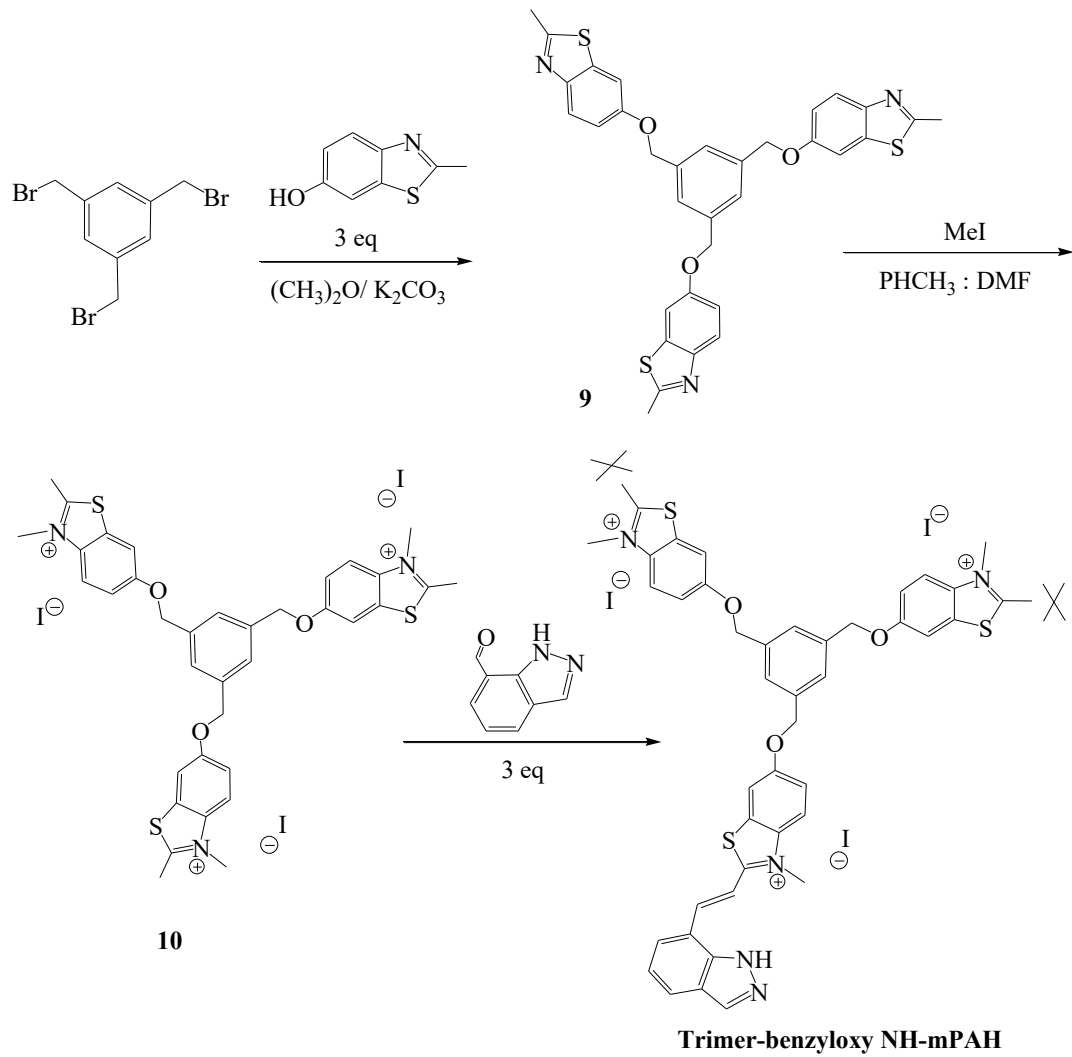
Scheme 3.5 Synthetic Route for the Compound 7 and 8.

3.6.2. Trimer-Benzoyloxy Thiazolium Iodide

The difficulty associated with low-solubility of trimer carboxamide-benzothiazolium led us to explore an alternative synthetic route of accessing trimer photoacid polymers with higher flexibility features. The linkage between the photoacid and the central benzene core was redesigned to be a benzyloxy bond instead of carboxamide, which may lead to better solubility in different solvents.

The proposed synthetic route started by reacting three equivalents of hydroxy-benzothiazole and 1,3,5-tris(bromomethyl)benzene to yield **9**, which was then dissolved in PhCH₃:DMF, 3:1, and refluxed overnight with methyl iodide to give try-(benzyloxy-thiazolium methyl iodide) benzene **10** (Scheme 3.6). The detailed procedure of synthesizing compounds **9** and **10** are given in chapter 6, but the last step, which was the Knoevenagel condensation reaction between the salt **10** and indazole-7-carbaldehyde, was unsuccessful despite using a more polar solvent such as DMSO or DMSO:EtOH, presumably due to the solubility issues of compound **10**.

We attempted the condensation reaction many times in a variety of solvent mixtures in a sealed tube. In one such attempt, we observed that only one unit of the trimer could be coupled with the aldehyde. The reaction was carried out by dissolving the trimer benzyloxy-thiazolium **10** (0.06 g, 0.57 mmol) in EtOH:H₂O, 1:3 mL. Then, 1H-indazole-7-carbaldehyde (0.28g, 0.18 mmol) and a catalytic amount of ammonium acetate were added to the reaction mixture, refluxed for two days, and then cooled to room temperature. The orange precipitate was filtered, washed with acetone, and left out to dry slowly in the open air.



Scheme 3. 6. Synthetic route of the trimer-benzyloxy NH-mPAH.

^1H NMR spectroscopy showed that the aldehyde condensation was coupled only with one unit of trimer-benzyloxy thiazolium to form trimer-benzyloxy thiazolium-NH-mPAH. We found shifting peaks and splitting in the ^1H -NMR spectra in the $\text{d}_6\text{-DMSO}$ and determined indazole-7-carbaldehyde and two units of the trimer benzyloxy-thiazolium unreacted peaks(Figure 3.5).

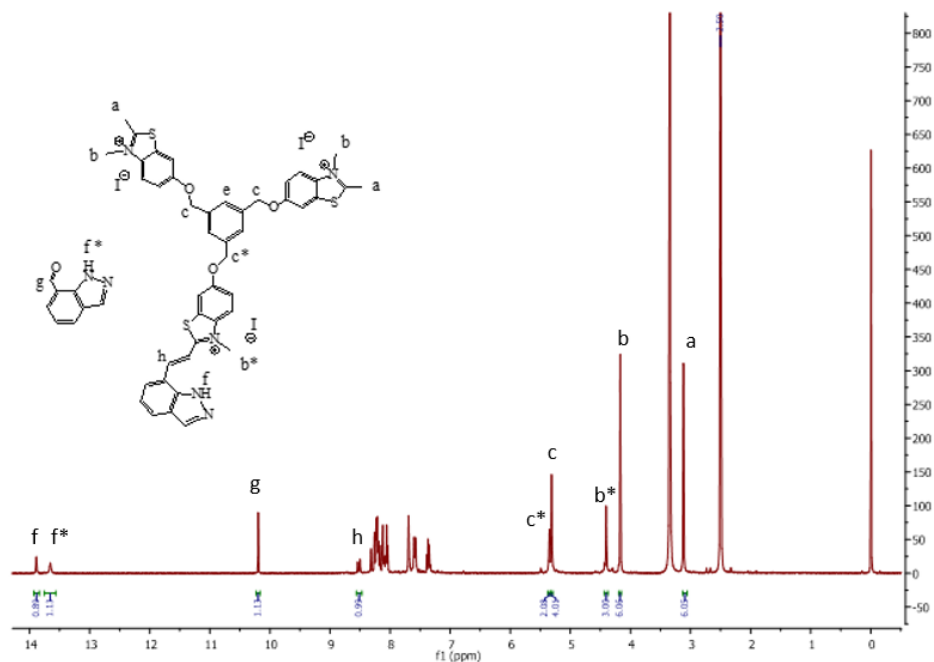


Figure 3.3. ^1H NMR overlay of trimer-benzyloxy thiazolium-NH-mPAH and indazole-7-carbaldehyde in $\text{d}_6\text{-DMSO}$.

We found that only one aldehyde could be condensed, and we could not go further to synthesize the trimer since the precipitate took place once one unit of three was coupled to aldehyde and precipitated to afford trimer-benzyloxy thiazolium-NH-mPAH. The resulting compound, considered a photoacid product in synthesizing oligomeric NH-mPAHs, can be useful in a specific application with one unit of NH-mPAH. However, increasing the solubility of tri-benzyloxy-thiazolium salt would result in an oligomer photoacid. Using methyl triflate instead of methyl iodide is one of the modifications that can be considered toward increasing solubility and synthesizing the oligomer photoacid.

The unsuccessful free radical polymerization attempts of monomer-**2** and -**3** towards high loading NH-photoacid and the difficulties associated with trimer solubility led us to explore alternative avenues such as norbornene monomers, which will be described in the next chapter.

3.7. References

1. Moad, G.; Rizzardo, E.; Thang, E. Toward Living Radical Polymerization, S. Acc Chem Res, **2008**, *41*,1133-1142.
2. Elgattar A.; Abeyrathna, N. and Liao, Y. Localized pH Pulses in PBS Buffer Repeatedly Induced by Visible Light, *J. Phys. Chem. B*, **2019**, *3*: 648-654.
3. Khalil, T.; Alharbi, A.; Baum, C.; Liao, Y. Facile Synthesis and Photoactivity of Merocyanine-Photoacid Polymers. *Macromolecular rapid Communications* **2018**, *15*, 1800319.
4. Montheard, M; Chatzopoulos, D. and Chappard, D. 2-Hydroxyethyl Methacrylate (HEMA): Chemical Properties and Applications in Biomedical Fields. *J. Macro. Sci.*, **1992**, *32*, 1-34.
5. Shekh, M. I.; Patel, D. M.; Patel, N. N.; Patel, U. S.; Patel, K. P; Patel, R. M. Methacrylate Copolymers and Their Composites with nano-CdS: Synthesis, Characterization, Thermal Behavior, and Antimicrobial Properties. *Int. J. Ind. Chem.*, **2018**, *9*, 153-166.

Chapter 4

ROMP of Norbornenes Containing mPAHs

4.1. Introduction

Materials covalently carrying indazole mPAH are still insufficient since the high-loading of a large local proton concentration was not achieved by free radical polymerization (Chapters 2 and 3). In most applications that have been reported, solutions of the mPAHs were used, and some of the applications displayed a low percentage of grafting or linking of the mPAHs to other host materials. While some suggest that using classic methods of polymerization via free-radical polymerization is viable for producing polymeric materials of mPAH, the inability to obtain reliable, consistent high-loading of mPAH and the difficulties associated with the solubility of acrylic amide monomers led us to focus specifically on norbornene (NB) monomers for metathesis polymerization.

Ring-opening metathesis polymerization (ROMP)¹⁻³ has been used successfully to synthesize polymeric materials with bulky structures⁴⁻⁵ and the

zwitterionic structures.⁶⁻⁸ NB derivatives are very attractive materials due to their high polymerization reactivity and commercial availability. At the same time, they can easily be prepared by Diels–Alder reactions with different substituents and reacted with a variety of functional groups in order to be employed for different purposes.^{9,10} Most importantly, the characteristic structure of NB shows the capability to polymerize via different mechanism routes to create advanced functional polymer architectures. Interestingly, the two common routes of polymerization, ROMP and addition, are driven by the ring strain energy of the cyclic NB structure in the presence of transition metal complexes. The main chain, which is the backbone polymer structure in each polymerization route, depends on the types of catalysts chosen.^{11,12}

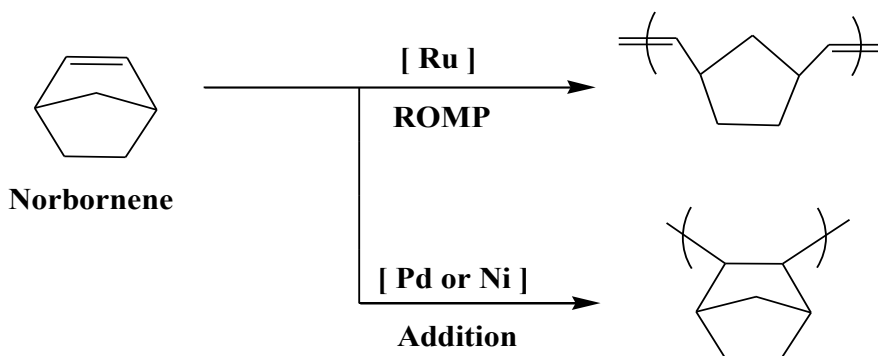


Figure 4.1. Common polymerization routes of NB-derivatives.

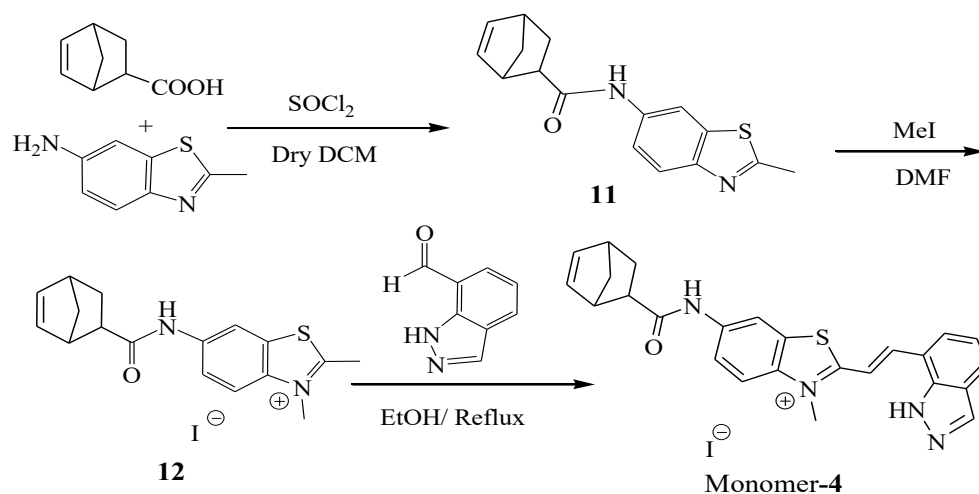
Worth noting is that the addition polymerization typically works in the presence of Ni- and Pd-complexes and forms a fully saturated main chain polymer

with more rigid backbones, but not all NB derivatives, especially those that have bulky groups, are active and easy to be polymerized with addition.¹³ Therefore, this method could not be useful for our mPAHs since the major problem is solubility, for the rigidity in the main chain decreases the solubility. Interestingly, ruthenium metathesis catalysts are commonly used to form flexible unsaturated backbones in polymeric materials. ROMP would be a preferential route for such mPAHs due to solubility issues. Specifically, the Grubbs second-generation catalyst (G2) was chosen for our experiment due to its tolerance of bulky functional groups. Lapinte *et al.*¹⁴ and Schrodi and Pederson studied the reactivity of Ru-catalysts and found that the G2 exhibited the highest reactivities for such polymerization compared to other Ru-catalysts.¹⁵ Gaining a more complete understanding of the NB structures and their polymers, we designed NB-monomers that have the desired physical properties of mPAHs and studied how we could synthesize NB-photoacid polymers. Thus, protons accumulated at a high concentration repeatedly induced by visible light.

4.2. NB Carboxamide-mPAH Polymerization

Thiol-NB, which is a type of thiol-ene reaction, has been utilized in many applications.¹⁶⁻²⁰ In 2018, Hoorick *et al.* reported that the thiol-NB reaction was more reactive than thiol-acrylate.²¹ The molecule was designed to have a NB-

carboxamide bond. Therefore, the first NB-NH-mPAH monomer was synthesized in a procedure that started with the condensation reaction between 5-NB-2-carboxylic acid and 6-amino-2-methyl-benzothiazole to yield NB carboxamide benzothiazole **11**. Then, methyl iodide was added to the solution of **11** in a minimum amount of DMF to yield **12**. In the last step, indazole-7-carboxylaldehyde was coupled to **12** in the present ammonium acetate as the catalyst to result in the monomer-4 (NH-mPAH4) (Scheme 4.1).



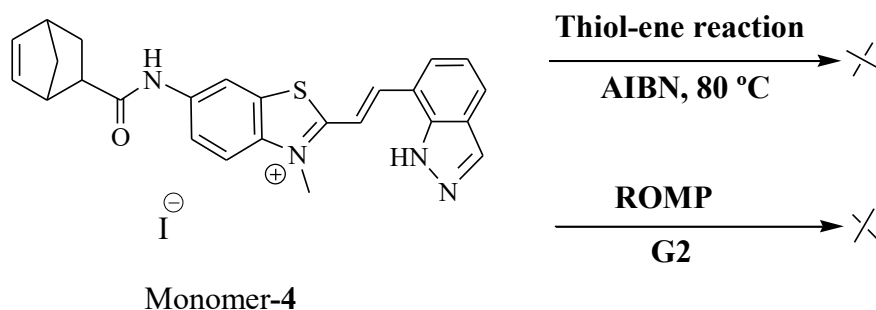
Scheme 4.1 Synthesis of monomer-4.

The thiol-NB click reaction was carried out thermally in DMSO using AIBN as a thermal radical initiator.¹⁷⁻¹⁹ Trimethylolpropane tris(3-mercaptopropionate) (tri-thiol) was selected to be coupled to the monomer-4 in the thiol-ene click polymerization. In a glass vial, 3 eq of the monomer-4, one eq of tri-thiol

polymer, and 2 mol % of AIBN were dissolved in a minimal amount of DMSO. The mixture was degassed via three freeze-pump-thaw cycles and then heated at 80 °C overnight. After cooling, the product was precipitated and washed three times in ether. Despite using a high percentage of AIBN, the reaction was unsuccessful because we used the thermal initiator instead of the radical photoinitiator. In this type of reaction, the photoinitiator is highly recommended to induce thiol-ene click reactions, which decomposed our mPAH, most likely because mPAH is a radical quencher. In fact, we are still interested to see if any other initiating system could circumvent the decomposition. Lack of success in our studies regarding the thiol-ene reaction led us to explore alternative avenues and to check any productive polymer formation with the monomer-4.

Interestingly, the reaction between mPAH and NB showed no side reactions. We were encouraged to investigate different polymerization techniques such as ROMP and addition polymerization using the monomer-4. Applying the monomer-4 to standard ROMP conditions was not successful, even though we increased the molar percentage of the catalyst to initiate and propagate a ruthenium catalyst (Scheme 4). Worthy of mention, DMF, HFIP, and DMSO are the only solvents that could be used due to the solubility limitation of the NH-mPAHs. The polymerization proceeded in different concentrated solvents, and no reaction occurred on the double bond. This observation was attributed due to steric

interactions in endo isomer during formation of metallocyclobutane or during the coordination of the double bond in propagation. The closeness of the groups to the double bonds inhibited efficient coordination of the G2 center.

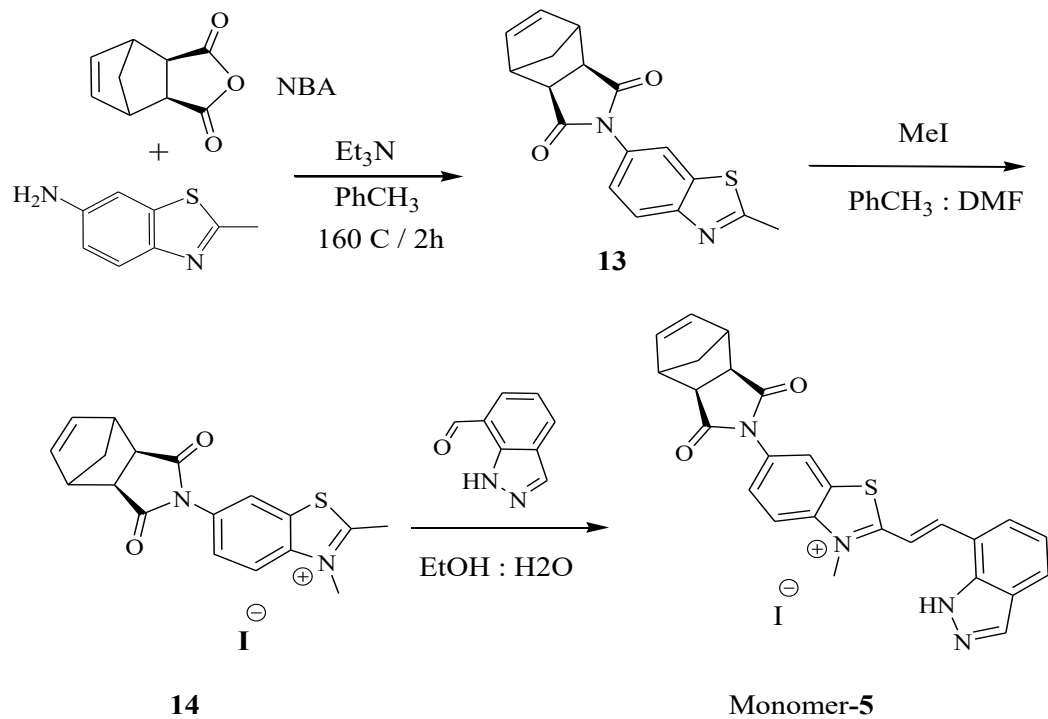


Scheme 4.2. Attempted thiol-ene polymerization and ROMP of the monomer-4.

Lacking polymerizability of some substituents on the NB monomers takes place in the orbital interactions between a close substituent and an olefinic double bond in monomer-4 carbonyl group in a carboxamide linker was close to the double bond in the NB. Thus, the bulk steric was hindered between the Grubbs center, and the double bond increased. Also, the closeness caused the deactivation of the coordination of the catalyst and prevented polymerization. The deactivation reduced the electron density on the double bond, making coordination with a Grubbs catalyst less favorable. Therefore, for a successful design, the substituents on the NB's derivative monomers must be distant enough from the olefinic double bond to be tolerated by ROMP.^{22, 23-}

3.4. Exo-NB Imide mPAH Polymerization

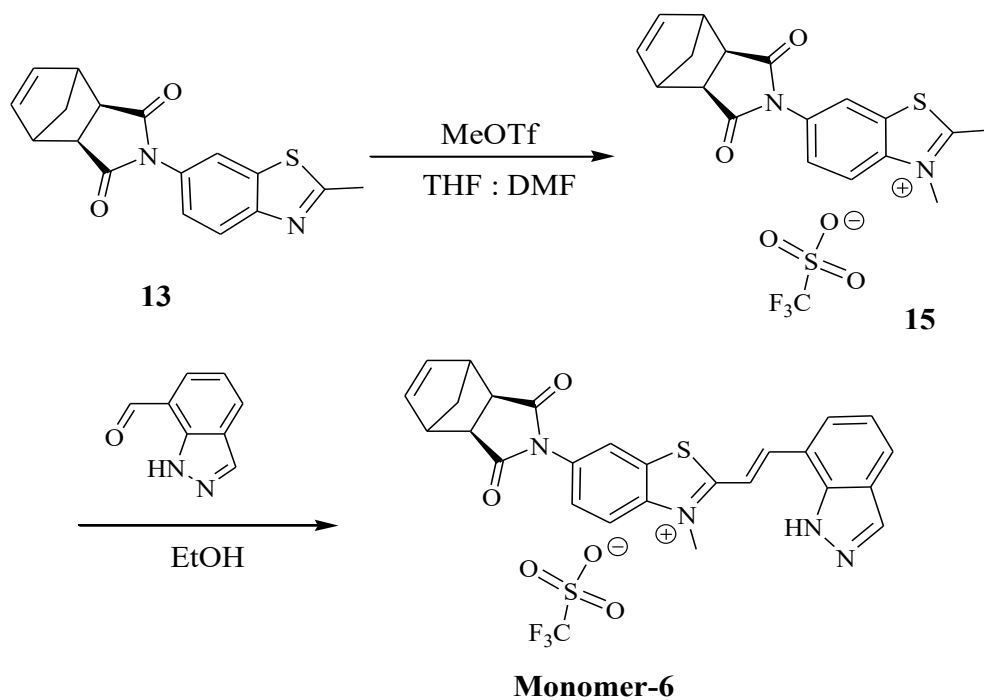
The exo-NB derivatives are more reactive in ROMP compared to endo-NBs. The endo-isomer could increase a chelating interaction between the double bond and close substituents in NB. Thus, the endo-isomer forms an intermolecular complex with the catalyst and inhibits polymerization.²⁴ Therefore, the exo-NB isomer was chosen as starting material to synthesize exclusively the NB mPAH monomers. The designing of the monomer-**5** was based on the anhydride NB structural (Scheme 4.4), and the detailed procedure is explained in Chapter 6. The synthesis started with the condensation reaction between exo-5-NB-2,3-dicarboxylic anhydride and 6-amino-2-methylbenzothiazole to yield exo-NB imide benzothiazole **13**. Then methyl iodide was added to the solution of **13** in PhCH₃:DMF to yield **14**. In the last step, indazole-7-carboxylaldehyde was coupled to **17** in present ammonium acetate as a catalyst to result in the monomer-**5** (NH-mPAH5).



Scheme 4.3. Synthesis monomer-5.

The successfully synthesized monomer-5 was expected to be the suitable monomer for ROMP (Scheme 4. 4). We were very interested to see any G2 activity on the double bond of the monomer-5 that could lead to polymer formation. Unfortunately, the problem was the lack of solubility of the monomer-5 in the DMF, HFIP, and other usable solvents, preventing polymerization. The unsuccessful polymerization of the monomer-5 led us to design monomer 6, which had the triflate instead of iodide counter ion to improve solubility.

The methyl triflate monomer-6 was successfully synthesized (Scheme 4.5). The modification was started in the second step by adding methyl triflate in a solution of compound **13** in the THF:DMF, resulting in a white solid of imide benzothiazolium **15**. Then indazole-7-carboxylaldehyde was coupled to yield the monomer-6 (NH-mPAH6) (Chapter 6).



Scheme 4.4. Synthesis monomer-6.

When we investigated the photoreaction and reversibility of the monomer-6 in the DMSO with 470 nm of light, a fast forward reaction was noted once the

monomer-6 was exposed to light. No thermal relaxation back to the ground state (reverse reaction) was observed in dark, mostly due to the presence of an imide group in the para-position of the nitrogen cation in the EA moiety. The resonance in the imide group made the amine group inductively EWG, which enhanced the ring closing reaction. Therefore, the monomer-6 became a fast light-responsive molecule, quickly disassociated the protons, and stabilized the equilibrium toward the CRF. The CRF could be analyzed from the $^1\text{H-NMR}$ spectrum stacked spectra of the monomer-6 after irradiation with 470 nm (Figure 4.2).

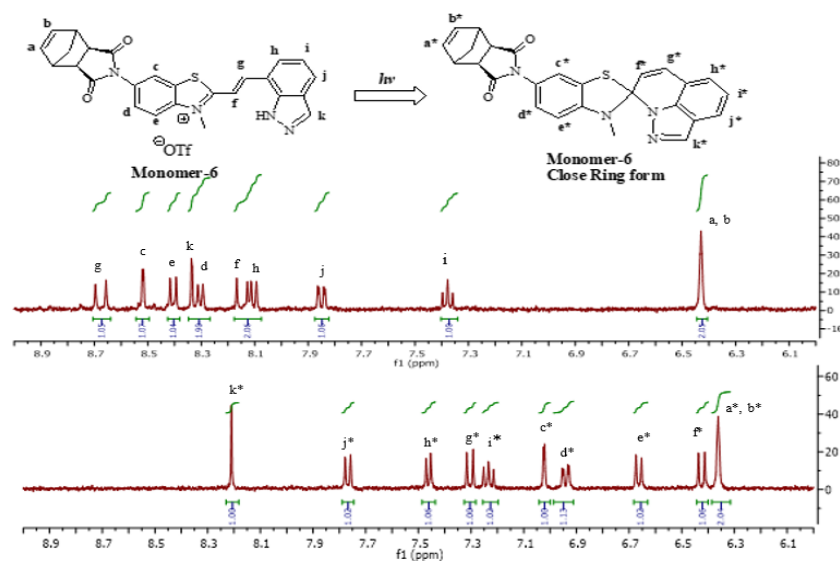


Figure 4.2. $^1\text{H-NMR}$ (DMSO- d_6) spectrum of monomer-6 before irradiation (top) and after irradiation, CRF (bottom).

We were curious to see if using a G2 with an exo-structure of mPAH leads to polymer formation and facilitates the reverse reaction activity of the monomer-6. ROMP was carried out in a test tube by dissolving 60 mg of the monomer-6 in 0.75 mL dry DMF and purged with N₂. Then, 5 mol % of G2 was taken separately in another test tube under N₂ atmosphere and dissolved in 0.25 mL dry DMF. The solution of G2 was added to the monomer solution while it heated at 80 °C. The mixture was left to reflux overnight. After the mixture was cooled to room temperature, ethyl vinyl ether (EVE) was added to quench the polymerization and stirred for 15 min. The polymer was precipitated in toluene, filtered, washed by THF, and then dried. The product was analyzed by ¹H NMR spectroscopy in the DMSO-d₆ (Figure 4.3).

After the reaction, the double-bond peak of monomer **6** at 6.4 ppm was no longer visible in the ¹H NMR spectroscopy (red circle, bottom). At the same time, the formation of a new broad resonance peak was observed between 5.9 and 5.3 ppm (blue circle) indicating ROMP. Finally, we found how to polymerize mPAHs, but the aromatic resonance peaks overlapped the CRF and ORF in the range of 6.5 to 8.7 ppm (Figure 4.3). The overlapping resonances in the aromatic range peaks and the downfield shift complicated definitive integration.

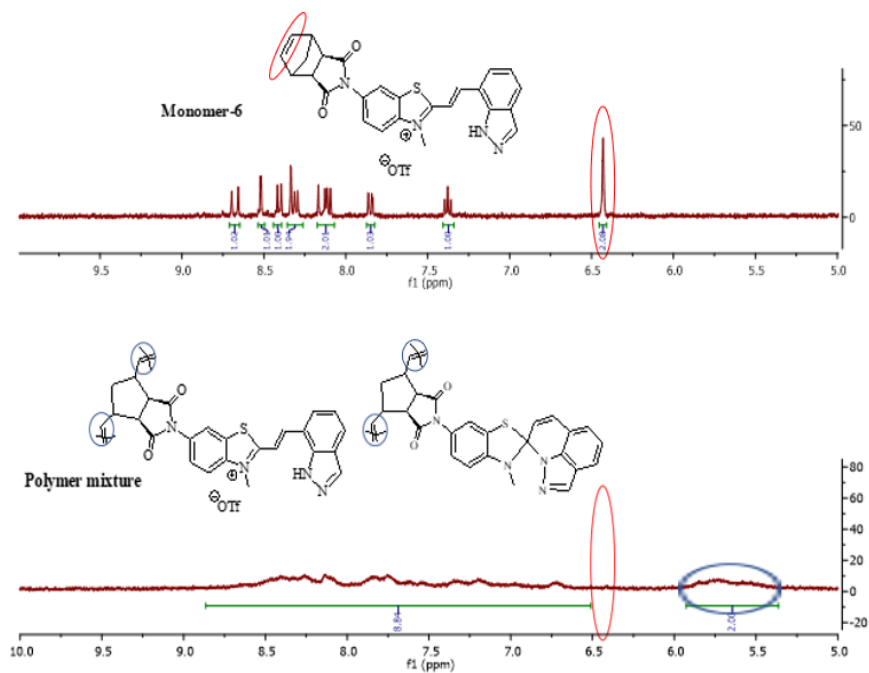


Figure 4. 3. ¹H NMR spectrum (DMSO-d₆) diagnostic of the polymer synthesized from the monomer-6, showing the disappearance of the monomer olefinic peaks at 6.4 ppm was observed (red circle, bottom) and new olefinic resonances of the product appeared 5.9-5.3 ppm (blue circle, bottom).

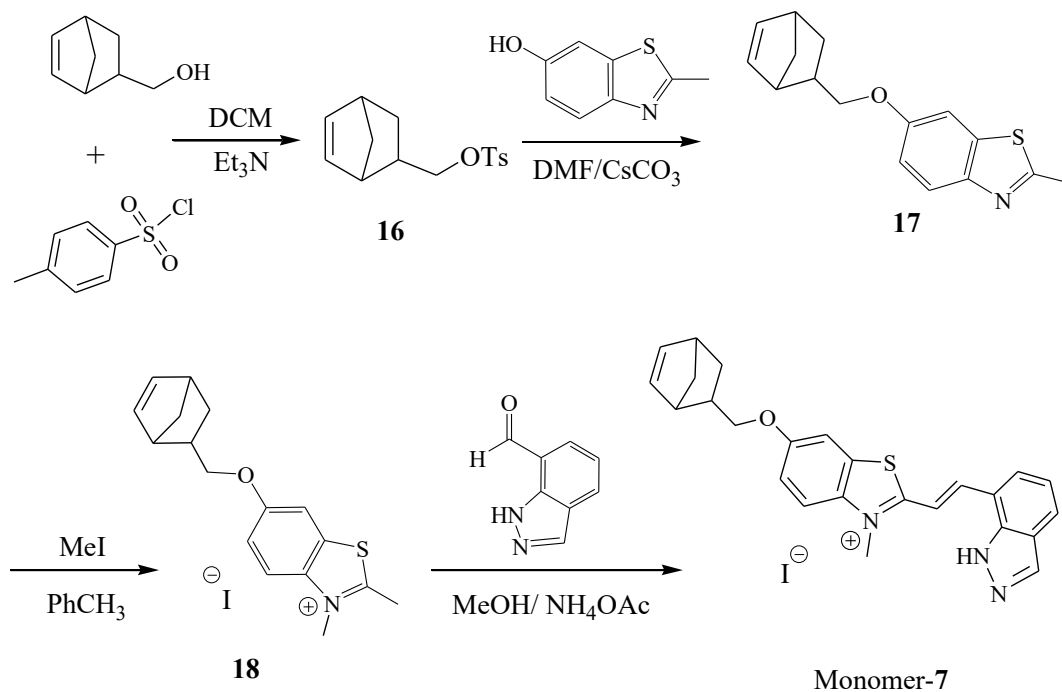
The successful polymerization of the monomer-6 via ROMP inspired us to explore alternative synthetic route by designing a monomer with more distance between the double bond and substituents.

4.4. Norbornenyloxy Benzothiazolium Polymer

The previous ROMP using the monomer-6 and G2 reached full conversion from the monomer to polymer NH-mPAH. The sluggish reversibility of NH-mPAH was believed to be due to the imide group in the EA moiety of the monomer-6 (Scheme 4.5). Also, in other considerations, the endo-NB structure isomers may prevent the ROMP due to their coordination between the ruthenium catalyst and the carbonyl bond. We designed an alternative synthetic route for a new monomer, making possible the polymerization of monomers even with bulky substituents. My coworker Osamah provided assistance by synthesizing the monomer-7. An mPAH substrate allowed us to use G2 with fast initiating and propagation rates in order to form polymeric mPAHs.

The norbornenyloxy-mPAH monomer was synthesized through a procedure that started with the tosylation of 5-NB-2-methanol adding *p*-tosyl chloride in presence of Et₃N, resulting in **16**, and then hydroxy-benzothiazole was added to replace the *p*-tosyl group, yielding norbornenyloxy-benzothiazole, **17** (Scheme 4.5). Then iodomethane was added to the solution of **17** in the PhCH₃ to result in MeI-benzothiazolium **18**. In the last step, indazole-7-carboxaldehyde was refluxed with

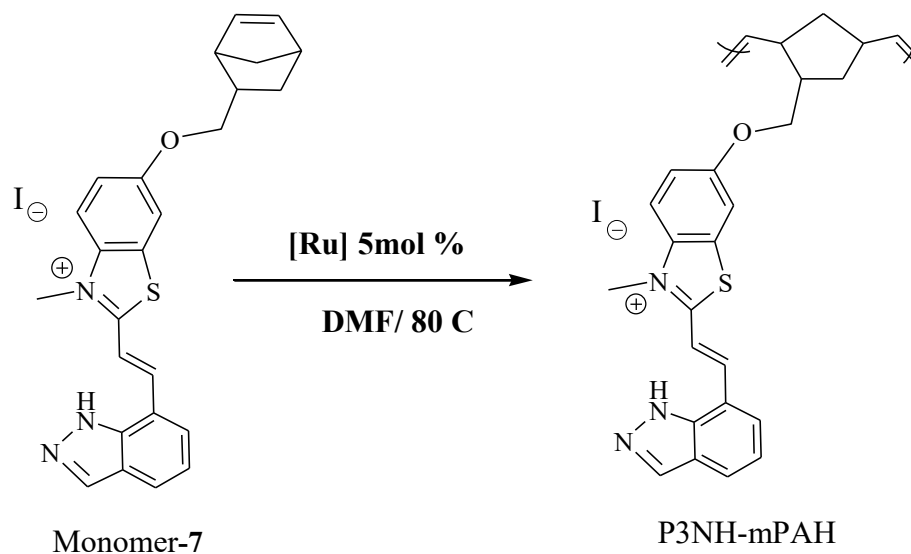
18 in MeOH with present ammonium acetate as the catalyst to result in the monomer-7 (NH-mPAH7). A detailed procedure is given in Chapter 6.



Scheme 4.5. Synthesis of the monomer-7.

The polymerization was carried out by preparing a solution of the monomer-7 in dry DMF, stirring, purging with N₂, and heating to 80 C. Another solution of 5 mol % of G2 was prepared under N₂ atmosphere. The catalyst solution was added to the monomer-7 solution while degassing and heating and kept overnight to reflux. After the reaction mixture was cooled to room temperature, EVE was added and stirred for 15 minutes. The polymer was precipitated in PhCH₃, filtered, washed with acetone, and then dried in open air (Figure 4.6). The

product was analyzed by ^1H NMR spectroscopy in the DMSO- d_6 . The notable shift in olefinic resonances from the monomer at 6.2-5.9 ppm to the ring-opened species at 5.3 ppm was diagnostic of polymerization formation. Detailed procedures for the synthesis of the monomer and the polymer are described in chapter 6.



Scheme 4.6. Polymerization of the monomer-7 to form the respective P3-mPAH.

This chapter describes my efforts in designing and synthesizing high-loading mPAH polymers using ROMP. Finally, the first photoacid NH-mPAH polymer with a single backbone was designed and synthesized, and ROMP proves to be an exciting new way to synthesize a homopolymer of NH-mPAHs. The ^1H NMR shows no aromatic side product, and the UV-vis spectra show reversible photoreaction in the DMSO. Using ROMP to generate a light-controllable mPAH

homopolymer, which allows protons to accumulate at high concentrations locally and repeatedly.

4.5. Future Expansion of NH-mPAH Polymer

Biological and medical applications require mPAH polymers that have a good reverse reaction in aqueous conditions. Modulation of pH changes using visible light may allow users to control enzymatic activity and find applications in biomedical and biotechnology. The ROMP of monomer-7 successfully produced a NH-mPAH homopolymer, which releases proton and changed charges upon irradiation in the DMSO observed. Unfortunately, though the NH-mPAH homopolymer can be dissolved in 0.5 % DMSO aqueous solution and can release protons upon irradiation, no reverse reaction was detected in the water media in the dark. The lack of reversibility in water was most likely due to the solubility limit of the polymeric surface in water, thus banning the reverse reaction.

Since we know how to design and synthesize a single backbone polymer (homopolymer) of mPAH and ROMP is an exciting new way to densely functionalized random and block copolymers of mPAHs. In addition, copolymerization is an adaptable method to synthesize copolymers from different monomers to result in a new copolymer with different properties than their individual homopolymers. Therefore, NH-mPAH water-soluble polymers can be

created using ROMP and G2 through copolymerization of the monomer-7 with different host water-soluble materials that contain three or five ethylene oxide units or the incorporation of the homopolymer in a block water-soluble copolymer to improv the solubility.

4.6. References

1. Choi, T.; Grubbs, R. H. Controlled Living Ring-Opening-Metathesis Polymerization by a Fast-Initiating Ruthenium Catalyst, *Angew. Chemie*, **2003**, *42*, 1743–1746.
2. Bielawski, C. W.; Grubbs, R. H. Living ring-opening metathesis polymerization, *Prog. Polym. Sci.*, **2007**, *32*, 1–29.
3. Smith, D.; Pentzer, E. B.; Nguyen, S. T. Bioactive and therapeutic ROMP polymers, *Polym. Rev.*, **2007**, *47*, 419–459.
4. Tlenkopatech, M.; Fomine, S.; Fomine, L.; Gavino, R.; Ogawa, T. Ring-Opening Metathesis Polymerization of Coumarin-Containing Norbornene. *Polym. J.*, **1997**, *29*, 622-625.
5. Finkelshtein, E. S.; Chapala, P. P.; Gringolts, M.L.; Rogan, Y. Polymerization of Tricyclonones. *Polym. Sci. Ser.*, **2019**, *16*, 17-30.
6. Samanta, S.; Locklin, J. Formation of Photochromic Spiropyran Polymer Brushes via Surface-Initiated, Ring-Opening Metathesis Polymerization: Reversible Photocontrol of Wetting Behavior and Solvent Dependent Morpholog changes. *Langmuir*, **2008**, *24*, 9558-9565.

7. Ren, L., Zhang, J., Bai, X., Hardy, C.G., Shimizu, K.D.; Tang, C. Preparation of cationic cobaltocenium polymers and block copolymers by “living” ring-opening metathesis polymerization. *Chem. Sci. J.* , **2012**, *3*, 580-583.
8. Pineda-Contreras, A., Hernández-Madrigal, J.V., Vázquez-Vuelvas, O.F. and Fomine, S. Synthesis; ROMP of new sulfobetaine and carboxybetaine norbornene. *e-Polymers*, **2016**, *16*, 181-188.
9. Grieco, P.A.; Abood, N. Cycloalkenone synthesis via Lewis acid-catalyzed retro Diels-Alder reactions of norbornene derivatives: synthesis of 12-oxophytodienoic acid (12-oxoPDA). *J. Org. Chem.*, **1989**, *54*, 6008-6010.
10. Horikawa, H., Nishitani, T., Iwasaki, T., Mushika, Y., Inoue, I.; Miyoshi, M. A synthesis of 2-aminonorbornene-2-carboxylic acid derivatives by diels-alder reaction using α,β -dehydroalaninates as a dienophile. *Tetrahedron Lett* ,**1980**, *21*, 4101-4104.
11. Grubbs, R. H.; Khosravi, E. *Handbook of Metathesis*, 2nd ed., Wiley-VCH, Weinheim, **2015**,
12. Elling, B. R.; Xia, Y. Living Alternating Ring-Opening Metathesis Polymerization Based on Single Monomer Additions, *J. Am. Chem. Soc.*, **2015**, *137*, 9922–9926.

13. Bermeshev, M. V.; Chapala, P.P. Addition polymerization of functionalized norbornenes as a powerful tool for assembling molecular moieties of new polymers with versatile properties, *Prog. Polym. Sci.*, **2018**, *84*, 1-46
14. Lapinte, V.; Brosse, J.; Fontaine, L. Ring-opening metathesis polymerization (ROMP) reactivity of endo-and exo-norbornenylazlactone using ruthenium Catalysts. *Macromol. Chem phys.* **2004**, *205*, 824-833.
15. Schrodi, Y.; Pederson, R.L. Evolution and Applications of Second-Generation Ruthenium Olefin Metathesis Catalysts. *Aldrichimica Acta*, **2007**, *40*, 45-52.
16. Lin, C.C., Ki, C.S.; Shih, H. Thiol-norbornene photo-click hydrogels for tissue engineering applications. *J. Appl. Polym. Sci.* , **2015** , *132*, 41563.
17. Lowe, A. B. Thiol–ene “click” reactions and recent applications in polymer and materials synthesis: a first update. *Polym. Chem.*, **2014**, *5*, 4820-4870.
18. Campos, L.M., Killops, K.L., Sakai, R., Paulusse, J.M., Damiron, D., Drockenmuller, E., Messmore, B.W.; Hawker, C.J. Development of thermal and photochemical strategies for thiol-ene click polymer functionalization. *Macromolecules*, **2008**, *41*, 7063-7070.
19. Uygun, M., Tasdelen, M.A.; Yagci, Y. Influence of type of initiation on thiol–ene “click” chemistry. *Macromol Chem Phys*, **2010**, *211*, 103-110

20. Fairbanks, B.D., Love, D.M.; Bowman, C.N. Efficient Polymer-Polymer Conjugation via Thiol-ene Click Reaction. *Macromol Chem Phys.*, **2017**, *218*, 1700073.
21. Hoorick, J.; Gruber, P.; Markovic, M.; Rollot, M.; Graulus, G. *et al.* Highly reactive thiol-Norbornene photo-Click hydrogels: toward improved processability. *Macromol. Rapid Commun.*, **2018**, *39*, 1800181.
22. Rule, J.D.; Moore, J.S. ROMP Reactivity of endo- and exo-Dicyclopentadiene. *Macromolecules*, **2002**, *35*, 7878-7882
23. Bielawski, C.W.; Grubbs, R.H. Living ring-opening metathesis polymerization. *Prog. Polym. Sci.*, **2007**, *32*, 1-29.
24. Diot-Néant, F.; Migeot, L.; Hollande, L.; Reano, F. A.; Domenek, S.; Allais, F. Biocatalytic synthesis and polymerization via ROMP of new biobased phenolic monomers: a greener process toward sustainable antioxidant polymers. *Front. Chem.*, **2017**, *5*, 126.
25. Alghazwat, O.; Elgattar, A.; Alharithy, H.; Liao, L. A Reversible Photoacid switched by different wavelengths of Ligh, **2020**
<https://doi.org/10.1002/cptc.202000256>

Chapter 5

Poly(butyl cyanoacrylate) Nanoparticle Containing an Organic PhotoCORM

“Reproduced from **Elgattar**, A.; Wasington, K.; Talebzadeh, S.; Alwagdani, A.; Khalil, T.; Alghazwat, O., Alshammri, H.; Pal, H.; Bashur, C. and Liao, Y. Poly(butyl cyanoacrylate) Nanoparticle Containing an Organic PhotoCORM. *Photochem. Photobiol. Sci.* **2019**, 18, 2666-2672, Copyright © 2019, with permission from The Royal Society of Chemistry."Royal Society of Chemistry.

5.1. Introduction

Carbon monoxide (CO) is a gasotransmitter produced naturally during heme catabolism. The production of CO plays a vital role in many physiological functions in the mammalian body, such as anti-inflammatory, anti-apoptotic, anti-coagulative, anti-hypertensive, and cell protective effects.¹ However, it is well

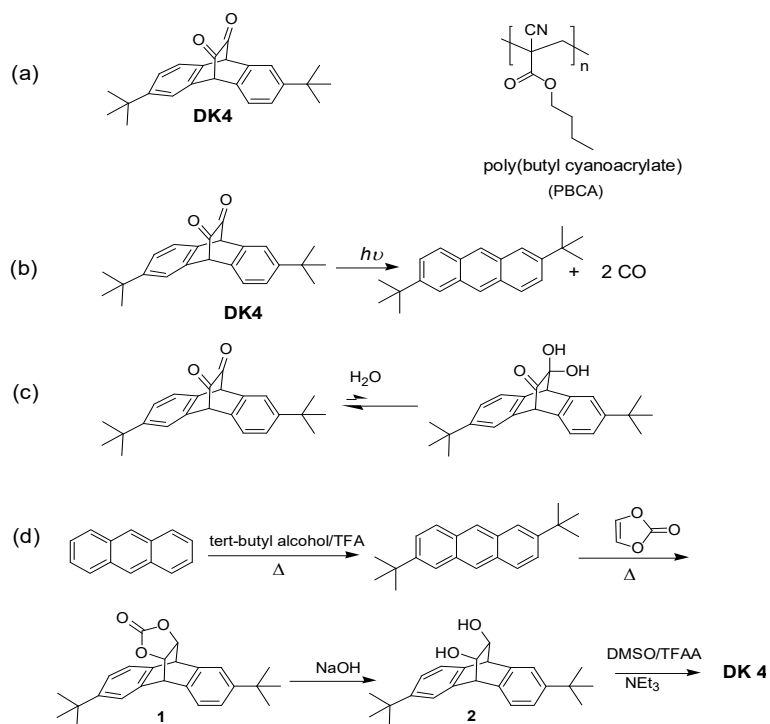
known that CO is toxic at high concentrations. The high affinity of CO for hemoglobin reduces the availability of O₂ in tissues causing death by asphyxiation. Previous work suggests that low concentrations of CO are not acutely toxic to humans.¹ When the cellular concentrations are considered, the rate and amount of CO production by Heme Oxygenase 1 within the body is in nanomolar levels.² However, in the past decade, inhaled, small-quantities of supplemental CO gas has been demonstrated in pre-clinical disease models to have therapeutic effects including reducing inflammatory and cardiovascular disorders³

The recent synthesis of CO-releasing molecules (CORMs), a group of compounds capable of releasing controlled quantities of CO in cellular systems, provides a promising delivery approach to reduce the safety concerns of systemic, inhaled CO gas. The potential to control the release of CO to a specific target is the major advantage of CORMs over gaseous CO as a therapeutic agent. The majority of CORMs studied contain transition metals including both essential trace elements (manganese, iron, cobalt) and non-physiological metals (ruthenium, tungsten, rhenium).^{1,4} Some nonmetallic CORMs have also been developed in recent years.⁵⁻
¹¹ CO release from these CORMs were triggered by protonation, thermal release, ligand exchange, ligand substitution, enzymatic reaction and light.^{1,5} In recent years, CORMs have also been incorporated into organic and inorganic nanoparticles to improve biocompatibility, control of CO release, and response to

magnetic field and near infrared light.¹²⁻¹⁷ In this work, we incorporated a new organic photoCORM into a nanoparticle of poly butyl cyanoacrylate (PBCA), which is used as tissue adhesive and has been studied for delivery of drugs to treat neural disorders such as Alzheimer disease.¹⁸⁻²⁰ The biocompatibility of the photoCORM loaded nanoparticles were also tested.

Previously, our group has reported a type of photoCORM with cyclic diketone (DK) structures.⁹ The DK photoCORMs can efficiently release two molecules of CO under visible light and simultaneously generate a fluorescent anthracene, which allows the CO release to be monitored by fluorescence spectroscopy and UV-vis spectroscopy. The clean photoreaction yields welldefined products and both the previously reported DKs and the anthracene photoproducts showed low cytotoxicity. However, the DK PhotoCORMs are hydrated in aqueous conditions, which diminishes its photoactivity. The hydration is a reversible reaction so it does not decompose the DK. If the equilibrium favors the hydrated form, which is not photosensitive, the rate of the photoreaction is significantly reduced since the hydrated form must change to the dehydrated form to react. Therefore, DKs need to be incorporated in micelles⁹ or polymers²¹ to avoid hydration for biological uses. In fact, previous work showed that photo-induced CO release increased with the hydrophobicity of the DK.

In this work, we studied a DK molecule with two highly hydrophobic tert-butyl groups (DK4 in Scheme 5.1). Although this molecule has been reported before,²² it has never been studied as a CORM. In addition, we used a different synthetic route, which led to the DK4 with good yield. As shown in Scheme 5.1, di-tert-butyl anthracene was prepared from anthracene and t-butyl alcohol following a literature procedure.²³ Then it was heated with vinylene carbonate in xylene to form the Diels Alder adduct 1. Compound 1 was then hydrolyzed by NaOH to yield the dihydroxy intermediate 2. DK4 was synthesized from 2 using Swern oxidation.



Scheme 5.1. (a) Structures of DK4 and PBCA, (b) photoreaction of DK4, (c) the potential hydration reaction, and (d) synthesis of DK4.

DK4 is not soluble in water but is well dissolved in DMSO and other common organic solvents such as THF. The UV-vis spectrum of DK4 in DMSO is shown in Figure 5.1 (a). It is similar to other DKs reported before.⁹ The n- π transition band of the diketone appears between 400 and 550 nm with the maximum absorption at 465 nm. Upon irradiation by a 470 nm LED, the absorption diminished to nearly zero. A strong absorption peaked at 266 nm and an absorption band with three peaks between 300 nm and 400 nm appeared, which indicates the formation of the anthracene side product. Among the three peaks between 300 nm and 400 nm the middle peak at 358 nm was the highest and the peak at 379 nm was the second highest. Previous studies on DKs have shown that the formation of the anthracene derivatives is accompanied by the release of CO.^{9,24} (Scheme 5.1) Therefore, CO release can be conveniently monitored by the formation of the anthracene.

As described above, hydration is a problem for using DKs as PhotoCORMs. Previous work showed that when DKs were dissolved in 1% DMSO in water, the n- π transition band of the diketone disappeared and the DKs became inactive under irradiation. ⁹ To test whether DK4 can be protected from hydration due to the hydrophobic t-butyl groups, a solution of DK4 in 1% DMSO in water was prepared. The UV-Vis spectrum of the solution is shown in Figure 5.1. Unlike other DKs, the n- π transition band in the visible range can still be observed. Upon

irradiation, the band disappeared and the absorption bands of the anthracene product showed in the spectrum. However, the position of the two peaks red-shifted to 366 and 387 nm. The shape of the absorption band was also different from that of the DMSO solution (Figure 5. 1). The peak at 387 nm was higher than that at the 366 nm. We attribute this change to the formation of aggregation or even small particles due to the low solubility of the photoproduct (di-t-butyl anthracene) in water. In fact, the baseline was high, especially at the lower wavelengths, which is commonly observed when there are small particles in the solution. To confirm this, DMSO was added to the irradiated solution until the DMSO/water ratio was 3:1. The position of the two peaks shifted back to 357 nm and 378 nm, and the former was higher than the latter as in the spectrum of the DMSO solution (Figure 5. 1b). In addition, the release of CO was confirmed by a direct measurement using a CO meter (Experimental section). The results showed that the hydration of DK4 is much lessened comparing to previously developed DKs and it is photoactive in 1% DMSO in water.

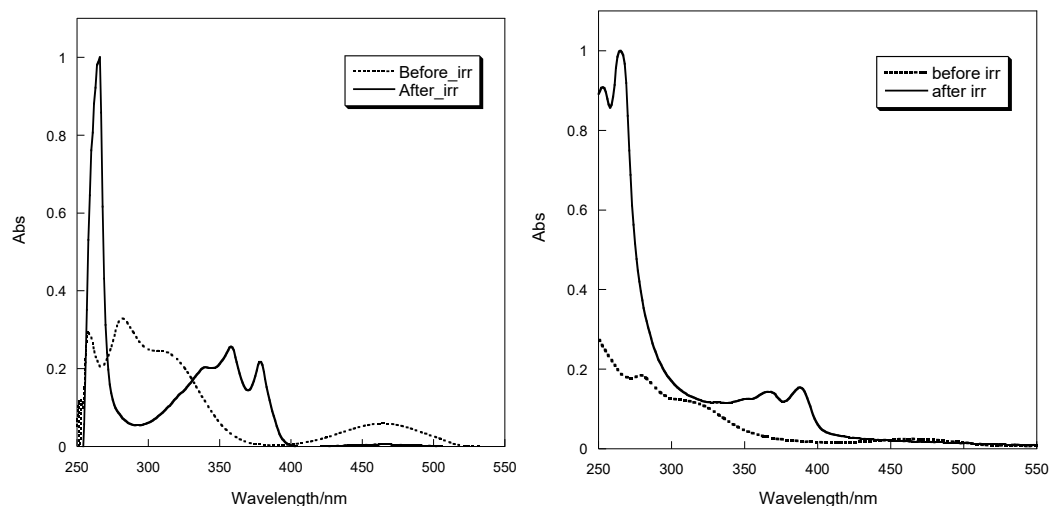


Figure 5.1. UV-Vis spectra of DK4 in DMSO (9×10^{-5} M) before and after irradiation [left, inserted figure: spectrum of di-*t*-butyl anthracene (the expected photoproduct)], and in 1% DMSO aqueous solution (4×10^{-5} M) before and after irradiation [right, inserted figure: spectra of the irradiated solution after addition of DMSO].

5.2. DK4 incorporated with PBCA nanoparticles

We incorporated DK4 in PBCA nanoparticles. As described above, incorporating CORMs in nanoparticles can improve their biocompatibility and achieve better control of CO delivery. PCBA is a well-known biocompatible polymer. It has previously been used to deliver drugs to pass the blood-brain barrier. PBCA nanoparticles are commonly prepared by anionic emulsion polymerization.^{19, 20} It combines the polymerization, nanoparticle formation and

drug incorporation in one step. However, much work needs to be done for optimizing the conditions and achieving good reproducibility. We synthesized PBCA using a nonconventional free radical polymerization (Experimental Section). The competing anionic polymerization was quenched by addition of dichloroacetic acid. This method allows us to prepare a relatively large scale of PBCA, which can be used many times for the preparation of the DK4/PBCA nanoparticles. In addition, it is possible to copolymerize common acrylates (not only cyanoacrylates) with BCA, which could be useful for tuning the nanoparticle properties.

The PBCA nanoparticle containing DK4 was prepared by addition of an acetone solution of DK4 and PBCA in a quickly stirred 1% Pluronic F-127 solution in water. The details are given in the Experimental Section. The nanoparticle was characterized by dynamic light scattering (DSL) method. The average size was measured to be 326 nm. After irradiation, the size was about the same (351 nm). Since a size of around 200 nm or less is preferred for drug delivery,²⁵ the nanoparticle suspension was filtered through a 2 μm filter. DSL showed that the average size was 214 nm before irradiation and 216 nm after irradiation. (Figure 5. 2) The zeta potential of the nanoparticle was -28.4 mV indicating a moderate stability.

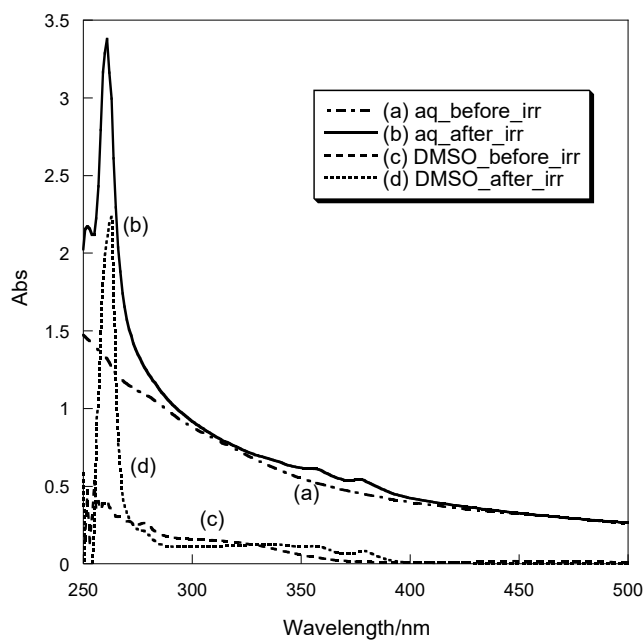
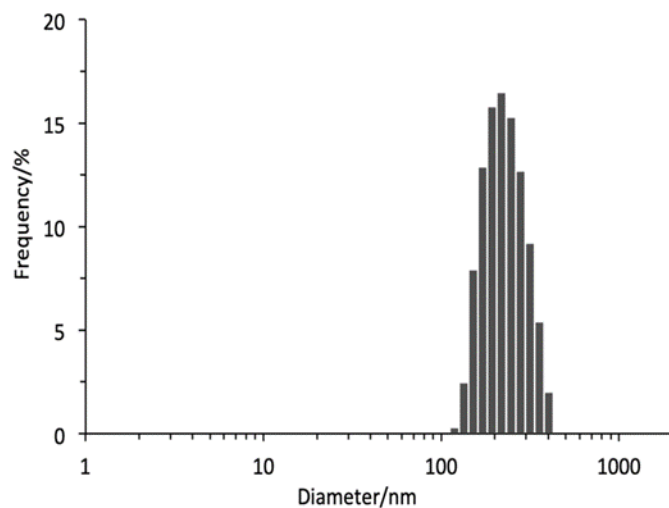


Figure 5.2. Size distribution of the PBCA/DK4 nanoparticle measured by DSL (up) and UV-Vis spectra of the nanoparticle in water and in DMSO before and after irradiation (down).

A suspension of the nanoparticles was irradiated by 470 nm light and its UV-Vis spectra were studied. A shallow bump appeared between 400 and 550 nm before irradiation. (Figure 5.2) The baseline was high, especially at the lower wavelengths, due to background light scattering of the nanoparticles. Upon irradiation, the bump disappeared and the anthracene peaks at 261 nm and between 300 to 400 nm appeared as expected (Figure 5. 2). To evaluate the photoreaction efficiency, a different sample from the same batch of the nanoparticle suspension was dried under nitrogen. Then DMSO with the same volume as that of the sample before drying was added to the residue to prepare a DMSO solution with the same concentration of DK4 as that of the aqueous sample. Since both the polymer and the DK4 are soluble in DMSO, the DMSO solution contained the dissolved polymer and DK4 but not the nanoparticle. The DMSO solution was irradiated and UV showed the anthracene absorption peaks. The peak absorption at 263 nm was 2.23, which was 1.9 units higher than the absorption before irradiation. For comparison, the absorption change of the aqueous suspension of the nanoparticle was 2.0 (Figure 5. 2), which is about same as that of the DMSO solution. The result shows that the photoreaction of DK4 in the nanoparticle was as effective as that of a DK4 solution in DMSO. As described above, the photoreaction of DK4 in DMSO is nearly quantitative. Therefore, the photoreaction of DK4/PBCA nanoparticle is nearly quantitative.

5.3. Cytotoxicity Screening

The cell toxicity of DK4 incorporated within PBCA nanoparticles was determined by delivering a single-dose of the DK4/PBCA nanoparticle suspension to endothelial cells (ECs) seeded on tissue culture polystyrene (TCPS). DK4-loaded nanoparticles were tested both for the nonactivated and pre-activated conditions. For pre-activated nanoparticles, the CORM was activated and CO released prior to adding the nanoparticles to the cells. This allows evaluation of the potential toxicity after the photoreaction. We prepared 0, 0.5, 5, and 50 $\mu\text{g}/\text{mL}$ of DK4 loaded nanoparticles (DK4+NP) in sterile EC complete growth media. Figure 5. 3 shows the DNA analysis results for density of ECs seeded on TCPS treated with varying concentrations of DK4 nanoparticle solutions (6 samples/condition). There was no significant difference in cell density between conditions, even with a dose of nanoparticles up to 50 $\mu\text{g}/\text{mL}$, which indicates negligible toxicity even at this relatively high dose. There is variability in the biocompatibility of different nanoparticle formulations in other studies. For example, some iron oxide nanoparticles formulations have demonstrated toxicity at the levels we tested in this study.²⁶ Overall, the results indicate good biocompatibility for DK4/PBCA nanoparticles. Live/Dead confocal images of ECs after 11 days of culture with high and low doses further supported this conclusion. (Figure 5.3) There was almost 100% cell viability, as indicated by the presence of calcein-AM stained live cells

but no ethidium homodimer stained dead cells. While the photo-product of DK4 is fluorescent, it does not absorb the 488 nm light that was used to excite the fluorescence of the live/dead stains. Thus, it did not provide background fluorescence.

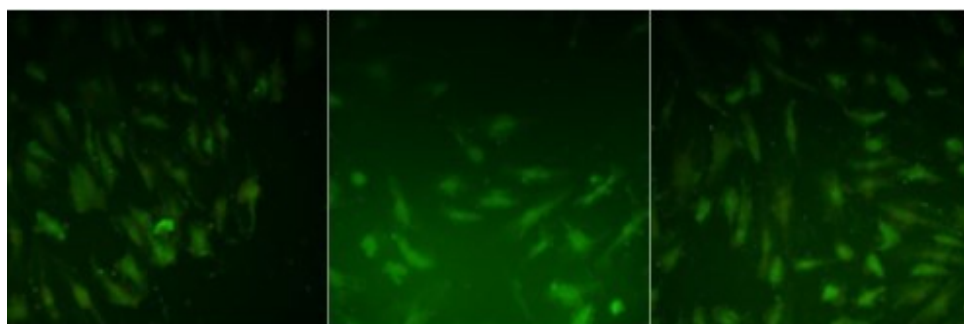
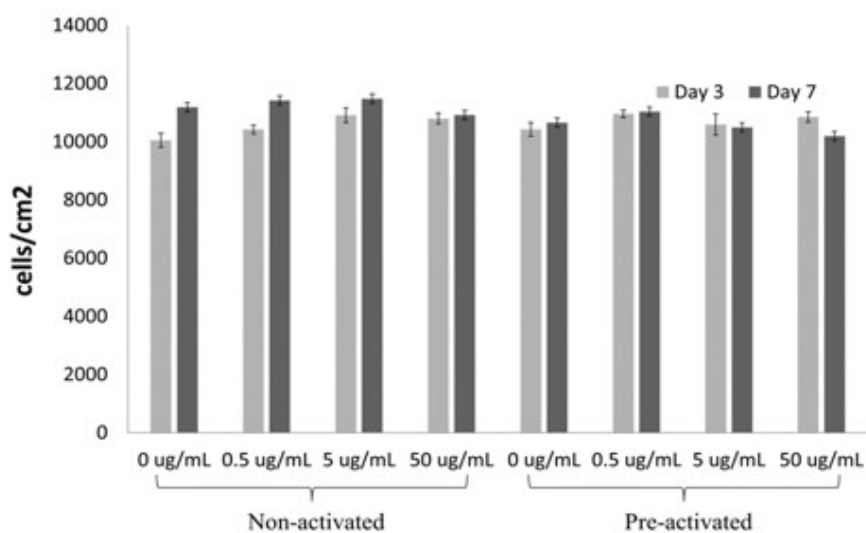


Figure 5.3. Top: DNA Analysis of Endothelial Cells seeded on TCPS treated with varying concentrations of DK4 Nanoparticle solutions ($n=6$). No significance was determined. **Bottom:** Live/Dead (green / red) confocal images of endothelial cells

with varying dose at A) no drug delivery of 0 $\mu\text{g/mL}$; B) low dose of 0.5 $\mu\text{g/mL}$, and C) at high concentration of 50 $\mu\text{g/mL}$ for DK4 Nanoparticle solution at Day 11.

5.4. Conclusion

The results show that DK4 is a promising organic photoCORM. The two hydrophobic t-butyl groups protect it from hydration, and allow it to react in a 1% DMSO/water solution. The well-defined photoreaction and efficient release of two molecules of CO makes DK4 a useful molecule for the study of CO. For example, it may be used to prepare a standard CO solution with low concentration. DK4 was incorporated into PCBA nanoparticles. The unconventional synthesis of PCBA and PCBA/drug nanoparticles is convenient for preparation of many batches with good consistency. The nanoparticles showed good photoactivity and low cytotoxicity. Given that PBCA has been applied to brain drug delivery, the PBCA/DK4 nanoparticle may be used for studying the effects of CO on brain cells, which will be investigated in the future.

5.5. References

1. (a) Heinemann, S. H.; Hoshi, T.; Westerhausen, M.; Schiller, A. Carbon monoxide–physiology, detection and controlled release. *Chem. Commun.*, **2014**, *50*, 3644-3660; (b) Ryter, S.W.; Otterbein, L. E. Carbon monoxide in biology and medicine. *Bioessays.*, **2004**, *26*, 270-280; (c) Ramao, C. C.; Blattler, W. A.; Seixas, J. D.; Bernardes, G. J. Developing drug molecules for therapy with carbon monoxide. *Chem. Soc. Rev.*, **2012**, *41*, 3571-3583. (d) Mann, B. E. CO-releasing molecules: a personal view. *Organometallics.*, **2012**, *31*, 5728-5735.
2. Wu, L.; Wang, R. Carbon monoxide: endogenous production, physiological functions, and pharmacological applications. *Pharmacol. Rev.*, **2005**, *57*, 585-630.
3. Wilbur, S.; Williams, M.; Williams, R.; Scinicariello, F.; Klotzbach, J. M.; Diamond, G. L.; Citra, M. Toxicological Profile for Carbon Monoxide. *Agency Toxic Subst. Dis. Regist. (US)*, **2012**, 9-23.

4. (a) Garcia-Gallego, S.; Bernardes, G. J. L. Carbon-monoxide-releasing molecules for the delivery of therapeutic CO in vivo. *Angew. Chem. Int. Ed.*, **2014**, *53*, 9712–9721. (b) Foresti, R.; Bani-Hani, M. G. ; Motterlini, R. Use of carbon monoxide as a therapeutic agent: promises and challenges. *Intensive Care Med.*, **2008**, *34*, 649-659. (c) Foresti, R.; Motterlini, R. Interaction of carbon monoxide with transition metals: evolutionary insights into drug target discovery. *Curr. Drug Targets.*, **2010**, *11*, 1595-1604. (d) Alberto, R.; Motterlini, R. Chemistry and biological activities of CO-releasing molecules (CORMs) and transition metal complexes. *Dalt. Trans.*, **2007**, *17*,1651-1660. (e) Motterlini, R.; Clark, J. E.; Foresti, R.; Sarathchandra, P.; Mann, B. E.; Green, C. J. Carbon monoxide-releasing molecules: characterization of biochemical and vascular activities. *Circ. Res.*, **2002**, *90*, E17-E24. (f) Clark, J. E. ; Naughton, P.; Shurey, S.; Green, C. J.; Johnson, T. R.; Mann, B. E. ; Foresti, R.; Motterlini, R. Cardioprotective actions by a water-soluble carbon monoxide–releasing molecule. *Circ. Res.*, **2003**, *93*, e2-e8.
5. Abeyrathna, N.; Washington, K.; Bashur, C.; Liao, Y. Nonmetallic carbon monoxide releasing molecules (CORMs). *Org Biomol Chem.*, **2017**, *15*, 8692-8699.

6. (a) Motterlini, R.; Sawle, P.; Hammad, J. ; Bains, S.; Alberto, R.; Foresti, R.; Green, C. J. CORM-A1: a new pharmacologically active carbon monoxide-releasing molecule. *FASEB J.*, **2005**, *19*, 284–286. (b) Alberto, R.; Ortner, K.; Wheatley, N.; Schibli, R.; Schubiger, A. P. Synthesis and properties of boranocarbonate: a convenient in situ CO source for the aqueous preparation of $[^{99m}\text{Tc}(\text{OH})_2)_3(\text{CO})_3]^+$. *J. Am. Chem. Soc.* , **2001**, *123*, 3135-3136.
7. Ayudhya, T. I.; Raymond, C. C. Dingra, N. N. Hexamethylenetetramine carboxyborane: synthesis, structural characterization and CO releasing properties. *Dalt. Trans.*, **2017**, *46*, 882–889.
8. Wang, D.; Viennois, E.; Damera, K. Ji. K. ; Draganov, A.; Zheng, Y.; Dai, C.; Merlin, D.; Wang, B. A click-and-release approach to CO prodrugs. *Chem. Commun.*, **2014**, *50*, 15890-15893.
9. Peng, P.; Wang, C.; Shi, Z.; Johns, V. K.; Ma, L.; Oyer, J.; Copik, A.; Igarashi, R.; Liao, Y. Visible-light activatable organic CO-releasing molecules (PhotoCORMs) that simultaneously generate fluorophores. *Org. Biomol. Chem.*, **2013**, *11*, 6671–6674.

10. (a) Antony, L. A. P.; Slanina, T.; Sebej, P.; Solomek, T.; Klan, P. Fluorescein analogue xanthene-9-carboxylic acid: a transition-metal-free CO releasing molecule activated by green light. *Org. Lett.*, **2013**, *15*, 4552-4555.
- (b) Palao, E.; Slanina, T.; Muchova, L. Solomek T, Vitek L, Klan P." , *J. Am. Chem. Soc.*, **2016**, *138*, 126-133.
11. (a) Popova, M.; Soboleva, T.; Ayad, S.; Benninghoff, A. D.; Berreau, L. M. Visible-light-activated quinolone carbon-monoxide-releasing molecule: prodrug and albumin-assisted delivery enables anticancer and potent anti-inflammatory effects. *J. Am. Chem. Soc.*, **2018**, *140*, 9721-9729. (b) Anderson, S.; N.; Richards, J.; M.; Esquer, H.; J.; Benninghoff, A.; D.; Arif, A.; M.; Berreau, L. M. A structurally-tunable 3-hydroxyflavone motif for visible light-induced carbon monoxide-releasing molecules (CORMs). *ChemistryOpen.*, **2015**, *4*, 590-594.
12. Ou, J.; Zheng, W.; Xiao, Z.; Yan, Y.; Jiang, X.; Dou, Y.; Jiang, R.; Liu, X. Core-shell materials bearing iron (ii) carbonyl units and their CO-release via an upconversion process. *J Mater Chem B Mater Biol Med.*, **2017**, *5*, 8161-8168.
13. Kautz, A. C.; Kunz, P. C.; Janiak, C. CO-releasing molecule (CORM) conjugate systems. *Dalton Trans.*, **2016**, *45*, 18045-18063.

14. Qureshi, O. S.; Zeb, A.; Kram, M. A.; Kim, M.; Kang, J.; Kim, H.; Majid, A.; Han, I.; Chang, S.; Bae, O.; Kim, J. Enhanced acute anti-inflammatory effects of CORM-2-loaded nanoparticles via sustained carbon monoxide delivery. *Eur. J. Pharm. Biopharm.*, **2016**, *108*, 178-195.
15. Nguyen, D.; Adnan, N. M. ; Oliver, S.; Boyer, C. The Interaction of CORM-2 with Block Copolymers Containing Poly (4-vinylpyridine): Macromolecular Scaffolds for Carbon Monoxide Delivery in Biological Systems. *Macromol Rapid Commun.*, **2016**, *37*, 739-744.
16. Kunz, P. C.; Meyer, H.; Barthel, J.; Sollazzo, S.; Schmidt, A. M.; Janiak, C. Metal carbonyls supported on iron oxide nanoparticles to trigger the CO-gasotransmitter release by magnetic heating. *Chem. Commun. (Cambridge, U. K.)*, **2013**, *49*, 4896-4898.
17. Dordelmann, G.; Pfeiffer, H.; Birkner, A.; Schatzschneider, U. Silicium dioxide nanoparticles as carriers for photoactivatable CO-releasing molecules (PhotoCORMs). *Inorg. Chem.*, **2011**, *50*, 4363-4367.
18. Rocha, S. Targeted drug delivery across the blood brain barrier in Alzheimer's disease. *Curr Pharm Des.*, **2013**, *19*, 6635-6646.

19. Wilson, B.; Samanta, M. K.; Santhi, K.; Kumar, K. P. S.; Paramakrishnan, N.; Suresh, B. Poly (n-butylcyanoacrylate) nanoparticles coated with polysorbate 80 for the targeted delivery of rivastigmine into the brain to treat Alzheimer's disease. *Brain Res.*, **2008**, *1200*, 159-168.
20. Joshi, S.A.; Chavhan, S. S.; Sawant, K. K. Rivastigmine-loaded PLGA and PBCA nanoparticles: preparation, optimization, characterization, in vitro and pharmacodynamic studies. *Eur. J. Pharm. Biopharm.*, **2010**, *76*, 189-199.
21. Michael, E.; Abeyrathna, N.; Patel, A.V.; Liao, Y.; Bashur, C. A. Incorporation of photo-carbon monoxide releasing materials into electrospun scaffolds for vascular tissue engineering. *Biomed. Mater.*, **2016**, *11*, 025009.
22. Breidenkötter, B.; Grzywa, M.; Alaghemandi, M.; Schmid, R.; Herrebout, W.; Bultinck, P.; Volkmer, D. Tribenzotriquinacene receptors for C60 fullerene rotors: towards C3 symmetrical chiral stators for unidirectionally operating nanoratchets. *Chem. Eur. J.*, **2014**, *20*, 9100-9110.
23. Niladari Raju, M. V.; Mohanty, M. E.; Bangal, P. R.; Vaidya, J. R. Synthesis and ultrafast dynamics of a donor–acceptor–donor molecule having optoelectronic properties. *J. Phys. Chem. C.*, **2015**, *119*, 8563-8575.

24. Mondal, R.; Okhrimenko, A. N.; Shah, B. K.; Neckers, D. C. Photodecarbonylation of α -diketones: a mechanistic study of reactions leading to acenes. *J. Phys. Chem. B*, **2008**, *112*, 11-15.
25. Hoshyar, N.; Gray, S.; Han, H.; Bao, G. The effect of nanoparticle size on in vivo pharmacokinetics and cellular interaction. *Nanomed.*, **2016**, *11*, 673-692.
26. (a) P. R. Gil, G. Oberdörster, A. Elder, V. Puentes; W. Correlating physico-chemical with toxicological properties of nanoparticles: the present and the future J. Parak, *ACS Nano.*, **2010**, *4*, 5527-5531. (b) George, S.; SPokhrel, S.; Xia, T.; Gilbert, B.; Ji, Z.; Schowalter, M.; Rosenauer, A.; Damoiseaux, R.; Bradley, K.; Mädler, L.; Nel, A; Use of a rapid cytotoxicity screening approach to engineer a safer zinc oxide nanoparticle through iron doping. *ACS Nano.*, **2010**, *4*, 15-29.

Chapter 6

Experimental

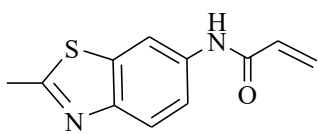
6.1. Materials and Instrumentation

Unless otherwise noted, reagents and solvents were commercially available and used as received without any further purification. Ultraviolet-visible (UV-vis) spectra were obtained from a Varian Cary 60 Scan UV-vis spectrophotometer. NMR spectra were determined in deuterated solvents on a Bruker av400 NMR spectrometer. Chemical shifts were reported in delta (δ) units, parts per million (ppm) downfield from TMS. Abbreviations for NMR assignments for peaks are as follows: s = singlet, d = doublet, t = triplet, q = quartet, sept = septet, m = multiplet and br = broad. The light sources for irradiation were 470 nm LED arrays with 120 LEDs purchased from www.theledman.com. Photon flux was measured by an apogee quantum meter. The polymer film thicknesses were measured using an

iGaging (0-1", 0.00005") digital electronic micrometer with large display inch/metric. Photoacids were synthesized following literature methods.^{1,2}

6.2. Chapter 2 Synthesis and Characterization

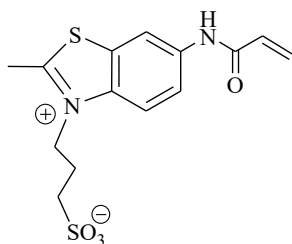
Synthesis of compound 1; 2-methylbenzothiazol-6-acrylamide



1

The starting material 2-methyl-6-amino-benzothiazole (1.50 g, 9.1 mmol) was dissolved in dry dichloromethane (18 mL). Then triethylamine (1.00 g, 10.0 mmol) was added, and the mixture was stirred for 5 minutes. Next, the mixture was cooled in an ice bath and acryloyl chloride (0.87 g, 9.60 mmol) was added dropwise. The reaction mixture was stirred for 24 h at ambient temperature and then poured into water. The product was poured into 100 mL water and vigorously stirred for one hour. After stirring, a light-yellow precipitate was filtered and washed with water, and dried out in the air. The TLC in the 5:3 hexane:EtOAc system showed that a single product was obtained, and no further purification was required (1.86 g, 93 % yield). ¹H NMR (400 MHz, DMSO, δ ppm): δ = 10.37 (s, 1H), 8.50 (s, 1H), 7.85 (d, 1H, J = 8.8 Hz), 7.56 (d, 1H, J = 8.8 Hz), 6.46 (dd, 1H, J = 10 Hz), 6.28 (d, 1H, J = 15.2 Hz), 5.78 (d, 1H, J = 10 Hz), 2.72 (s, 3H).

Synthesis of compound 2: acrylamido-2-methylbenzothiazio-propane sulfonate

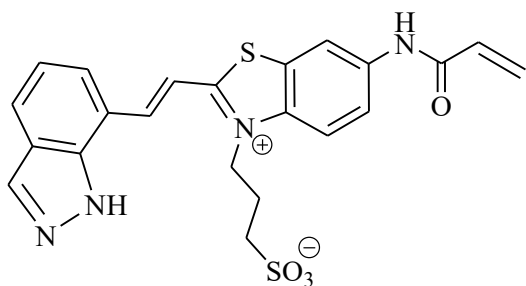


2

A mixture of compound 1 (0.2 g, 1.00 mmol) and 1,3-propanesultone (0.16 g, 1.40 mmol) and 1.00 mg of butylated hydroxytoluene (BHT) in ~ 1 mL of THF were stirred and heated on plate at 90 °C in a sealed vial for 4 days. The precipitate was washed with THF

to yield the product (0.24g, 78% yield). ¹H NMR (400 MHz, d6-DMSO, δ ppm): δ = 10.72 (s, 1H), 8.96 (s, 1H), 8.37 (d, 1H, J=9.2 Hz), 7.86 (d, 1H, J=9.2 Hz), 6.46 (dd, 1H, J=10 Hz), 6.35 (d, 1H, J= 15.2 Hz), 5.86 (d, 1H, J=10Hz), 4.86 (t, 2H, J=8.4Hz), 3.15 (s, 3H), 2.63 (t, 2H, J=6.4Hz), 2.14 (m, 2H, J=6.8 Hz).

Synthesis of monomer-1; NH-mPAH1



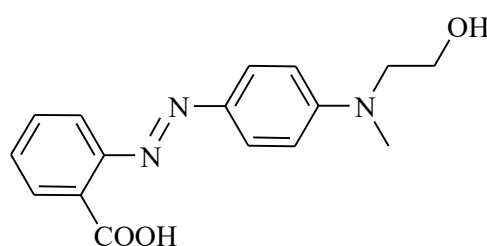
Monomer-1
NH-mPAH1

A mixture of compound 2 (90 mg, 0.26 mmol), 1H-indazole-7-benzaldehyde (0.44 g, 0.3 mmol), catalytic amount of ammonium acetate, and 1 mg of BHT were stirred in 1.5 mL of ethylene glycol and heated at 70 °C overnight.

The orange precipitate was washed with THF and acetone to obtain a dark reddish orange solid (69 mg, 56 %). ¹H NMR (400 MHz, d6- DMSO δ ppm): δ = 13.95 (s, 1H), 10.75 (s, 1H), 8.99 (s, 1H), 8.55

molar concentration of the NH-mPAH on the polymer was calculated by dividing the absorbance at 438 nm by the extinction coefficient of the photoacid ($2.9 \times 10^4 \text{ M}^{-1} \text{ cm}^{-1}$). The weight of the NH-mPAH unit was then calculated from the molar concentration, the solution volume, and the molecular weight of the NH-mPAH monomer. The wt % was the weight of the NH-mPAH unit divided by the weight of the polymer used in preparing the solution.

Synthesis of compound 5;(2-((4((2hydroxyethyl)(methyl)amino)phenyl)diazenyl)-benzoic acid).



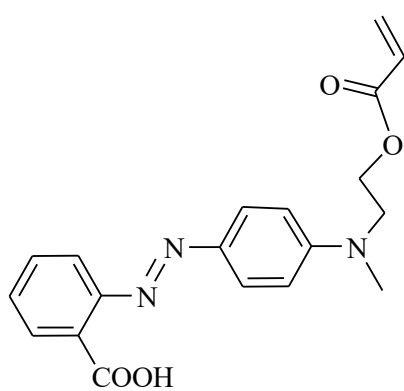
3

A mixture of anthranilic acid (0.5 g, 3.6 mmol), concentrated HCl (0.5 mL), and water (1 mL) was placed in an ice bath and then was diazotized by adding a cold solution of sodium nitrite (0.25 g, 3.6 mmol, 0.5 mL water) dropwise; then, a cold solution of 2-(N-methylanilino)ethanol (0.82 g, 5.4 mmol, 1 mL water) was added to the cold diazonium salt. After that, the reaction mixture was stirred for 15 min in an ice bath; then, a solution of sodium acetate (0.52 g in 1 mL water) was added and stirring was continued for 1 h. The mixture was kept in a refrigerator for 12 h and then left for 2 h at room temperature. A solution of NaOH (2 mL, 20 %) was added to the reaction mixture and left at room temperature for 1 h. The product was filtered and washed many

times with water and acetic acid (3 mL, 10 %) to remove unreacted 2-(N-methylanilino)ethanol. The dried product material was a dark-red powder in a 65 % yield. $^1\text{H NMR}$ (400 MHz, $\text{d}_6\text{-DMSO}$, δ ppm): δ = 13.17 (s, 1H), 7.75 (d, 2H, J = 8.8 Hz), 7.71 (d, 1H, J = 2.4 Hz), 7.61 (d, 1H, J = 2.4 Hz), (t, 1H, J = 2.4 Hz), 7.48 (m, 1H), 6.88 (d, 2H, J = 9.2 Hz), 4.80 (t, 1H, J = 5.2 Hz), 3.60 (q, 2H, J = 5.6 Hz), 3.56 (t, 2H, J = 5.2 Hz), 3.09 (s, 3H).

Synthesis of compound 4; Indicator monomer

(2-((4-((2-(Acryloyloxy)ethyl)- (methyl)- amino)phenyl)diazenyl)benzoic acid).

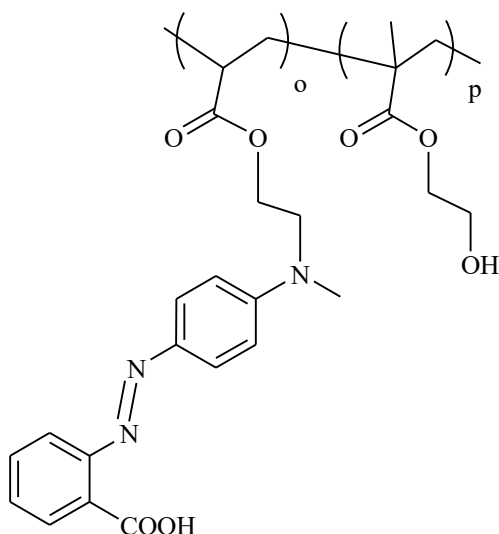


4

The mixture of **3** (0.45 g, 1.50 mmol) and triethylamine (0.3 g, 3.00 mmol) was dissolved in anhydrous THF (10 mL). A solution of acryloyl chloride (0.27 g, 3.00 mmol) in anhydrous THF (1.5 mL) was added dropwise to the above solution with temperature kept below 10 °C. The solution was then stirred overnight at an ambient temperature. The solvent was evaporated under reduced pressure, and the crude product was purified by column chromatography using dichloromethane and ethyl acetate (9:1) as the eluent to obtain a dark red product (0.10 g, 20 %). $^1\text{H NMR}$ (400 MHz, $\text{d}_6\text{-DMSO}$, δ ppm): δ = 13.12 (s, 1H), 7.76 (d, 2H, J = 9.2 Hz), 7.74 (d, 1H, J = 2 Hz), 7.61 (d, 1H, and t, 1H, J = 3.2 Hz), 7.48 (m, 1H, J = 3.2

Hz), 6.97 (d, 2H, J = 9.2 Hz), 6.28 (d, 1H, J = 16 Hz), 6.13 (dd, 1H, J = 10.4 Hz), 6.95 (d, 1H, J = 10.4 Hz), 4.33 (t, 2H, J = 5.2 Hz), 3.81 (t, 2H, J = 5.6 Hz), 3.08 (s, 3H).

Synthesis of Indicator polymer P-MR.



P-MR

An indicator monomer **4** (30 mg), 2-hydroxyethyl methacrylate (570 mg), and AIBN (3 mg) were dissolved in DMSO (1.5 mL). The solution was degassed with nitrogen and heated at 60 °C overnight to obtain a viscous solution. The solution was added dropwise to diethyl ether to precipitate out the polymer product as a dark-red solid polymer (530 mg) ¹H NMR

(400 MHz, d₆-DMSO, δ ppm): δ 7.71, 7.58, 7.46, and 6.87 (b, MR peaks, 0.14 H), 4.78 (b, 1H), 3.86 (b, 2H), 3.53 (b, 2H), 1.75 (b, 2H), 0.90 and 0.73 (b, 3H).

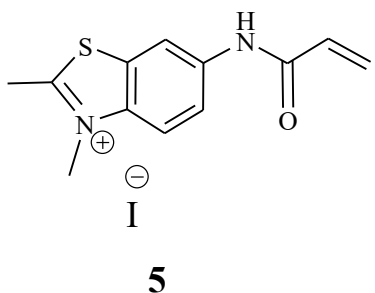
Preparation of thin film to test photo-induced pH pulse.

To test the photo-induced pH pulse in the P1-mPAH/P-MR film, a mixture of 20 mg of P1NH-*m*PAH and 5 mg of P-MR was dissolved in 0.5 mL of methanol assisted by ultrasonication. The solution was drop casted on glass slides and dried in a ventilation hood for 15 min at room temperature and then on a heat plate (plate

temperature 70 °C) for 15 min. A reddish thin film was obtained and kept in the dark until it was tested. Before the test, the thin film on a glass substrate was cut into small pieces that fitted into a regular quartz cell for a UV-Vis spectrometer. The sample was soaked in water for 15 min and then in PBS buffer for 30 min, after which the color of the film changed to orange. It was then put into a quartz cell filled with a PBS buffer with a tilt angle (Figure 5.2). The sample was irradiated from the top by a 470 nm LED array, and the UV-Vis absorption change was monitored by a UV-Vis spectrometer during and after irradiation. The photon flux of the irradiation ($\sim 425 \mu\text{mol s}^{-1} \text{m}^{-2}$, 11 mW/cm^{-2}) was measured by putting the detector of a handheld quantum meter at the same distance to the LED as the center of the sample. As described above, the sample was irradiated three times. Each irradiation lasted about 1 min, and the interval between the irradiation was ~ 8 h. To quantify the pH change, PBS buffer was removed from the cell 8 h after the last irradiation. A pH 6 buffer (citric acid/ Na_2HPO_4) was added slowly to the cell without moving the position of the sample. A UV-Vis spectrum was collected after the sample was kept in the new buffer for ~ 15 min. The pH 6 buffer was then substituted by a pH 5.5 buffer, and UV-Vis spectrum was collected after the sample was kept in the new buffer for ~ 15 min.

6.3. Chapter 3 Synthesis and Characterization

Synthesis of compound 5: 6-acrylamid-2, 3-dimethyl-benzothiazolium iodide.

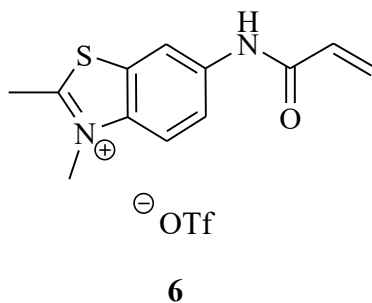


6-acrylamide-2-methyl-benzothiazole **1** (0.5 g, 2.3 mmol) was dissolved in a minimum amount of DMF ~2mL, and then iodomethane (0.57 mL, 9.0 mmol) was added dropwise with a syringe. 1 mg of (BHT) was added to avoid any polymerization

reaction. The mixture was refluxed overnight and then cooled to room temperature. The resulting precipitate was filtrated and washed thoroughly with EtOAc and dried at room temperature, yielding (93%, yellow). **¹H NMR** (400 MHz, d6-DMSO, δ ppm): δ = 10.71 (s, 1H), 8.91 (s, 1H), 8.23 (d, 1H, J = 9.2 Hz), 7.91 (d, 1H, J = 9.2 Hz), 6.5 (dd, 1H, J = 10 Hz), 6.34 (d, 1H, J = 16.8 Hz), 5.86 (d, 1H, J = 10Hz), 4.15 (s, 3H), 3.11 (s, 3H).

Synthesis of compound 6: 6-acrylamidee 2, 3-dimethyl-benzothiazolium triflate.

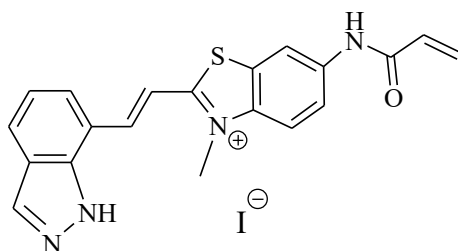
6-Acrylamide-2-methyl-benzothiazole **1** (0.5 g, 2.3 mmol) was dissolved in a minimum amount of DMF ~1.5 mL and then add 3 mL of PhCH₃. The solution was stirred at room temperature 15 mins



under N₂. After that, 1 mg of (BHT) was added, and methyl

trifluoromethanesulfonate (0.8 mL, 7.0 mmol) was added dropwise by syringe. The mixture was heated up to 60 °C and kept stirring overnight. Then the resulting precipitate was filtered and washed out with DCM to yield the final product #6 white-pale (70% yield). ¹H NMR (400 MHz, d6-DMSO, δ ppm): δ = 10.71 (s, 1H), 8.91 (s, 1H), 8.23 (d, 1H, J = 9.2 Hz), 7.86 (d, 1H, J = 9.2 Hz), 6.46 (dd, 1H, J = 10 Hz), 6.35 (d, 1H, J = 15.2 Hz), 5.86 (d, 1H, J = 10Hz), 4.86 (t, 2H, J = 8.4Hz), 3.15 (s, 3H), 2.63 (t, 2H, J = 6.4Hz), 2.14 (m, 2H, J = 6.8 Hz).

Synthesis monomer-2; NH-mPAH2



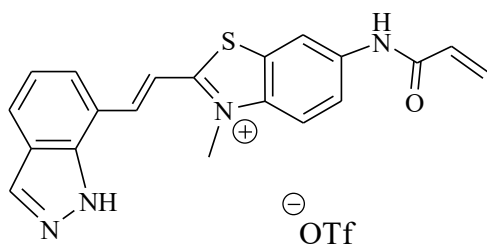
Monomer-2
NH-mPAH2

6-Acrylamide-2,3-dimethyl-benzothiazolium iodide **5** (0.2 g 0.58 mmol) was dissolved in 6 mL of mixed solvents ACN: MeOH, 3: 1 in a sealed tube. Then 1H-indazole-7-benzaldehyde (100 mg, 0.68 mmol), a catalytic amount of ammonium

acetate, and 1mg of BHT were added and refluxed for 2 days. The precipitate was filtered and washed with acetone to give a dark orange pure product (monomer-1, 60 % yield). ¹H NMR (400 MHz, d6-DMSO δ ppm): δ = 13.93 (s, 1H), 10.77 (s, 1H), 8.98 (s, 1H), 8.54 (d, 1H, J = 16 Hz), 8.3 (s, 1H), 8.24 (d, 1H, J = 9.2 Hz), 8.23 (d, 1H, J = 7.6), 8.00 (d, 1H, J = 16 Hz), 8.06 (d, 1H, J = 8 Hz), 7.90 (d, 1H, J

= 9.2 Hz), 7.34 (t, 1H, J = 7.6 Hz), 7.5 (dd, 1H, J = 10 Hz), 6.37 (d, 1H, J = 16.8 Hz), 5.88 (d, 1H, J = 10 Hz), 4.38 (s, 3H).

Synthesis of monomer-3; NH-mPAH3



Monomer-3

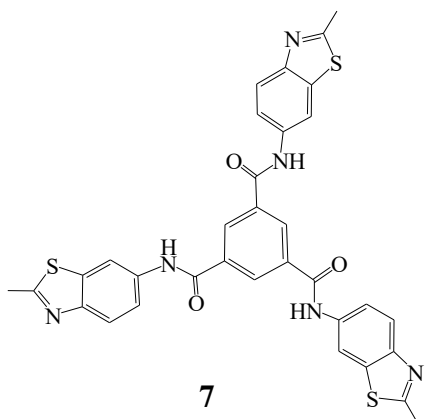
NH-mPAH3

6-acrylamide 2, 3-dimethyl-benzothiazolium triflate; **6** (0.3 g 0.78 mmol) was dissolved in 5 mL of mixed solvents EtOH: ACN, 4: 1 in a sealed tube. Then 1H-indazole-7-benzaldehyde (0.12 g, 0.82 mmol), a catalytic amount

of ammonium acetate, and 1mg of BHT were added and refluxed for 2 days. The dark orange precipitate was filtered and washed with acetone to give the pure product (monomer-3, 70 % yield). ¹H NMR (400 MHz, d₆-DMSO δ ppm): δ = 13.93 (s, 1H), 10.77 (s, 1H), 8.98 (s, 1H), 8.54 (d, 1H, J = 16 Hz), 8.3 (s, 1H), 8.24 (d, 1H, J = 9.2 Hz), 8.23 (d, 1H, J = 7.6), 8.00 (d, 1H, J = 16 Hz), 8.06 (d, 1H, J = 8 Hz), 7.90 (d, 1H, J = 9.2 Hz), 7.34 (t, 1H, J = 7.6 Hz), 7.5 (dd, 1H, J = 10 Hz), 6.37 (d, 1H, J = 16.8 Hz), 5.88 (d, 1H, J = 10 Hz), 4.38 (s, 3H).

Synthesis of compound 7: 1,3,5-tricarboxamide-tris(2-methylbenzothiazol-6-yl)

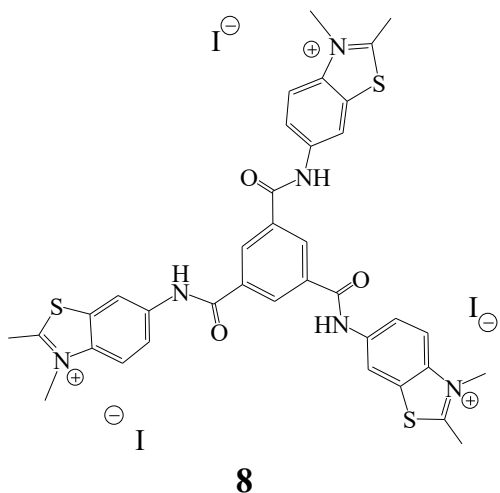
benzene



In a 25 mL round bottom flask, 2-methylbenzothiazol-6-acrylamide (0.2 g, 2.25 mmol) was dissolved in 2 mL DCM and cooled to 0 °C using an ice bath. C₅H₅N (0.18 mL, 2.27 mmol) was added to the solution.

Then, a solution of 1,3,5-benzenetricarbonyl trichloride (0.2 g, 0.75 mmol) in 2 mL DCM was added dropwise to the ice-cooled solution. The mixture was stirred overnight at room temperature. After that, the crude product was poured into 20 mL water, and then the insoluble precipitate was filtered off and washed vigorously with water and dried in open air. (70 % yield). ¹H NMR (400 MHz, d₆-DMSO δ ppm): δ = 10.85 (s, 3H), 8.76 (s, 3H), 8.60 (s, 3H), 7.92 (d, 3H, J = 8.8 Hz), 7.81 (d, 3H), 2.78 (s, 9H).

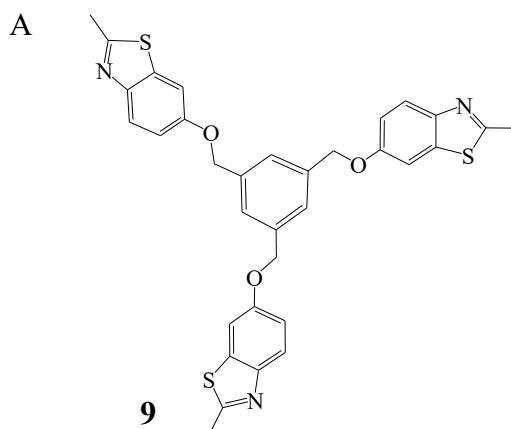
Synthesis of compound 8: Trimer (carboxamide-bezothiazolium iodide)-benzene



Tri-carboxamide **7** (0.10 g 0.15 mmol) was dissolved in PhCH₃:DMF 2:1 mL and stirred vigorously at room temperature 15 min. Iodomethane (0.11 mL, 1.84 mmol) was syringed into the mixture dropwise, and the mixture was refluxed overnight, cooled to room temperature, filtered, and washed with EtOAc. White precipitate was

left out to dry slowly in open air (85% yield). ¹H NMR (400 MHz, d₆-DMSO δ ppm): δ = 10.85 (s, 3H), 8.76 (s, 3H), 8.60 (s, 3H), 7.92 (d, 3H, J = 8.8 Hz), 7.81 (d, 3H), 2.78 (s, 9H). Including DMF peaks at 7.95, 2.89, and 2.73 ppm.

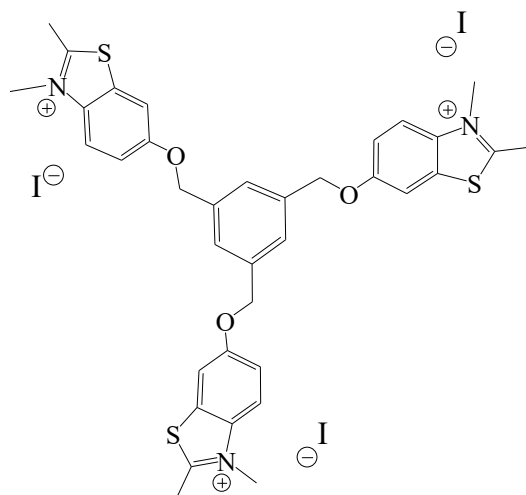
Synthesis of compound 9: Tri-(benzyloxy-thiazole)-benzene.



mixture of 6-hydroxy-2-methylbenzothiazole (0.28 g, 1.69 mmol) and 1,3,5-tris(bromomethyl)benzene (0.2 g, 0.56 mmol) and potassium carbonate (0.38, 2.80 mmol) in acetone was refluxed under nitrogen overnight. After completion of the reaction, the mixture was filtrated and washed with DCM (3X).

The filtrate was concentrated under vacuo, and the crude obtained was purified by column chromatography on silica gel with DCM:EtOAc (7:3) as an eluent to afford the pure **9** (83% yield). $^1\text{H NMR}$ (400 MHz, CDCl_3): δ = 7.83 (d, 3H, J = 9.2), 7.51 (s, 3H), 7.34 (s, 3H), 7.12 (d, 3H, J = 9.2 Hz), 5.15 (s, 6H), 2.79 (s, 9H). Impurities that appeared included ethyl acetate at 4.12, 2.05, and 1.31 ppm as well as acetone at 2.17 ppm.

Synthesis of compound 10: Try-(benzyloxy-thiazolium methyl iodide) benzene.



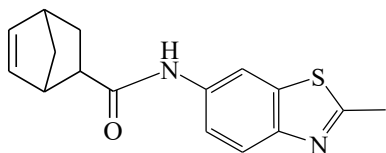
10

Tri-(benzyloxy-thiazole)-benzene, **9** (0.10 g 0.17 mmol) was dissolved in minimum PhCH_3 :DMF 2:1 and stirred vigorously. Iodomethane (0.11 mL, 2.00 mmol) was added to the mixture dropwise. The mixture was refluxed overnight and cooled to room temperature, filtered, and washed with acetone. Bright yellow solid precipitate

was dried out in open air (85 % yield). $^1\text{H NMR}$ (400 MHz, d_6 -DMSO δ ppm): δ = 8.20 (d, 3H, J = 9.6 Hz), 8.10 (s, 3H), 7.66 (s, 3H), 7.56 (d, 3H, J = 9.6Hz), 5.28 (s, 6H), 4.15 (s, 9H), 3.10 (s, 9H). Including acetone peak at 2.09 ppm.

6.4. Chapter 4 Synthesis and Characterization

Synthesis of compound 11: Carboxamide norbornene benzothiazole



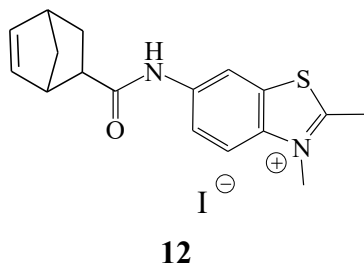
11

5-Norbornene-2-carboxylic acid, a mixture of endo and exo, (0.4 g, 2.42 mmol) was dissolved in 5 equivalents of thionyl chloride. A drop of DMF was added to the mixture, refluxed overnight under nitrogen, and then cooled to room temperature.

Unreacted thionyl chloride was removed under reduced pressure, resulting in norbornene carbonyl chloride (NBCOCl). In situ, 2 mL dry DCM was added to the resultant NBCOCl, and then a cooled solution of 2-methyl-6-amino-benzothiazole (0.4g, 2.42 mmol) was added. The reaction mixture was dissolved in dry DCM and 1.2 equivalents of Et₃N, stirred 15 min at room temperature, and then refluxed overnight. After cooled to room temperature, the mixture was diluted with DCM (20 mL), washed with water (2 x 20 mL) followed by a saturated aqueous NaHCO₃ solution (2 x 20 mL), dried over anhydrous Mg₂SO₄, filtered, and concentrated in the vacuo. The crude material was purified by column chromatography eluting with hexane/hexane (4:1) to yield a white powder product (50% yield). ¹H NMR (400 MHz, d₆-DMSO δ ppm, mixture of endo and exo isomers): δ = 10.1, 9.97 (s, 1H), 8.45, 8.36 (d, 1H, J = 2.0 Hz), 7.8 (t, 1H, J = 8.4 Hz), 7.49 (d, 1H, J = 2.0 Hz), 6.20,

6.16, 5.85 (s, m, m, 2H), 3.29, 2.94 (br, 1H), 3.05, 2.88 (s, 2H), 2.75 (s, 3H), 2.32, 1.88, 1.39 (m, m, m, 2H), 1.32 (m, 2H).

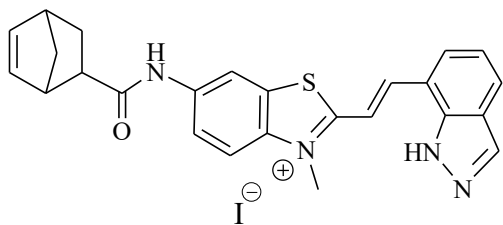
Synthesis of compound 12: Carboxamide norbornene benzothiazolium



Carboxamide norbornene benzothiazole **11** (0.3, 1.00 mmol) was dissolved in minimum DMF ~ 0.6 mL. Then, iodide methane (0.26 mL, 4.17 mmol) was syringed dropwise, and the reaction mixture was refluxed overnight. The white precipitate was

collected by filtration and washed with EtOAc and kept drying in open air (93 % yield). **¹H NMR** (400 MHz, d₆-DMSO δ ppm, mixture of endo and exo isomers): δ = 10.56, 10.35 (s, 1H), 8.89, 8.80 (d, 1H, J = 2.0 Hz), 8.19 (t, 1H, J = 8.4 Hz), 7.83 (d, 1H, J = 2.0 Hz), 6.22, 6.19, 5.85 (s, m, m, 2H), 4.13 (s, 3H), 3.32, 2.98, (s, 1H), 3.12, 3.04, 2.90 (m, 2H), 3.10 (s, 3H), 2.35, 1.85, 1.39 (m, m, 2H), 1.35 (m, 2H).

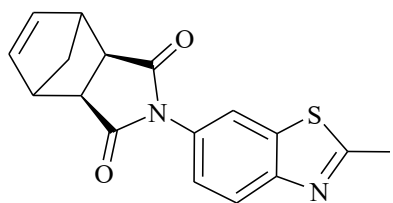
Synthesis of monomer 4: NHmPAH4



In a sealed tube, carboxamide norbornene benzothiazolium, **12** (0.2 g, 0.46 mmol) was dissolved in 4 mL EtOH. 1H-indazole-7-benzaldehyde (0.08 g, 0.56 mmol) was added and then refluxed for

two days. After cooled to room temperature, the the dark orange precipitate was filtered and washed with cooled EtOH to give a pure product (76% yield). **¹H NMR** (400 MHz, d₆-DMSO δ ppm, mixture of endo and exo isomers): δ = 13.90 (s, 1H), 10.63, 10.42 (s, 1H), 8.96, 8.87 (s, 1H), 8.52 (d, 1H, J = 16 Hz), 8.30 (s, 1H), 8.21 (m, 2H), 8.06 (m, 2H), 7.81 (d 1H, J = 9.2 Hz), 7.33 (t, 1H, J = 7.2 Hz), 6.23, 6.20, 5.87 (s, m, m, 2H), Hz) 4.37 (s, 3H), 3.14, 2.38, (m, m 1H), 3.00, 2.93, 1.69 (s, d, d, 2H), 1.89, 1.45 (m, m, 2H), 1.36 (m, 2H).

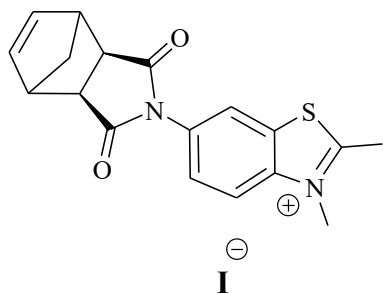
Synthesis of compound 13: Imide norbornene benzothiazole.



13

In a sealed tube, cis-5-norbornene-exo-anhydride (0.68 g, 4.13 mmol) was stirred in 10 mL of PhCH₃: DMF (4:1) at room temperature. An equivalent of Et₃N and a solution of 2-methyl-6-amino-benzothiazole (0.67 g, 4.08 mmol) in PhCH₃: DMF (4:1) 5 ml were added to the mixture. The reaction mixture was heated at 160 °C for 4 h and allowed to cool to room temperature. Then the solvents were removed in vacuo, filtrated, washed by ether, and dried out in the air to give a pure white solid (78%, yield). **¹H NMR** (400 MHz, d₆-DMSO δ ppm = 8.00 (d, 2H, J = 8.8 Hz), 7.35 (d, 1H, J = 8.4 Hz), 6.42 (t, 2H, J = 4 Hz), 3.23 (m, 2H), 2.89 (m, 2H), 2.83 (s, 3H), 1.49 (m, 2H).

Synthesis of compound 14: Imide norbornene benzothiazolium methyl iodide.

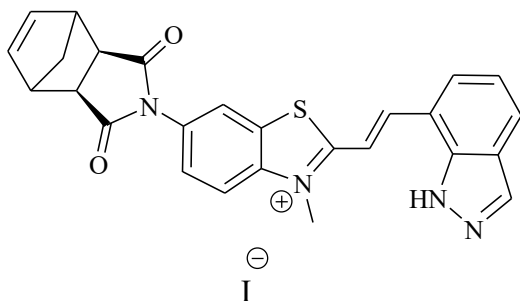


14

Imide norbornene benzothiazole, **13** (0.3 g 0.97 mmol) was dissolved in 2 mL DMF:THF (4:1) and stirred vigorously at room temperature 15 min. Iodomethane (0.24 mL, 3.82 mmol) was syringed into the mixture dropwise, and the mixture was refluxed overnight, cooled to room temperature,

filtered, and washed with THF. White precipitate was left out to dry slowly in open air (85 % yield). $^1\text{H NMR}$ (400 MHz, d_6 -DMSO δ ppm = 8.42 (d, 2H, $J = 9.2$ Hz), 7.83 (d, 1H, $J = 9.2$ Hz), 6.40 (m, 2H, $J = 1.6$ Hz), 4.2 (s, 3H), 3.25 (m, 2H), 3.17 (m, 3H), 2.94 (m, 2H), 1.49 (m, 2H).

Synthesis of monomer 5: NH-mPAH5



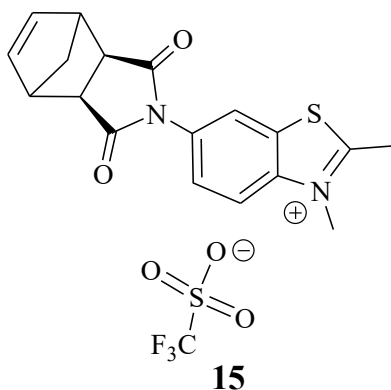
Monomer-5

Imide norbornene benzothiazolium **14** (0.15 g, 0.13 mmol) was dissolved in 3 mL EtOH:H₂O (2:1). A catalytic amount of ammonium acetate and 1H-indazole-7-benzaldehyde (0.06 g, 0.41 mmol) were added and refluxed for two

days. After cooled to room temperature, the dark orange precipitate was filtered and washed with cooled EtOH to give a pure product (62% yield). $^1\text{H NMR}$ (400 MHz,

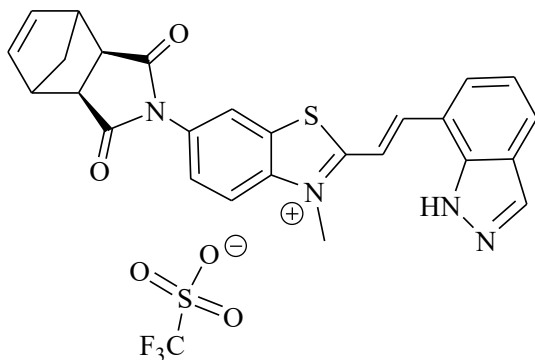
d₆-DMSO δ ppm = 13.94 (s, 1H), 8.60 (d, 1H, J = 16 Hz), 8.50 (s, 1H), 8.39 (d, 1H, J = 9.2 Hz), 8.30 (m, 2H), 8.13 (d, 1H, J = 7.7 Hz), 8.08 (d 1H, J = 8 Hz), 7.83 (d, 1H, J = 9.2 Hz), 7.36 (t, 1H, J = 9.2 Hz), 6.41, (m, 2H), 4.43 (s, 3H), 3.27 (m, 2H), 2.96, (m, 2H), 2.1 (m, 2H). included ethanol peaks.

Synthesis of compound 15: Imide norbornene benzothiazolium methyl triflate.



Imide norbornene benzothiazole **13** (0.5 g 1.61 mmol) was dissolved in 7 mL of THF:DMF (6:1) and stirred vigorously under nitrogen at room temperature 15 min. Methyl trifluoromethanesulfonate (0.55 mL, 4.83 mmol) was syringed into the mixture dropwise, and the mixture was refluxed overnight, cooled to room temperature, filtered, and washed with THF. White precipitate was left out to dry slowly in open air (70% yield). ¹H NMR (400 MHz, d₆-DMSO δ ppm = 8.40 (, 2H, J = 10 Hz), 7.83 (d, 1H, J = 8,8 Hz), 6.40 (t, 2H, J = 1.6 Hz), 4.2 (s, 3H), 3.24 (m, 2H), 3.17 (s, 3H), 2.94 (m, 2H), 1.50 (m, 2H).

Synthesis of monomer 6:

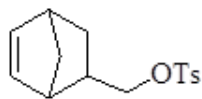


Monomer-6

Imide norbornene benzothiazolium triflate, **15** (0.15, 0.31 mmol) was dissolved in 2 mL MeOH, catalytic amount of ammonium acetate, and 1H-indazole-7-benzaldehyde (0.06 g, 0.37 mmol) and then added to a reaction solution. Then the mixture was

refluxed for two days. After allowed to cool to room temperature, the dark orange precipitate was filtered and washed with cooled MeOH to give the pure product of monomer-6 (52% yield). ¹H NMR (400 MHz, d₆-DMSO δ ppm = 13.96 (s, 1H), 8.67 (d, 1H, J = 16 Hz), 8.51 (s, 1H), 8.40 (d, 1H, J = 9.2 Hz), 8.30 (m, 2H), 8.14 (d, 1H, J = 7.7 Hz), 8.05 (d 1H, J = 8 Hz), 7.84 (d, 1H, J = 9.2 Hz), 7.37 (t, 1H, J = 9.2 Hz), 6.42, (s, 2H), 4.43 (s, 3H), 3.27 (s, 2H), 2.96, (s, 2H), 1.53 (s, 2H). included ethanol peaks.

Synthesis of compound 16;³ Exo, endo-(5-norbornenyl)methyl tosylate

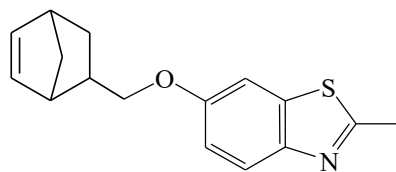


16

To a cooled solution of exo, endo-5-norbornene-2-methanol (1 g, 7.81 mmol) in DCM (10 mL), Et₃N was added (0.95g, 9.4 mmol) and *p*-tosyl chloride (6 g, 31 mmol). The mixture was

stirred overnight at room temperature. Upon the completion of the reaction as monitored by TLC, the solvent was concentrated in vacuo, and the crude product was purified by column chromatography on the silica gel eluting with EtOAc:Hexane; 1:4 to give a pure colorless oily product **16** (90% yield). ¹H NMR (400 MHz, CDCl₃ δ ppm, mixture of *endo* and *exo* isomers): δ = 7.78 (d, 2H, J = 8.1 Hz), 7.49 (d, 2H, J = 8.1 Hz), 6.10 (dd, , 1H J = 5.8, 3.0 Hz), 5.59 (dd, , 1H J = 5.8, 2.9 Hz), 3.74 (dd, 1H, J = 9.6, 6.5 Hz), 3.49 (t, 1H, J = 9.6 Hz), 2.76 (d, 2H, J = 13.2 Hz), 2.45 (s, 3H), 2.28 – 2.10 (m, 2H), 1.74 (ddd, 1H, J = 12.4, 9.3, 3.8 Hz), 1.26 – 1.34 (m, 1H), 1.20 (d, 1H, J = 8.2 Hz).

Synthesis of compound, 17 Exo, endo-(5-norbornenyl)methyl methoxybenzothiazole⁴

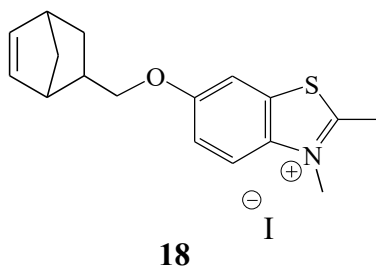


17

A mixture of *exo*, *endo*-(5-norbornenyl)methyl tosylate, **16** (1.1 g, 3.98 mmol), CsCO₃ (1.76 g, 5.43 mmol), and 6-hydroxy-2-methyl benzothiazole (0.5 mg, 3.6 mmol) were dissolved in DMF (10mL) and then heated at reflux for 24 h. Upon the completion of the reaction, the solvent was removed in *vacuo*, and water (50 mL) was added to the residue and then extracted with EtOAc (3 x 50). The combined organic layers were dried over MgSO₄, filtered, and concentrated in *vacuo*. The crude product was purified by flash column chromatography on silica gel using EtOAc:Hexane (10:1)

to obtain pure **17**, a colorless liquid (yield 73%). $^1\text{H NMR}$ (400 MHz, CDCl_3 δ ppm, mixture of *endo* and *exo* isomers): $\delta = 7.80$ (d, 1H, $J = 8.2$ Hz), 7.29 (m, 1H), 7.04 (m, 1H), 6.17-5.96 (m, 2H), 4.12-3.4 (m, 2H), 3.05-2.4 (m, 2H), 2.5-1.9 (m, 1H), 1.5-1.3 (m, 2H), 1.3-0.58 (m, 2H). Included DMF at 8.00, 2.09, and 2,80 ppm. This compound was used without any more purification.

Synthesis of compound 18: Exo, endo-5-norbornenyl methoxybenzothiazolium methyl iodide.

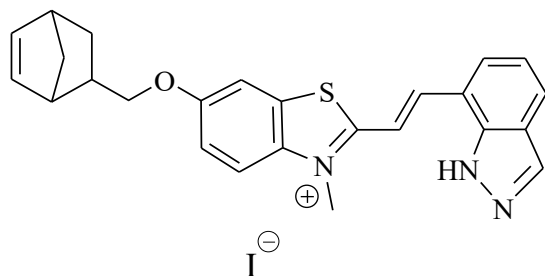


Exo, endo-5-norbornenyl methoxybenzothiazole, **17** (0.2g, 0.73 mmol) was dissolved in minimum PhCH_3 . Iodomethane (0.20 mL, 3.82 mmol) was syringed into the mixture dropwise, and the mixture was refluxed overnight, cooled to room

temperature, filtered, and washed with THF. White precipitate was left out to dry slowly in open air (75% yield).

$^1\text{H NMR}$ (400 MHz, d_6 -DMSO δ ppm, mixture of *exo* and *endo* isomers): $\delta = 8.17$ (m, 1H), 7.98 (d, 1H, $J = 8.1$ Hz), 7.48 (m, 1H), 6.23-5.92 (m, 2H), 4.20-3.6 (m, 2H) 4.15 (s, 3H), 3.09 (s, 3H), 2.90-2.06 (m, 2H), 2.51 (m, 1H), 1.99-1.32 (m, 2H). 1.32-0.57 (m, 2H).

Synthesis of monomer 7: Norbornenyl methoxybenzothiazolium iodide monomer



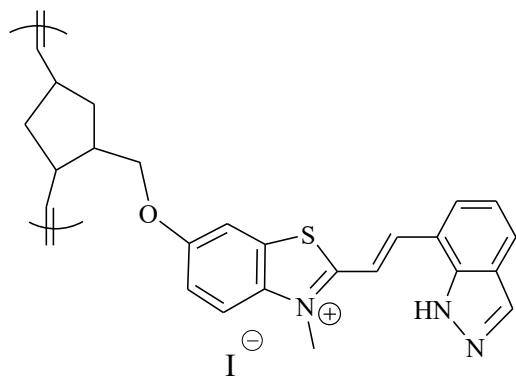
Monomer-7

Exo, endo-5-norbornenyl-methoxybenzothiazolium methyl iodide, **18** (0.1g, 0.24 mmol) was dissolved in 2 mL MeOH, 1H-indazole-7-carbaldehyde (0.34 g, 0.24 mmol), and a catalytic amount of ammonium

acetate was added to the reaction mixture, which was refluxed overnight. After allowed to cool to room temperature, the solid orange precipitate was filtered and washed with cooled MeOH to result in the pure product of monomer-7 (75% yield).

¹H NMR (400 MHz, d₆-DMSO δ ppm, mixture of exo and endo isomers): δ = 13.89 (s, 1H), 8.51 (d, 1H, J= 16Hz), 8.30 (s, 1H), 8.20 (m, 2H), 8.06 (m, 3H), 7.49 (m, 1H), 7.30 (t, 1H, J= 8Hz), 6.29-5.96 (m, , 2H) J = 5.3, 2.8 Hz), 4.39 (s, 3H), 4.29-3.66 (m, 2H), 3.06-2.81 (m, 2H), 2.60 (m, 1H), 1.99-1.39 (m, 2H), 1.34-0.58 (m, 2H).

Synthesis polymer-3: Norbornenyl methoxybenzothiazolium iodide polymer



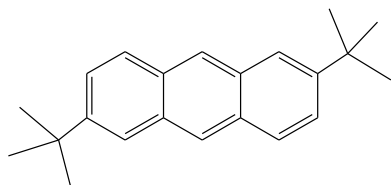
P3NH-mPAH

To a stirred, degassed solution of monomer-7 (60 mg, 0.11 mmol) in DMF (1 mL) at 80° C was syringed a degassed solution of G2 (60 mg, 0.07 mmol) in DMF (0.5 mL). The reaction was left to stir under nitrogen for 20 min and then continued refluxing overnight. The

reaction was cooled to room temperature and quenched with EVE (0.05 mL). The polymer, precipitated in 20 mL PhCH₃, filtered, and washed by acetone to give a solid dark red powder, was kept drying in open air. ¹H NMR (400 MHz, d₆-DMSO δ ppm, mixture of exo and endo isomers): δ = 13.90 (s, 1H), 8.53 (d, 1H, J= 16Hz), 8.30 (s, 1H), 8.23 (d, 1H, J= 8Hz), 8.18 (br, 1H), 8.87-6.81 (br, 9H, mPAH), 6.67-5.03 (br, 2H), 4.66-3.620 (br, 5H), 3.20-1.00 (br, overlapping resonances in NBs range peaks complicate definitive integration peaks including acetone peak at 2.09 ppm

6.5. Chapter 5 Synthesis and Characterization

Synthesis of compound **19**; 2, 6-di-tert-butylanthracene⁵

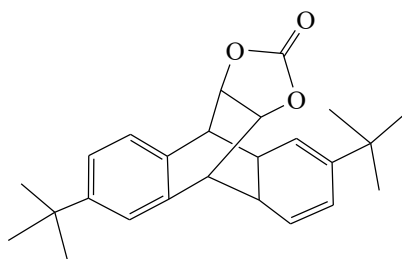


19

A mixture of anthracene (05.00 g, 28.05 mmol), tert-butyl alcohol (08 mL, 84.16 mmol), and trifluoroacetic acid (TFA) (35 mL) was refluxed overnight. The crude, black product was cooled to

room temperature and then treated with solid Na₂CO₃. Afterwards, the DI water (80 mL) and hexane (80 mL) were added to the mixture. The organic phase was extracted, and then dichloromethane (DCM) ~20 mL was added to make a clear solution, which was dried by MgSO₄ and filtered. After the solvent was removed by vacuo, the product was treated with hexane and refrigerated about 1 hour. Then it was filtered, washed with cold hexane, and dried to obtain white solid **19** (04.63g, 57%). ¹H NMR (400 MHz, CDCl₃, δ ppm): δ = 8.32 (s, 2H), 7.94-7.92 (d, 2H, J= 8.8Hz), 7.86 (s, 2H), 7.55-7.53 (dd, 2H, J= 8.8Hz), 1.44 (S, 18H).

Synthesis of compound **20**:

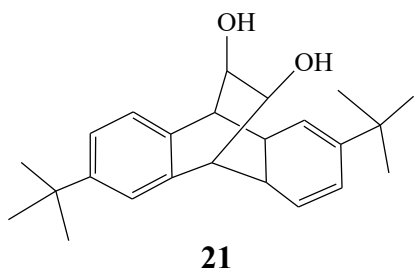


20

Compound **20** was prepared by a Diels Alder reaction. A solution of **19** (1.0 g, 3.5 mmol) and 2 mL of vinylene carbonate in dry xylene (4 mL) was refluxed in an autoclave at 180 C for 3 days. The solvent was removed in vacuo. The crude

product was collected by filtration and washed with cold hexane. The final product was a white solid after drying (1.0 g, 77%). $^1\text{H NMR}$ (400 MHz, CDCl_3 , δ ppm): $\delta = 7.38$ (s, 2H), 7.38-7.22 (m, 4H), 4.87 (t, 2H), 4.64 (d, 2H), 1.29 (s, 18H).

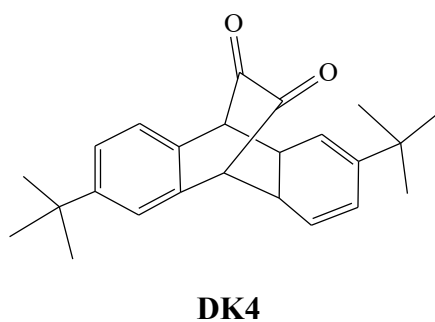
Synthesis of compound 21:



The compound **20** (1.0 g, 2.6 mmol) was added to a mixture of 1,4-dioxane (10 mL) and 4 M NaOH (10 mL). The mixture was refluxed under nitrogen for 2 h and then cooled down to room

temperature. The solution was then neutralized by 1 M HCl, diluted with water, and extracted with DCM twice. The combined organic phases were dried over Na_2SO_4 . The solvent was removed in vacuo, and the crude product was washed with cold hexane to yield a white solid (0.9 g, 96%). $^1\text{H NMR}$ (400 MHz, CDCl_3 , δ ppm): $\delta = 7.38$ (d, 1H), 7.32 (d, 1H, $J=8$ Hz), 7.31-7.14 (m, 4H), 4.35 (s, 2H), 4.04 (s, 2H).

Synthesis of compound DK4:

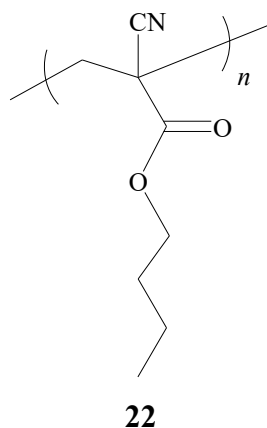


Under nitrogen, trifluoroacetic anhydride (0.62 mL, 4.2 mmol) was added dropwise to a mixture of anhydrous DMSO (0.4 mL, 0.5 mmol) and anhydrous DCM (22 mL) at -78 °C.

After stirring for 10 min, a solution of **2** (0.52 mg, 1.5 mmol) in anhydrous DCM/DMSO (2:1; 6 mL) was added to the above

mixture over 20 min and stirred for an additional 2 hours at the same temperature. Next, triethylamine (1.4 mL, 10.0 mmol) was added dropwise and stirred for 2 hours. Then the mixture was warmed to room temperature and poured into 50 mL of 2 M HCl. DCM was added to the mixture, and the organic phase was separated and dried over Na₂SO₄. The solvent was removed by vacuo, and the crude product was purified by column chromatography using Hexane:EtOAc (5:1) in the dark to yield a yellow solid (0.21g, 48%). ¹H NMR (400 MHz, CDCl₃, δ ppm): δ = 7.461 (s, 2H), 7.40 (s, 4H), 4.944 (s, 2H), 1.3 (s, 18H) IR: 1735 cm⁻¹ (C=O stretch). HRMS (ESI) M+Na⁺ (369.1798, cal. 369.1831).

Synthesis of compound 22: poly butylcyanoacrylate (PBCA)



To a test tube in a glove box was added 2 mL of n-butyl cyanoacrylate, BCA, 20 mg of dichloroacetic acid, and 12 mg of AIBN. The mixture was thoroughly degassed and then heated at 60° C overnight. The resultant polymer was dissolved in a small amount of THF. The THF solution was dropped into methanol to precipitate the poly butyl

cyanoacrylate PBCA as a white solid. ¹H NMR (400 MHz, CDCl₃): δ = 4.8-3.7 (br, 2H), 1.97-1.57 (br, 2H), 1.57-1.28 (br, 2H), 1.14-0.74 (br, 3H).

Synthesis of DK4/PBCA nanoparticles:

To synthesize the DK4/PBCA nanoparticles, 5.0 mg of DK4 and 20 mg of PBCA were dissolved in 1.0 mL acetone. The solution was added dropwise using a syringe needle to aqueous solution of pluronic F127 (1.0%, 30.0 ml) and stirred at 700 rpm. After addition, the mixture was stirred in a ventilation hood for an hour to evaporate the acetone. The resultant nanoparticle suspension was diluted to 200 mL and stored in a refrigerator at 4 °C. The procedure was conducted in the dark, and the final suspension was protected from light using aluminum foil.

Measurement of CO Release from DK4 Under Irradiation

A solution of DK4 in a mixture of DMSO (5%) and water (0.250 mM, 2.5 mL) was prepared in the dark in a glass vial, which was then put in a glass container with a Drager Pac3500 CO detector. The container was sealed, and the solution was irradiated by a 470 nm LED light outside the container. The reading of the meter was recorded after 20 min. Calculations from the average of three separate experiments show that $88.0 \pm 9\%$ of CO (two for each molecule) was released. The uncertainty of the CO is estimated from the weight, volume, and concentration measurements. The number of released CO, N_{CO} (mol) was calculated using the following equation⁵:

$$N_{CO} = \frac{pV_g}{RT} + cV_l = p\left(\frac{V_g}{RT} + \frac{V_l}{k}\right)$$

where p is the partial pressure of the CO detector readings. V_g is volume of the gas phase (373 mL); V_l is liquid phase (2.5 mL); R is $0.08205 \text{ L}\cdot\text{atm}\cdot\text{mol}^{-1}\cdot\text{K}^{-1}$; T is Temperature; c is CO concentration in the liquid phase; and k is Henry's law constant of CO in water ($1052.63 \text{ L}\cdot\text{atm}\cdot\text{mol}^{-1}$ at $25 \text{ }^\circ\text{C}$).

Cell Culture Analysis

Primary human umbilical vein endothelial cells (HUVECs) were cultured in standard cell culture conditions (95% air, 5% CO₂, and 37 °C). The culture media were Endothelial Cell Growth Medium MV, ECs growth supplement, and 1% penicillin/streptomycin. For nanoparticle biocompatibility, ECs seeded at a density of 5,000 cells/cm² on TCPS, and single doses of DK4+NP suspensions were added after 24 hours of seeding to allow for attachment of cells before treating. The biocompatibility of nanoparticles was tested both with (pre-activated) and without (non-activated) activation of the nanoparticles prior to adding the cells. Pre-activation was performed with a 470 nm LED light for 5 min. Regular media changes were performed every 2 days until the endpoints. The DNA Assay was used to measure cell density at days 3 and 7 following standard procedures. A cell-permeant nuclear counterstain emits blue fluorescence when bound to dsDNA. Significance was determined using one-way ANOVA with Tukey comparison for six samples per condition ($p < 0.05$). Cells were also stained with a Live/Dead stain (calcein-AM/ethidium homodimer) and imaged at day 11 with a Nikon DEclipse

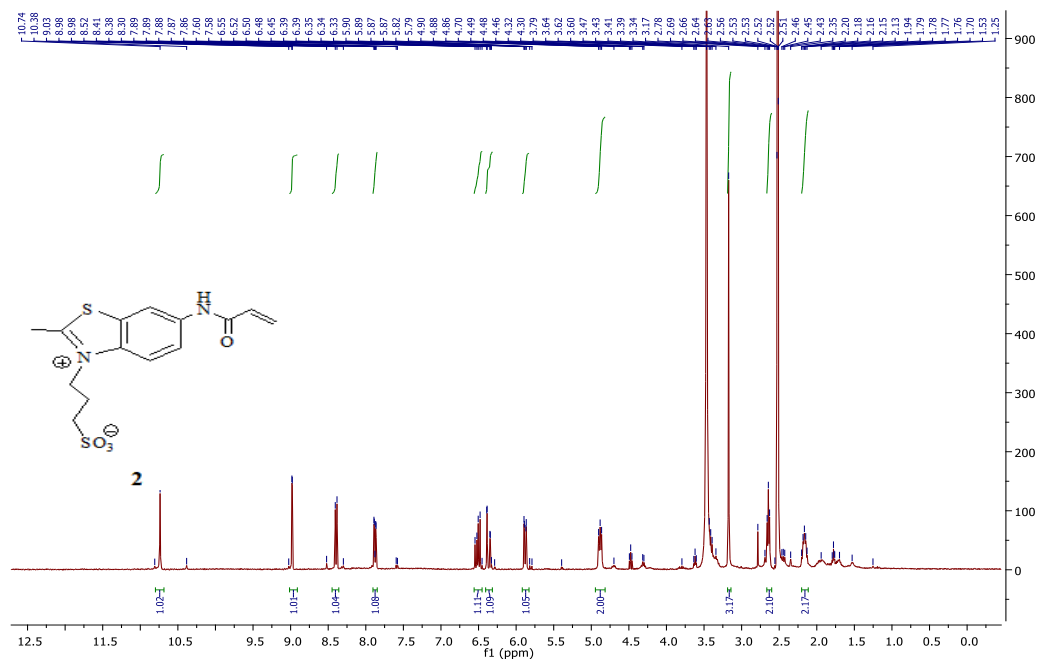
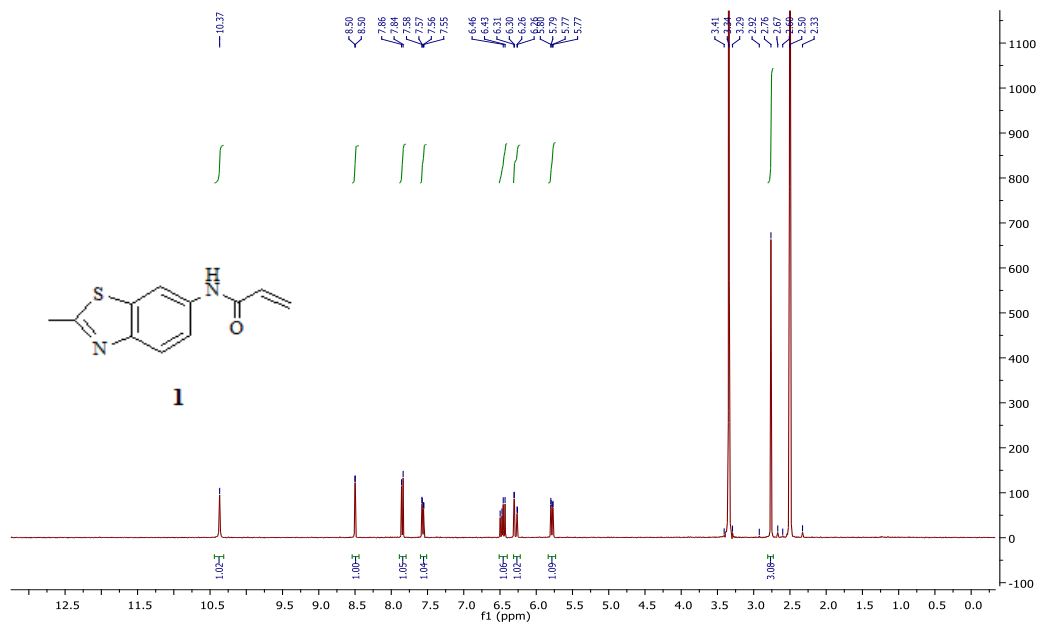
confocal microscope. For calcein-AM, a 488 nm laser and 515 ± 30 nm bandpass filter were used. For ethidium homodimer, a 561 nm laser and 605 ± 75 nm bandpass filter were used.

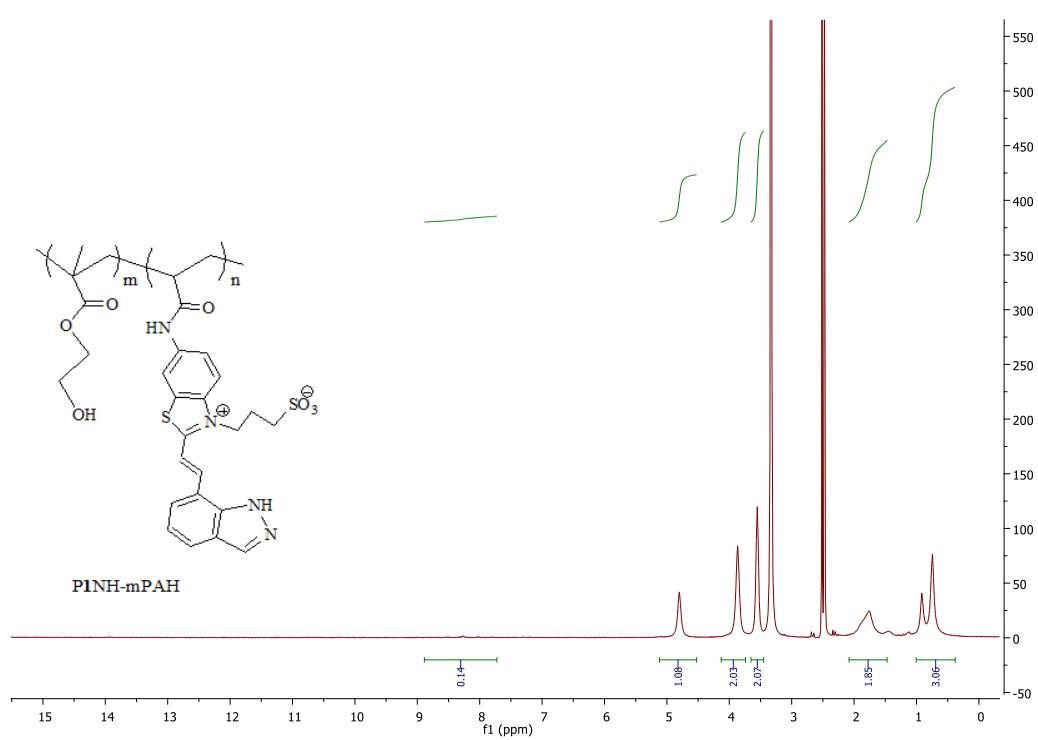
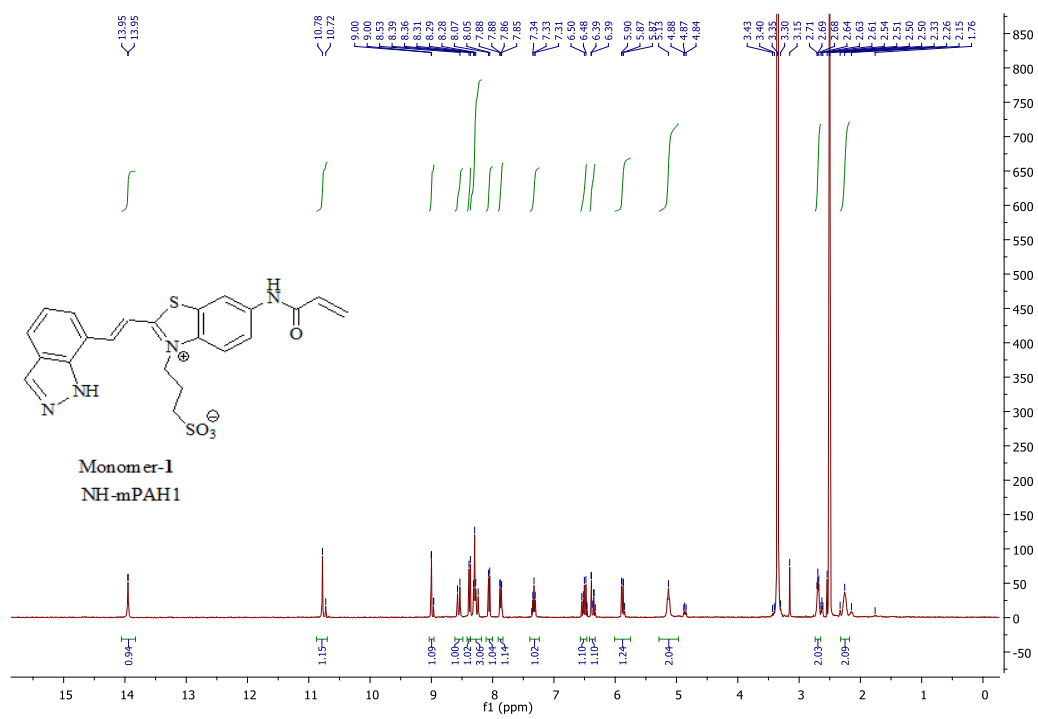
6.6. References.

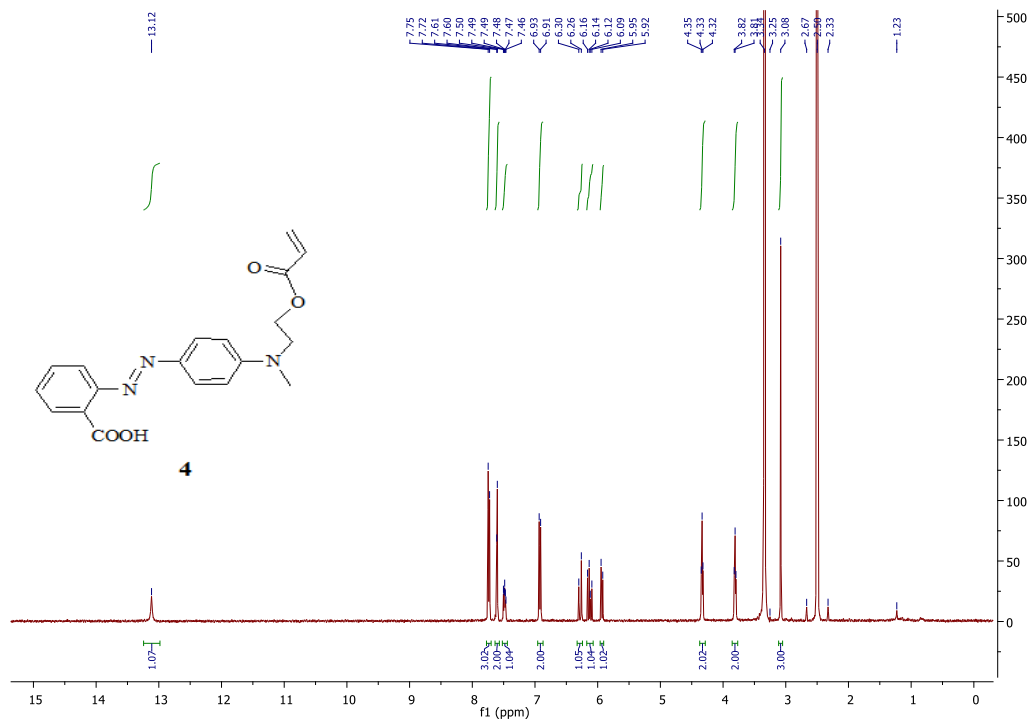
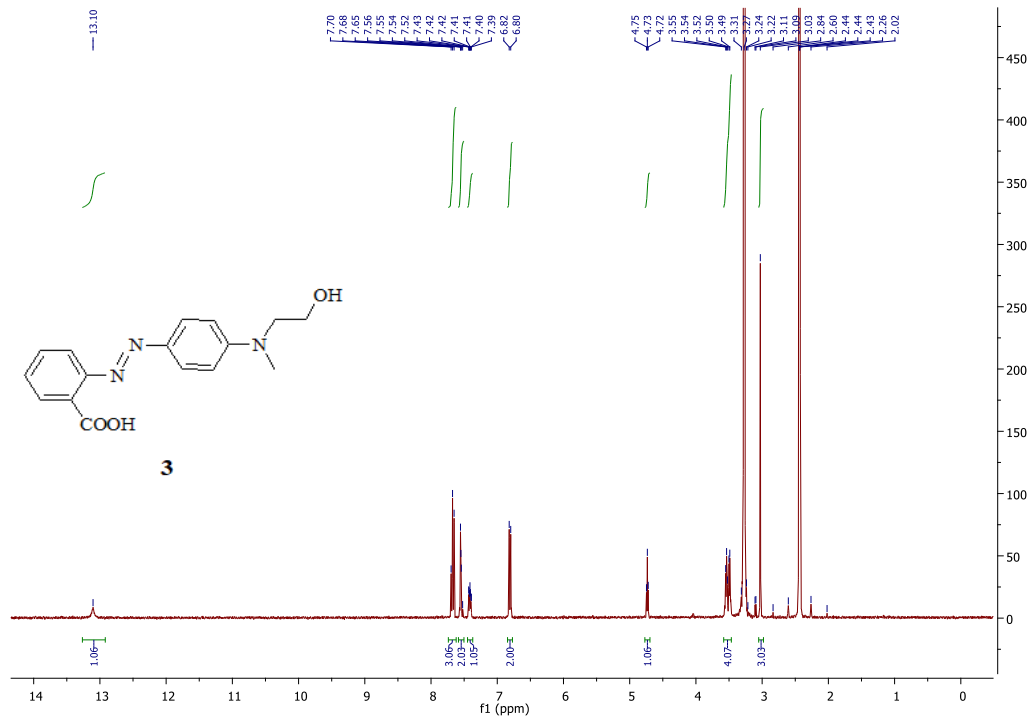
1. Shi, Z.; Peng, P.; Strohecker, D.; Liao, Y. Long-Lived Photoacid Based upon a Photochromic Reaction. *J. Am. Chem. Soc.* **2011**, *133*, 14699–14703.
2. Abeyrathna, N.; Liao, Y. A reversible photoacid functioning in PBS buffer under visible light. *J. Am. Chem. Soc.*, **2015**, *137*, 11282-11284.
3. Wanner, J., Romashko, D., Werner, D. S., May, E. W., Peng, Y., Schulz, R., ... and Thomson, S. Reversible linkage of two distinct small molecule inhibitors of Myc generates a dimeric inhibitor with improved potency that is active in myc over-expressing cancer cell lines. *PloS one*, **2015**, *10*, e0121793
4. Dewick, P. M. Benzyl p-toluenesulphonate as an O-benzylating agent for the protection of phenols. *Synth. Commun.*, **1981**, *11*, 853-857.
5. Niladari Raju, M. V.; Mohanty, M. E.; Bangal, P. R.; Vaidya, J. R. Synthesis and ultrafast dynamics of a donor–acceptor–donor molecule having optoelectronic properties. *J. Phys. Chem. C.*, **2015**, *119*, 8563-8575.
6. Hasegawa, U.; Van Der Vlies, A.; Simeoni, E.; Wandrey, C.; Hubbell, J. Carbon monoxide-releasing micelles for immunotherapy, *J. Am. Chem. Soc.*, **2010**, *132*, 18273-18280.

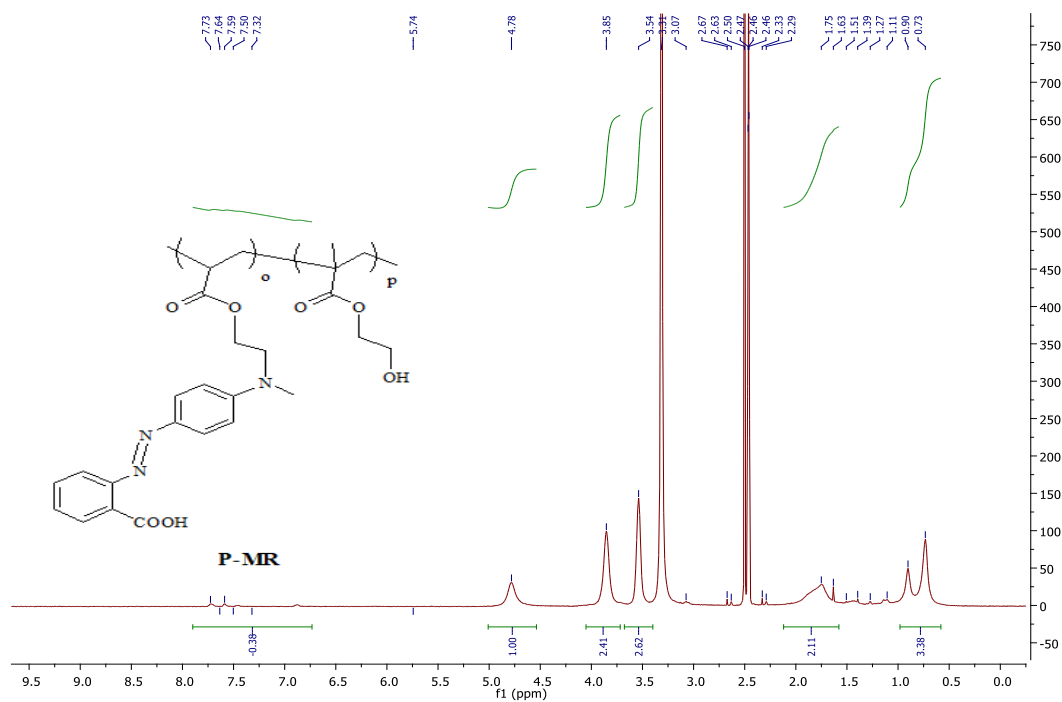
6.7. Appendices

6.7.1. Selected NMR Spectra for Chapter 2

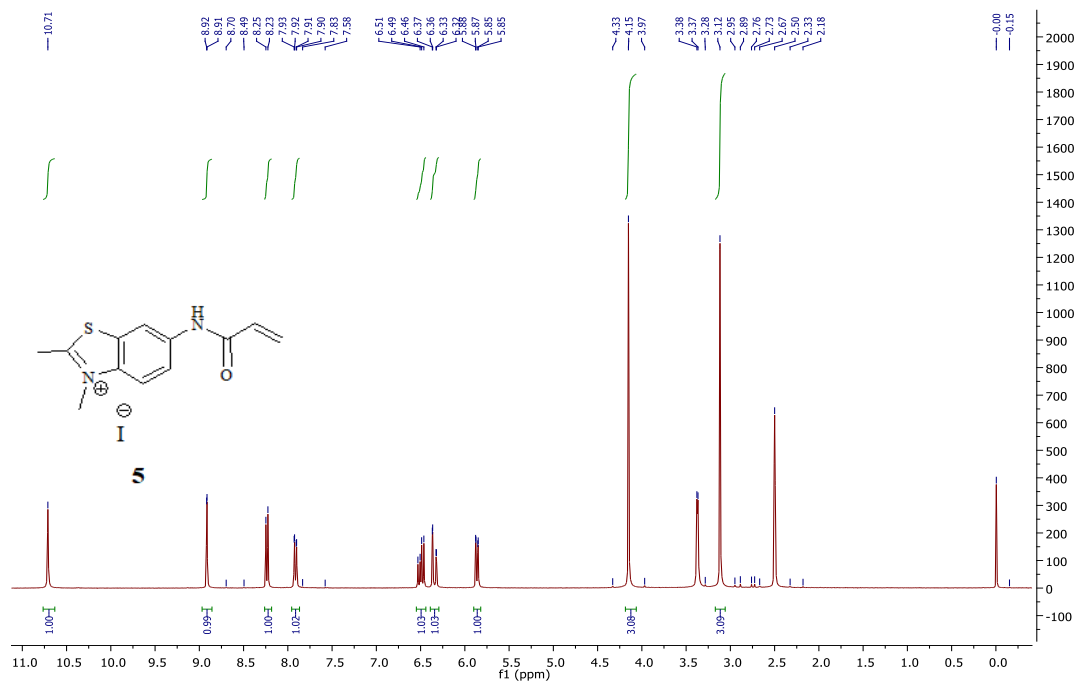


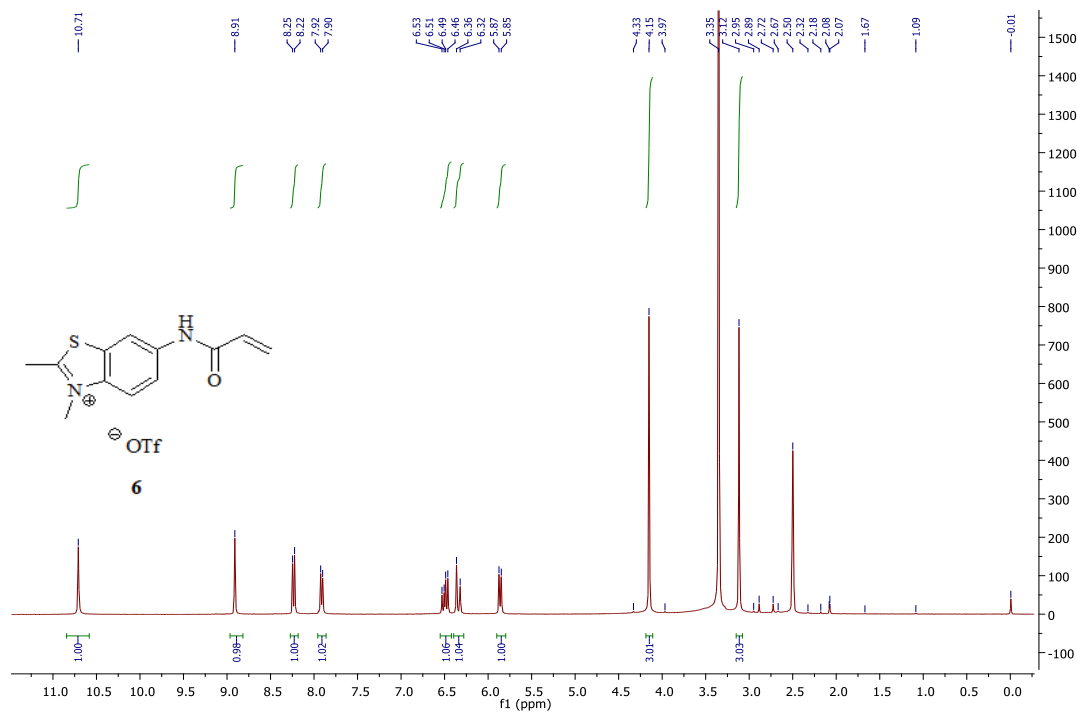
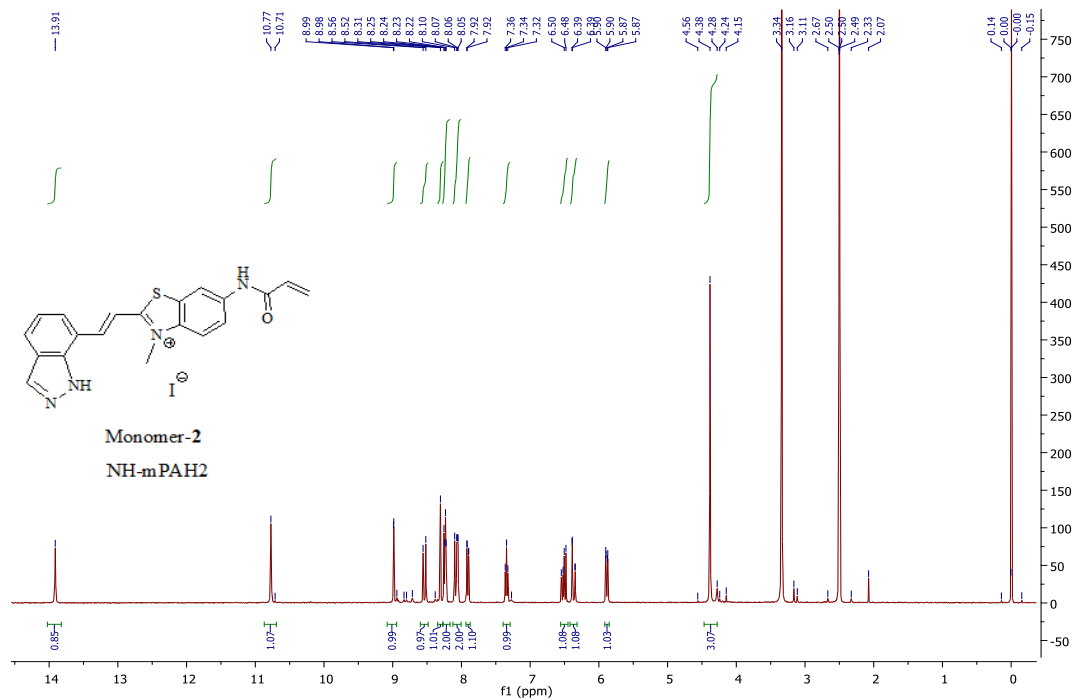


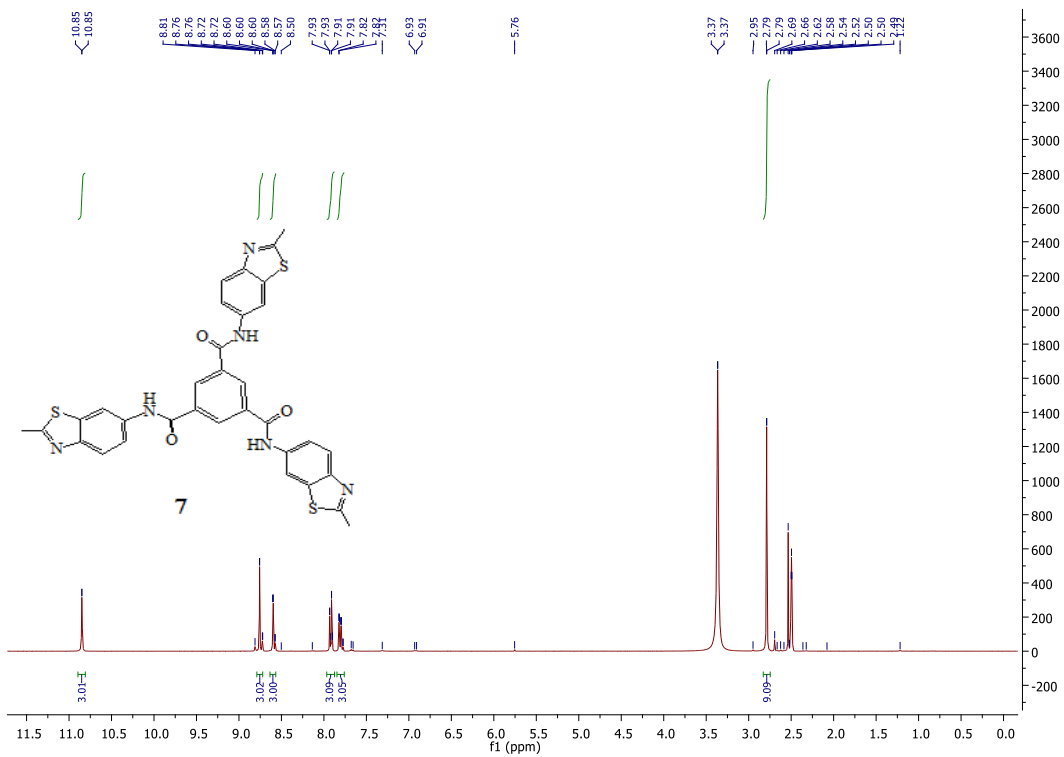
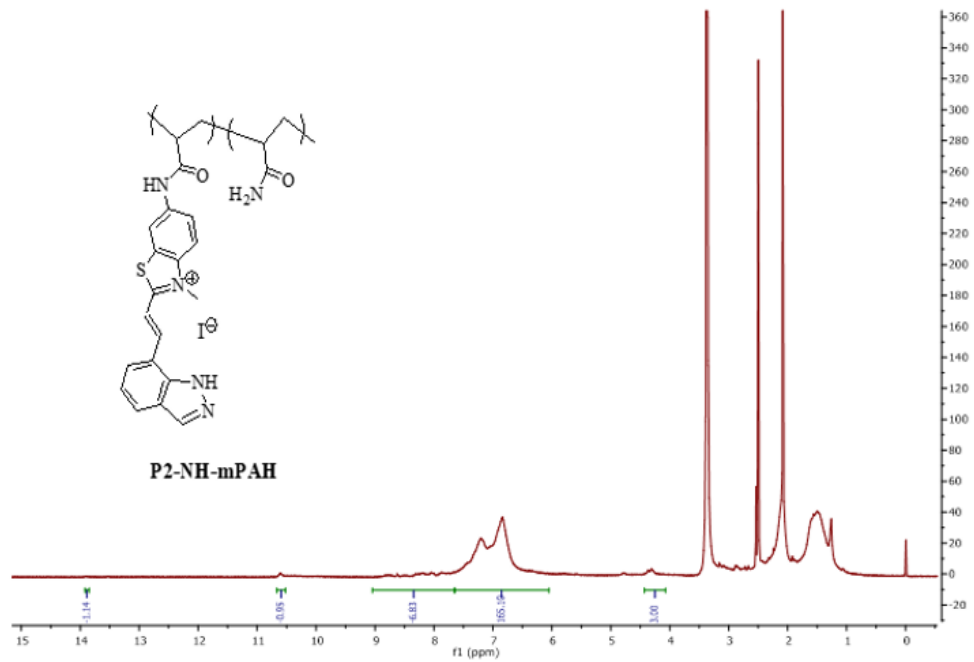


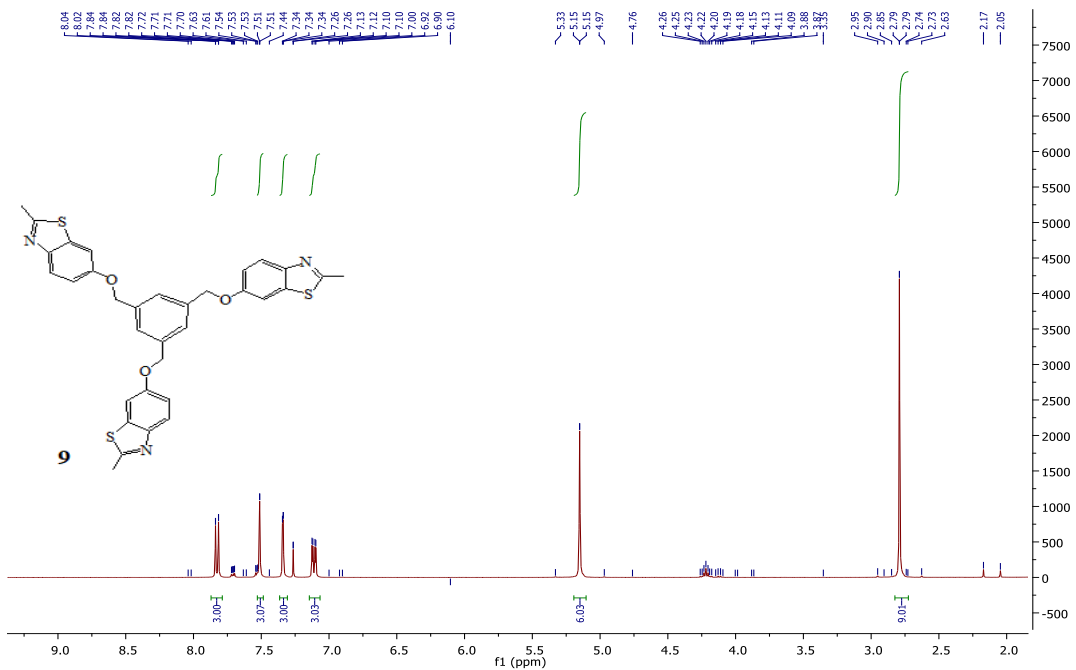
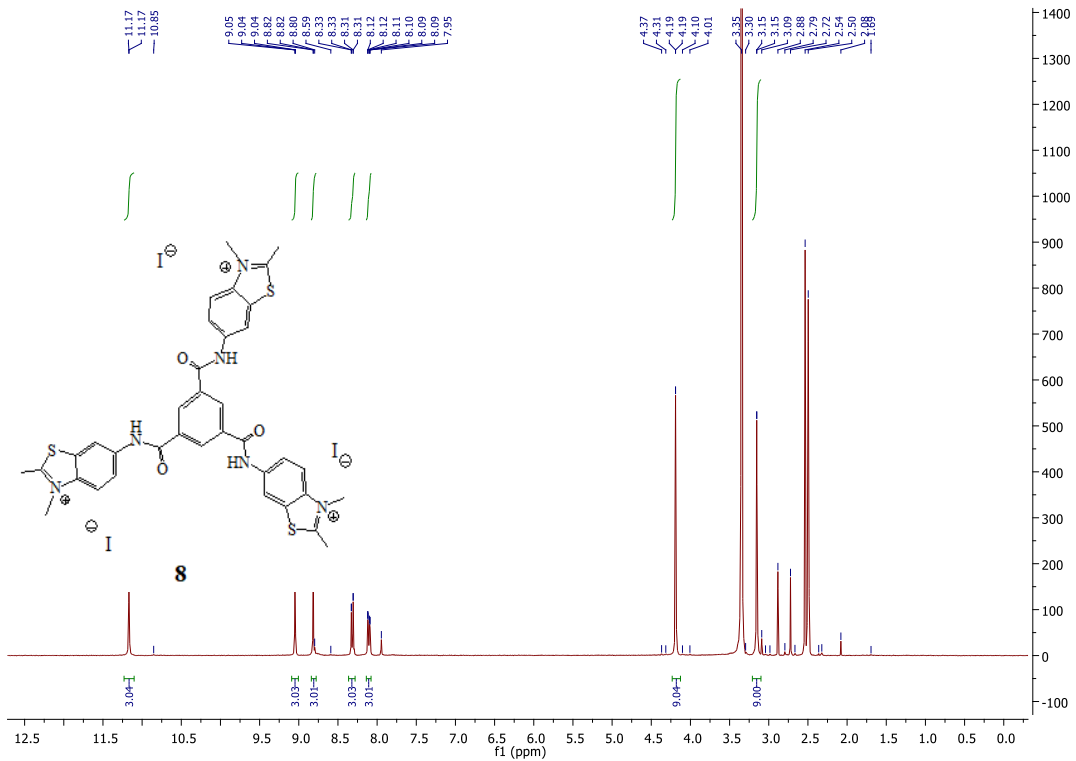


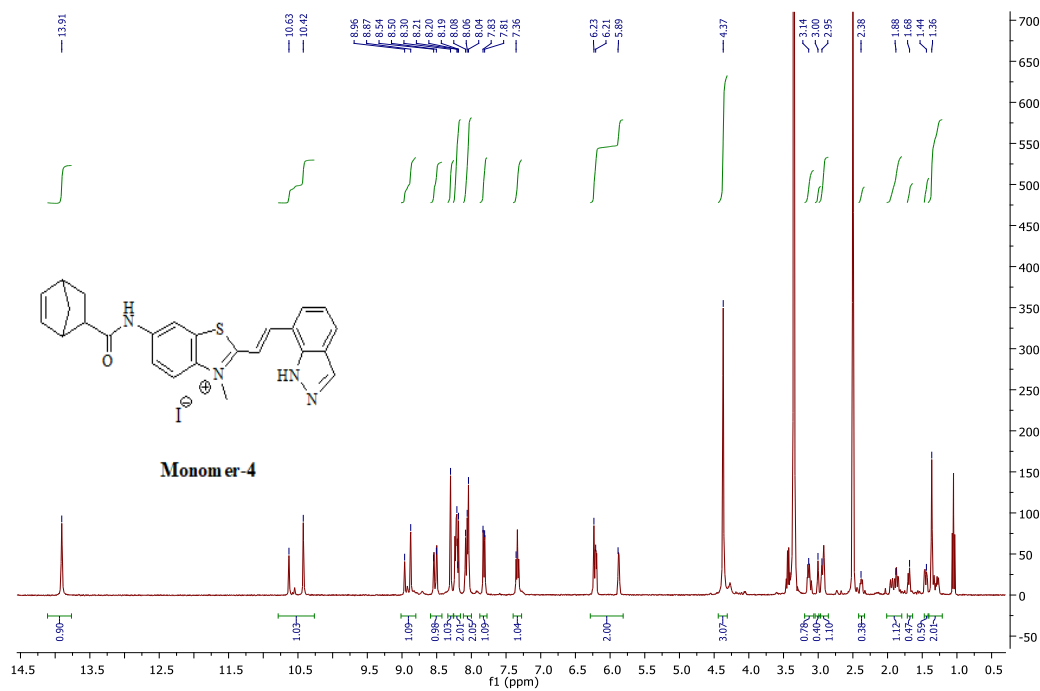
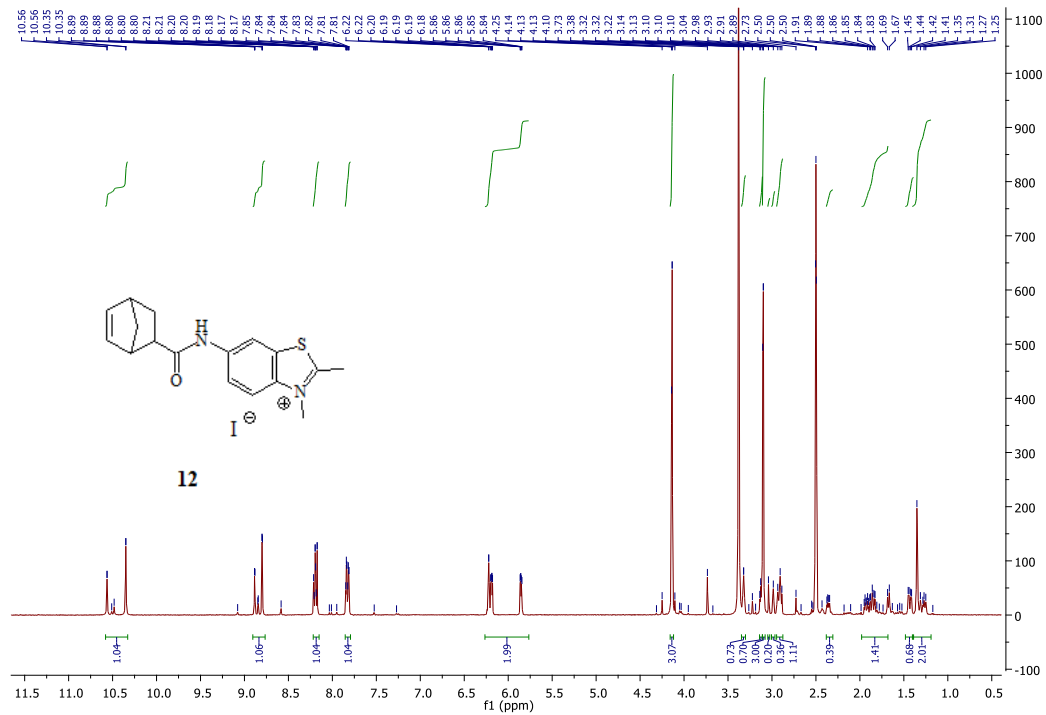
6.7.2. Selected NMR Spectra for Chapter 3

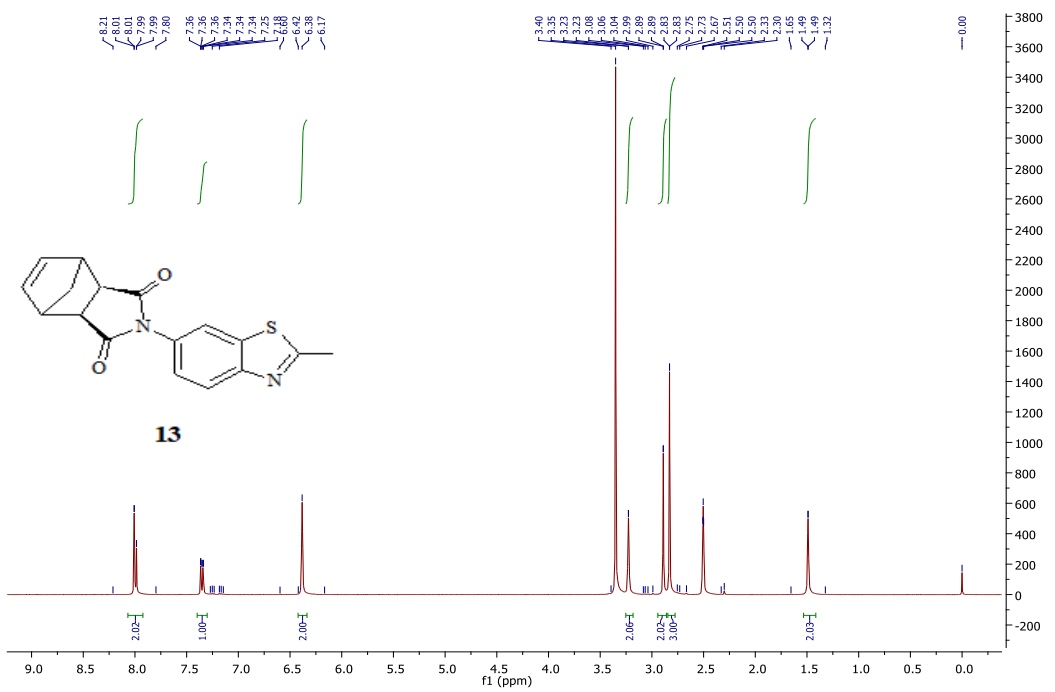
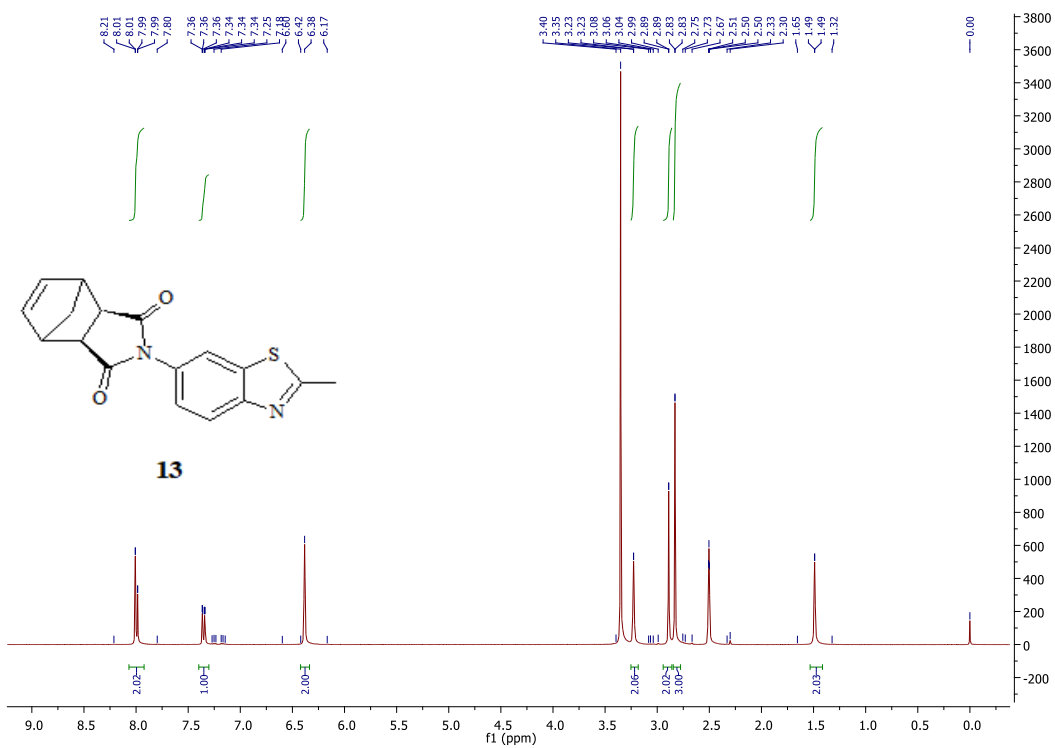


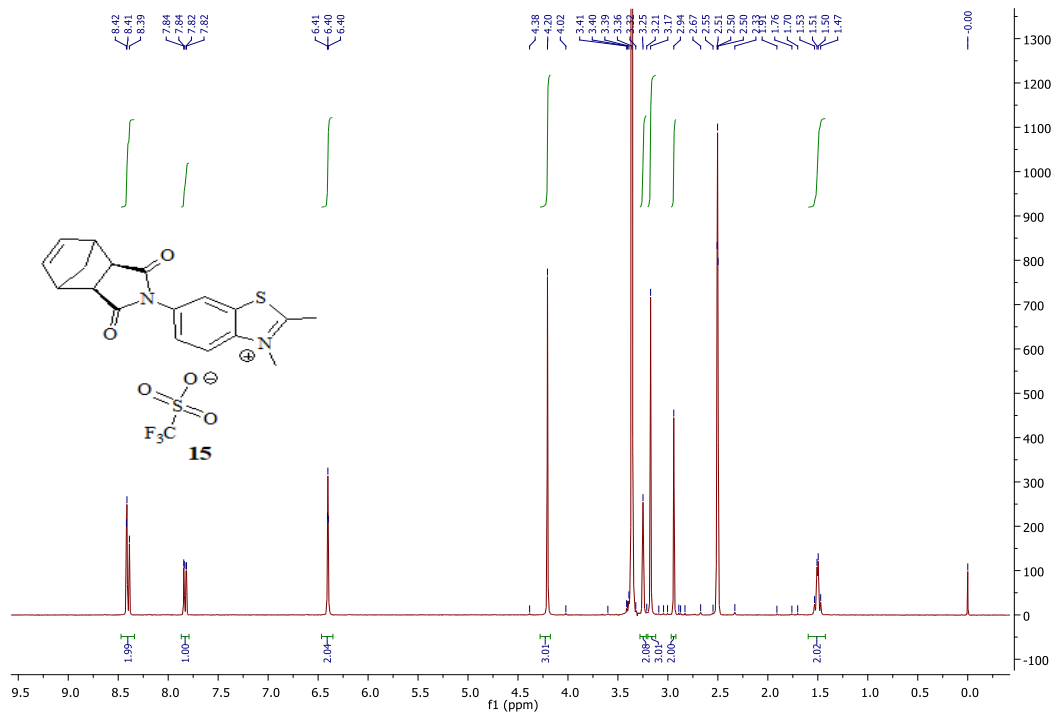
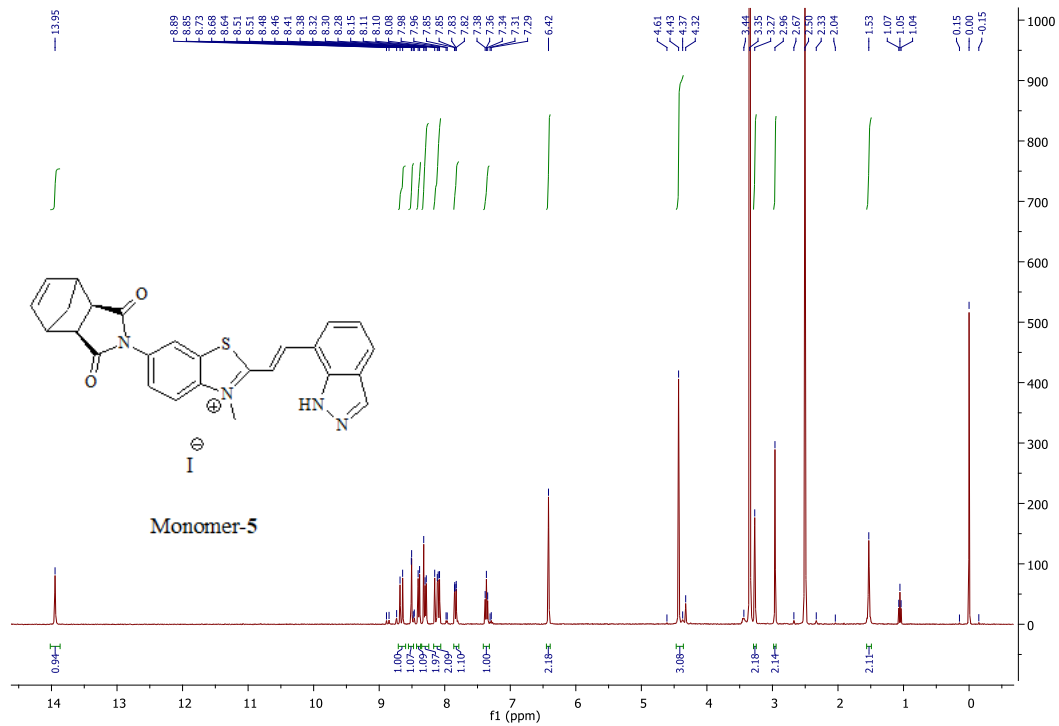


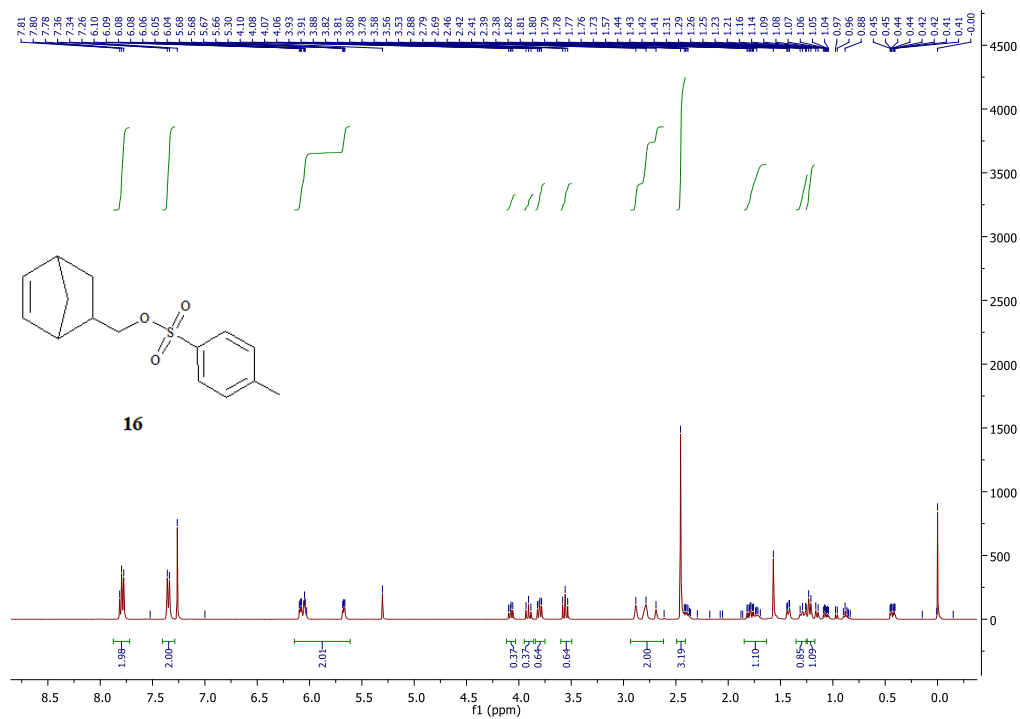
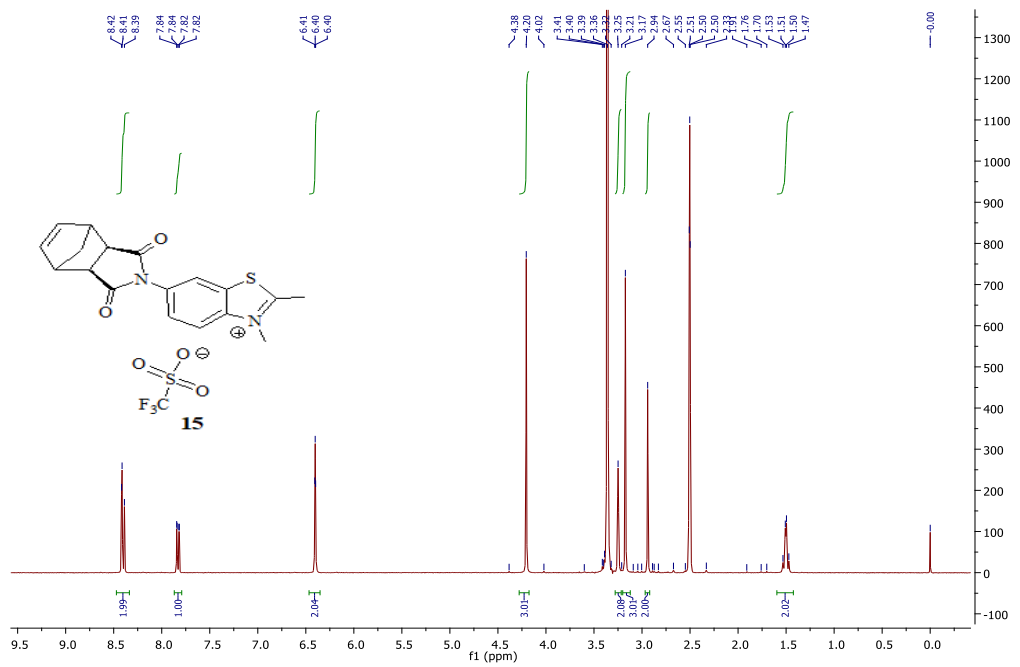


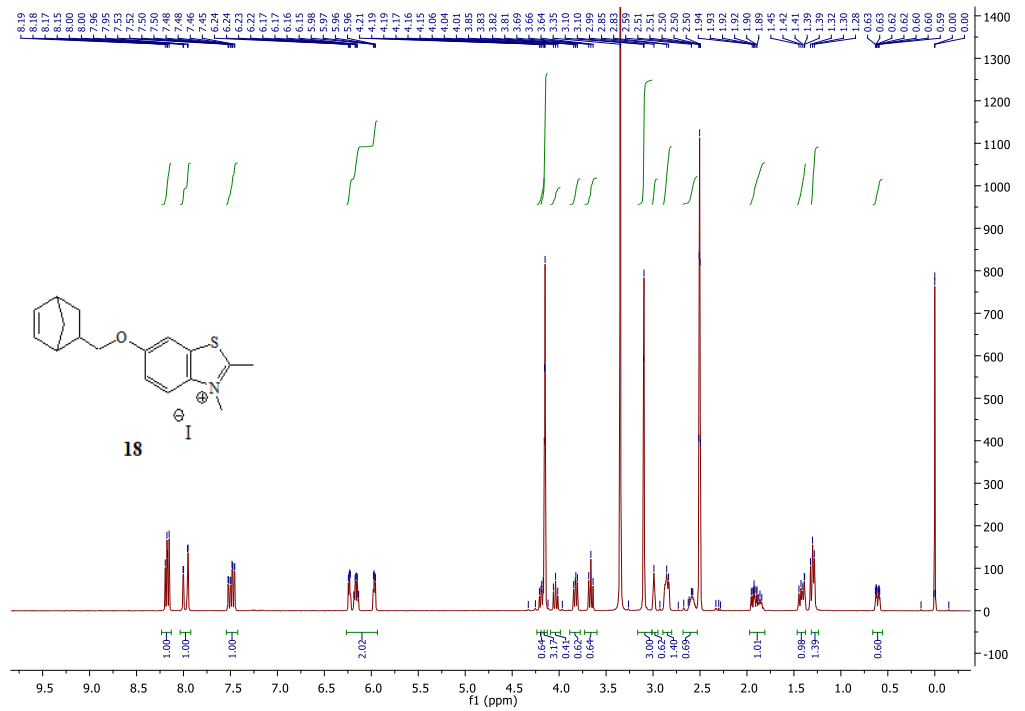
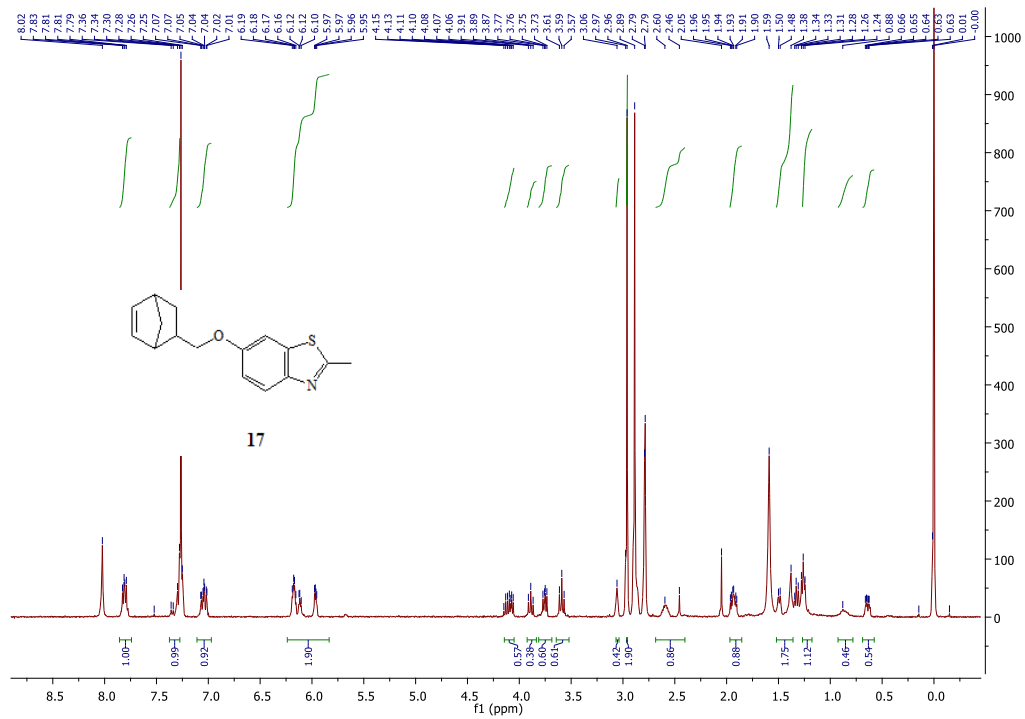


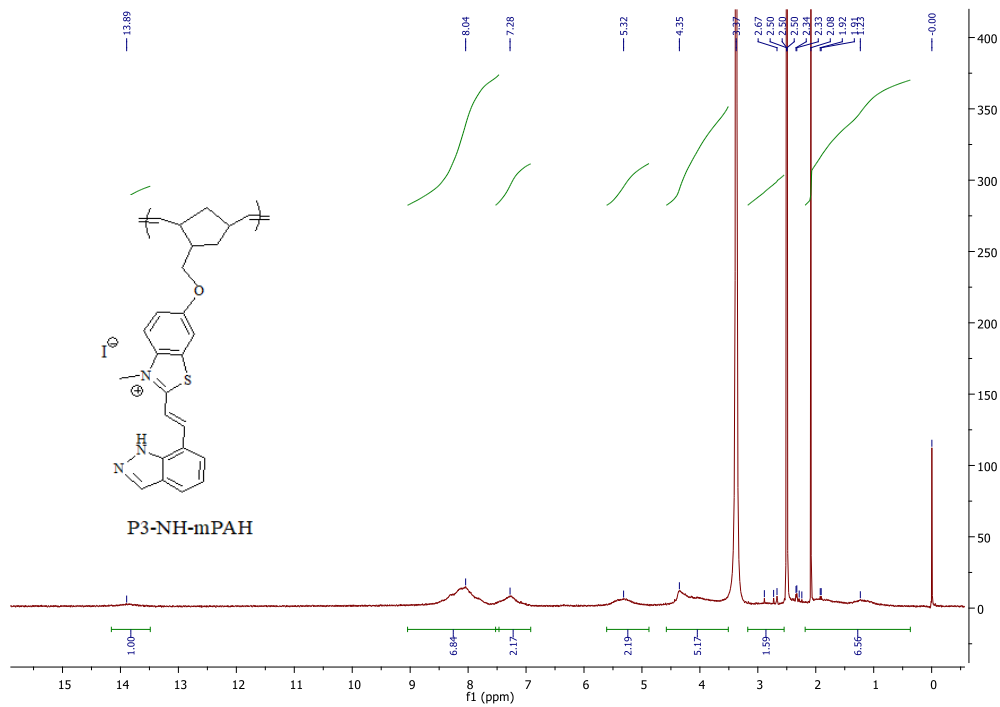
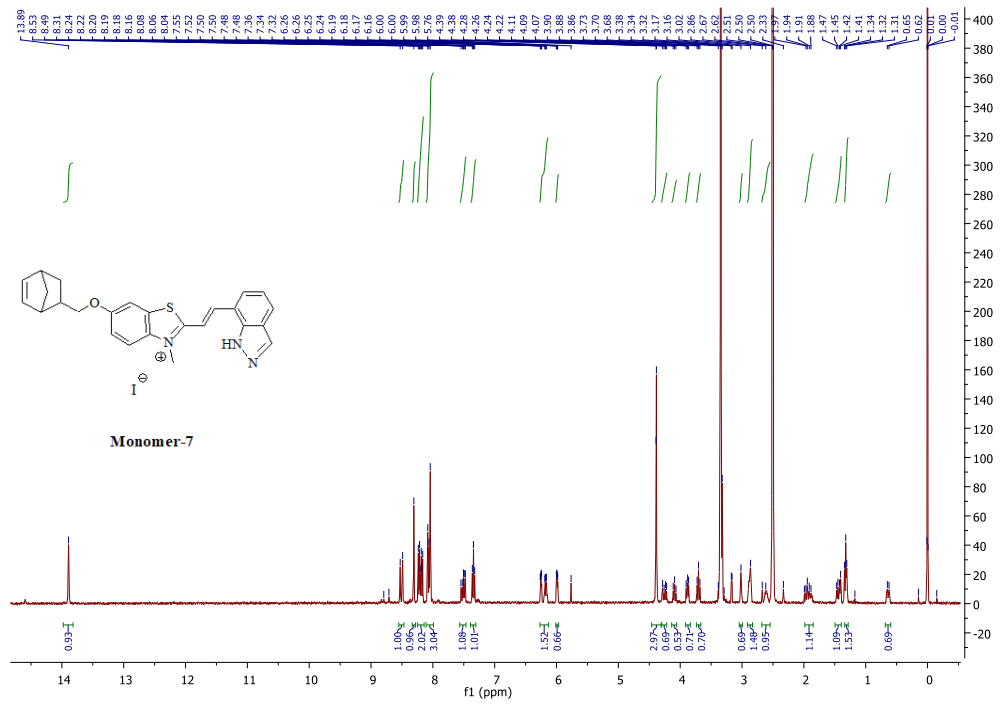












6.7.4. Selected NMR Spectra for Chapter 5

